10. SITE 1007[1]

Shipboard Scientific Party[2]

HOLE 1007A

Position: 24°30.261′N, 79°19.34′W

Start hole: 0800 hr, 24 March 1996

End hole: 1130 hr, 24 March 1996

Time on hole: 3 hr, 50 min

Seafloor (drill pipe measurement from rig floor, mbrf): 661.9

Total depth (drill pipe measurement from rig floor, mbrf): 668.5

Distance between rig floor and sea level (m): 11.6

Water depth (drill pipe measurement from sea level, m): 650.3

Penetration (mbsf): 6.6

Coring totals:
Type: APC; No: 1; Cored: 6.6 m; Recovered:100.8%

Formation:
Unit I: 0–6.65 mbsf, Pleistocene
Nannofossil ooze and unlithified wackestones and packstones

HOLE 1007B

Position: 24°30.261′N, 79°19.34′W

Start hole: 1130 hr, 24 March 1996

End hole: 2245 hr, 25 March 1996

Time on hole: 1 day, 11 hr, 15 min

Seafloor (drill pipe measurement from rig floor, mbrf): 659

Total depth (drill pipe measurement from rig floor, mbrf): 1036.7

Distance between rig floor and sea level (m): 11.6

Water depth (drill pipe measurement from sea level, m): 647.4

Penetration (mbsf): 377.7

Coring totals:
Type: APC; No: 10; Cored: 89.7 m; Recovered: 97.1%
Type: XCB; No: 31; Cored: 286 m; Recovered: 38.9%

Formation:
Unit I: 0–203.1 mbsf, Pleistocene to late Pliocene
Nannofossil ooze and unlithified to partially lithified wackestones and packstones
Unit II: 203.1–302 mbsf, early Pliocene
Foraminifer nannofossil chalk
Unit III: 302–362.6 mbsf, late Miocene
Foraminifer wackestones, foraminifer nannofossil chalks, and nannofossil limestones

HOLE 1007C

Position: 24°30.254′N, 79°19.348′W

Start hole: 2245 hr, 25 March 1996

End hole: 2015 hr, 3 April 1996

Time on hole: 8 days, 21 hr, 30 min

Seafloor (drill pipe measurement from rig floor, mbrf): 659

Total depth (drill pipe measurement from rig floor, mbrf): 1894.4

Distance between rig floor and sea level (m): 11.7

Water depth (drill pipe measurement from sea level, m): 647.3

Penetration (mbsf): 1235.4

Coring totals:
Type: RCB; No: 97; Cored: 933.4 m; Recovered: 53.9%

Formation:
Unit III: 302–362.6 mbsf, late Miocene
Foraminifer wackestones, foraminifer nannofossil chalks, and nannofossil limestones
Unit IV: 362.6–696.4 mbsf, late to middle Miocene
Light gray, gray, and olive gray foraminifer wackestones
Unit V: 696.4–832.7 mbsf, middle Miocene
Light gray to light brownish to olive gray foraminifer wackestones with minor intervals of packstones and mudstones
Unit VI: 832.7–986.2 mbsf, middle to early Miocene
Light gray to light olive or brownish foraminifer wackestones with minor intervals of fine-grained bioclastic packstones and wackestones
Unit VII: 986.2–1187.3 mbsf, early Miocene
Foraminifer wackestones with minor intervals of mudstones and wackestones to packstones
Unit VIII: 1187.3–1235.4 mbsf, early Miocene to late Oligocene
Pale yellow and light gray foraminifer wackestones and bioclastic wackestones

Principal results: Site 1007, at the crossing of seismic Lines 106 and 102B, was located on the toe-of-slope of the western Great Bahama Bank (GBB) in 647 m of water. The target horizon was the base of the Neogene, estimated to be at approximately 1230 mbsf. The site was positioned to penetrate the thin basinal portions of 17 prograding sequences and, in the upper part, a thick onlapping wedge that could be either a drift deposit or an accumulation of mass-gravity flows. To the west, the distal portions of the prograding clinoforms interfinger with the drift deposits of Site 1006. Site 1007, therefore, was the link between the basinal Site 1006 and the proximal slope Sites 1003, 1004, and 1005 to the east. In addition, a higher content of microfossils with good preservation was expected in the sediments of Site 1007 than in the more proximal Sites 1005, 1004, and 1003. The main objectives of this site in regard to sea level were to (1) precisely date the sequence boundaries, (2) determine the facies in the distal portions of carbonate sequences, and (3) assemble a data set suitable to compare the sedimentary record with the oxygen isotope record of the Neogene to Holocene sea-level fluctuations. Similarly as for the sea-level objectives, Site 1007 was also an intermediate site for the fluid-flow objectives. Interstitial-water chemistry and in situ temperature measure-

[1]Eberli, G.P., Swart, P.K., Malone, M.J., et al., 1997. *Proc. ODP, Init. Repts.*, 166: College Station, TX (Ocean Drilling Program).
[2]Shipboard Scientific Party is given in the list preceding the Table of Contents.

Previous Chapter Table of Contents Next Chapter

ments of this site should provide information about the fluid movement in the lower slope and, by comparison with the three previously drilled proximal sites, allow assessment of lateral changes in fluid chemistry. A logging suite, including a vertical seismic profile experiment, was performed for optimal correlation between the cores and the seismic data.

At Site 1007, the entire Neogene section and 20 m of Oligocene sediments were penetrated in a 1235.4 mbsf hole, providing the complete sedimentary record of Neogene sea-level changes. The sedimentation pattern displayed an alternation of more platform-derived intervals and thinner intervals with more pelagic material. This pattern occurred on a large scale (50–100 m) and on a small scale (1–5 m). Platform-reduced sediment input is interpreted to coincide with sea-level lowstands when the platform is exposed. The occurrence of this sedimentation pattern on different scales indicates that sea-level changes of various frequencies occurred throughout the Neogene. The planktonic foraminifers and nannofossils were more abundant and better preserved than in the sediments of the proximal sites. As a result, a detailed biostratigraphy was established for the entire Neogene section. This good biostratigraphic control enabled the sequence boundaries to be dated and allowed a comparison of the ages of the boundaries with the other sites. The comparison showed that an excellent correlation between the sites could be made and documented the age consistency of the sequence boundaries and the chronostratigraphic significance of these seismic reflections. With the ability to date the boundaries and several horizons within the sequences, the timing of these sea-level changes can be established. In addition, the well-preserved foraminifers at this site and Site 1006 will provide the oxygen isotope record of the Neogene sea-level changes in the same transect. Furthermore, the biostratigraphic dating was of sufficient quality to record sedimentation rates within several individual seismic sequences, thus providing an independent record of the platform-derived sedimentation during sea-level highstands and the reduced pelagic sedimentation during sea-level lowstands. Seventeen seismic sequences were distinguished prior to drilling Site 1007. The cores provide the facies content of these sequences. The facies succession indicates reduced or absent platform-derived sedimentation during the formation of the sequence boundaries, probably as a result of platform exposure during sea-level lowstands. Miocene sequences contained in the lower portion redeposited carbonates, such as turbidites and slump packages, in a more pelagic background sediment (lowstands), and biowackestones with more platform-derived material in the upper portions (highstands). With the transition into a steep-sided platform in the Pliocene, redeposited carbonates become more abundant in the upper parts of the sequences. This difference documents the influence of platform morphology on the highstand vs. lowstand shedding in carbonates. On a low-inclined carbonate, slope shedding is similar as in siliciclastics, but is 180° out of phase at steep-sided margins. Facies and diagenesis act in concert to produce petrophysical differences within the sedimentary section. As a result, the logs image closely the sedimentary and stratigraphic record. All sequence boundaries can be clearly identified on the log data. A core to log to seismic correlation is possible by the time-depth conversion using the vertical seismic profile that was acquired in the open hole after logging.

With regard to the fluid-flow objectives, Site 1007 is also a link between the basinal and the proximal sites. As in all other sites, it shows evidence of a flushed zone in the upper 20 mbsf that is somewhat thinner than in the proximal sites. The lower portion of the profile is dominated by diffusion, with local reactions involving the oxidation of organic material, the formation of pyrite, the precipitation and dissolution of carbonate minerals, and diagenesis of the clay minerals and cherts that control the concentration of various pore-water constituents.

A nearly continuous section of Pleistocene to upper Oligocene sediments was recovered at Site 1007 at the toe-of-slope of present-day GBB. Deposits recovered at Site 1007 contain elements identified at the more proximal Site 1003 and the more distal Site 1006. This sedimentary succession is interpreted to record an interplay among (1) a change in platform-to-basin morphology, (2) sea-level variation, (3) pelagic input, and (4) ocean currents. In contrast to other sites drilled during Leg 166, the section at Site 1007 is characterized by an increased occurrence of turbidites and slumped intervals and by a relatively high amount of clay- and silt-sized siliciclastics in the upper Pliocene and Pleistocene parts of the section. In addition, below 1120 mbsf, sediments at Site 1007 are marked by the presence of compaction-dissolution features, namely anastomosing or wispy solution seams.

The Pleistocene section at Site 1007 is characterized by a meter-scale alternation between silt- and clay-rich sediment and silt- and clay-poor sediment. These alternations are similar to the clay cycles observed in the Pleistocene section at Site 1006 and are interpreted to reflect erosion of continent-derived siliciclastics during sea-level lowstands and incipient sea-level rises, along with a subsequent increase in neritic and pelagic input following flooding. Seismic stratigraphy and biostratigraphic data suggest that the upper Pliocene section is thicker and characterized by a higher sedimentation rate relative to other sites. This thickness variation is caused by two processes: (1) an accumulation of mass-gravity flow deposits, which bypassed the upper slope and accumulated at Site 1007; and (2) an increase in the amount of current drift deposits. This latter increase could reflect a migration of the northward-flowing, Santaren Channel Current toward the platform during the late Pliocene and early part of the Pleistocene.

As at other sites drilled during Leg 166, the sedimentary succession at Site 1007 records an important change in the mode of neritic carbonate production. At the base of Unit I (base of upper Pliocene), there is a sudden increase in the occurrence of aragonite needles and peloids in the platform-derived material, whereas below this level it consisted mostly of skeletal debris. The turnover from skeletal- to aragonite needle-/ peloid-dominated sediments probably reflects the coupled effects of climate change and the transition of the GBB from a carbonate ramp, characteristic of the Miocene, to the present-day, flat-topped carbonate platform.

The Miocene section at Site 1007 is nearly identical to the Miocene sections recovered at Sites 1003, 1005, and 1006 and consists of alternating intervals of well-cemented, decimeter- to meter-scale light-colored, clay-free intervals, which show no evidence of compaction, and decimeter-scale dark-colored, relatively clay-rich intervals that show evidence of compaction. These alternations are interpreted to reflect changes in the rate of neritic carbonate input and the subsequent impact on the primary diagenetic potential of sediments. In this regard, light-colored, well-cemented intervals may reflect periods of higher neritic (aragonite and high-Mg calcite) input and the deposition of sediments with a higher diagenetic potential. In contrast, dark-colored, weakly cemented intervals may reflect periods of decreased neritic input, and the deposition of sediments with higher amounts of low-Mg calcite.

On a large scale, sediments at Site 1007 are divided into eight lithologic units on the basis of compositional and textural changes. Most unit boundaries correspond to inferred periods of reduced sedimentation, change in sediment composition, and intervals of increased mass-gravity flow deposits. The Pleistocene to upper Pliocene Unit I (0–231 mbsf) consists of a succession of nannofossil ooze and variable lithified wackestones to packstones. Aragonite needles and peloids are an important but variable component in the fine sand- and silt-sized fraction. The disappearance of peloids marks the lower boundary of this unit. Unit I is subdivided into four subunits. Subunit IA (0–10.9 mbsf) is a sequence of nannofossil ooze, unlithified wackestone and packstone, which is interrupted by gravity-flow deposits. Subunit IB (10.9–43.5 mbsf) is characterized by meter-scale alternations between intervals of silt- and clay-rich sediments and intervals of silt- and clay-free sediments. The contact between Subunit IB and Subunit IC occurs at the top of the lowermost of two hardgrounds. Subunit IC (43.5–165 mbsf) encompasses a succession of faintly laminated, unlithified peloidal wackestone to packstone. This succession is interrupted by an interval of partially lithified foraminifer wackestone and a slumped interval containing interbeds of unlithified packstone to floatstone. The contact between Subunits IC and ID is defined by a change in degree of lithification that coincides with a firm-

ground. Subunit ID (165.8–203.1 mbsf) consists of slightly dolomitized wackestone and packstone. The lower Pliocene Unit II (203.1–302.0 mbsf) consists entirely of bioturbated light gray to pale yellow foraminifer nannofossil chalk. Foraminifers are the dominant allochem, whereas other bioclastic debris are minor constituents.

The upper Miocene Unit III (302.0–362.6 mbsf) displays variable degrees of lithification of foraminifer wackestone, nannofossil chalk, and nannofossil limestone. In the upper part of the unit a series of coarse-grained turbidites are intercalated. The boundary of the underlying Unit IV (362.6–696.4 mbsf) is placed above a series of fine-grained, laminated packstones. The upper to middle Miocene Unit IV is made up of 5- to 10-cm-thick layers of fine-grained packstone and an alternation between decimeter- to meter-scale intervals of densely cemented sediment with intervals of weakly cemented sediment that show evidence of compaction. These alternations probably reflect the rate of neritic input and are related to sea-level changes (see above).

Unit V is of middle Miocene age and consists primarily of a succession of bioturbated foraminifer wackestone with minor intervals of packstone and mudstone. Turbidites are concentrated in the upper part of Unit V, whereas the lower part of the unit contains similar cyclic alternations of better and less cemented wackestones described above. The middle to lower Miocene Unit VI (832.7–986.2 mbsf) also contains bioturbated biowackestones with a small amount of packstones. In addition, several firmgrounds and thin clay-rich layers are observed within the unit. The lower Miocene Unit VII (986.2–1187.3 mbsf), like Units IV, V, and VI, is characterized by an alternation between well-cemented decimeter- to meter-scale intervals and decimeter-scale dark-colored intervals. In addition, the unit also contains numerous calcareous turbidite deposits and clay-rich layers. The lower Miocene to upper Oligocene Unit VIII (1187.3–1235.4 mbsf) consists of foraminifer wackestone and bioclastic wackestone arranged in alternations of decimeter- to meter-scale light- and dark-colored intervals that are generally similar to those described in the overlying units. Black chert nodules and compaction/dissolution seams discriminate this unit form the overlying ones.

Nannofossil and planktonic foraminiferal biostratigraphy indicates that the top of Hole 1007B is older than 0.95 Ma. Obviously, current action along this part of the slope increased during the last 1 m.y. and caused nondeposition and/or erosion. A hiatus just below the Pliocene/Pleistocene contact that lasted for approximately 0.4 m.y. might also be the result of current activity. The upper Pliocene interval is highly expanded with an average sedimentation rate of 21 cm/k.y. This is much higher than in time equivalent intervals at the other transect sites, where sedimentation rates of about 2–3 cm/k.y. were found. The increased sedimentation is the combined result of deposition of platform-derived material that bypassed the upper slope and was deposited at the toe-of-slope and the accumulation of drift sediments at Site 1007. The lower Pliocene package is bounded by a hiatus. The duration of the hiatus spanning the early/late Pliocene boundary is approximately 1 m.y. (3.2–4.2 Ma). The sedimentation rate below this hiatus is 17.5 cm/k.y. and is similar to the sedimentation rate at the more proximal slope sites (Sites 1003 and 1005) or in the Straits of Florida at Site 1006. Below 304 mbsf, an interval of poor preservation of the calcareous microfossils represents either an interval of very low sedimentation (<1 cm/k.y.) or contains a hiatus that straddles the Miocene–Pliocene boundary.

A late Miocene hiatus was detected at approximately 328 mbsf and spanned a period of approximately 2 m.y. Just above this unconformity, approximately 20 m of uppermost Miocene sediment was found. The sedimentation rate for this short section cannot accurately be determined, but is probably in the order of 1 cm/k.y. This interval may provide evidence for some platform production during the Messinian, or it represents a lowstand wedge. The late Miocene is characterized by a high sedimentation rate (13 cm/k.y.). Sedimentation rates at the proximal Sites 1003 and 1005 were very similar, whereas Site 1006 farther out in the basin shows a much lower sedimentation rate that is pelagic in nature (3 cm/k.y.). This sedimentation rate pattern shows that the GBB was shedding material to the gently dipping slope during the late Miocene. The middle and early Miocene sedimentation rates show four cycles with alternating low (<2 cm/k.y.) and high (>5 cm/k.y.) rates. Slow sedimentation intervals occurred from 9.5 to 11.5 Ma, 13 to 15 Ma, 16.5 to 17.5 Ma, and 20.5 to 23 Ma and correlate to hiatuses of similar duration at Site 1003. Periods of faster deposition occurred from 11.5 to 13 Ma, 15 to 16.5 Ma, 17.5 to 20.5 Ma, and older than 23 Ma, corresponding to intervals at Site 1003 with similarly high sedimentation rates. These cycles represent the turning off and on of platform production in response to relative sea-level changes.

Geophysical and geochemical data acquired during logging of Hole 1007C provide detailed information on the sedimentary properties and structure of the strata. Log-to-core correlation permits significant interpretations about variations in sedimentation patterns on the toe-of-slope of GBB from the earliest early Miocene to Pleistocene. The general compatibility of the discrete data points from shipboard petrophysical measurements with the log data supports the integrity of the data sets. In general, there is a downhole trend of increasing resistivity and sonic velocity. Small-scale and long-term excursions are superimposed over this general trend. These variations reflect the lithologic and diagenetic variations in the core. Higher resistivity and velocity can be correlated approximately with sediments described as firmgrounds, hardgrounds, or turbidites. In addition, logs display little variation through monotonous units. As the high values of the logs coincide with sequence stratigraphic important sedimentary units, they display precisely all sequence boundaries.

Seventeen seismic sequences were distinguished prior to drilling. Ages of the sequence boundaries were postulated from the biostratigraphic information of the adjacent sites. These predictions proved to be very accurate. In addition, the better preservation of the biostratigraphic markers at Site 1007, when compared to the more proximal sites, permits a refinement of some of the ages. For example, the lower Pliocene sequence was not datable in the more proximal Sites 1003 and 1005 due to the absence of age-diagnostic marker species. At this more distal site, a precise stratigraphy through this interval is possible and the basal sequence boundary is now dated as the top of the Messinian. For an intersite comparison of the ages of the seismic reflections that mark the sequence boundaries, a vertical seismic profile was acquired for an accurate time to depth conversion at Site 1007. All the seismic sequence boundaries yield the same ages as in the adjacent sites. This age consistency of seismic reflections proves the basic assumption of sequence stratigraphy that assumes a chronostratigraphic significance to seismic reflections. The good age control in this site and the entire transect allows the dating of the sequence boundaries and thus for the sea-level changes throughout the Neogene.

Site 1007 shows three basic geochemical zones that relate to zones seen previously. First, there is an upper flushed zone in which there are no changes in the conservative elements and only minimal changes in the nonconservative elements such as Sr^{2+}, Ca^{2+}, and alkalinity. This zone is similar to that found at the upper slope sites (Site 1003, 1004, and 1005), but differs in that minimal changes were observed in the concentration of Sr^{2+}. This is in contrast to the more proximal slope sites that exhibited no change in nonconservative parameters such as Sr^{2+} over this interval. Site 1007 is similar to the more distal Site 1006 in this regard. This flushed zone is also thinner than in the proximal sites, with a thickness of only 20 m compared to 40 m. Below the flushed zone, the concentration of the conservative elements (Cl^- and Na^+) shows a diffusional relationship to the bottom of the hole. The concentration of K^+ shows a major decrease between 900 and 1000 mbsf related to diagenesis of clay minerals. In geochemical Zone 2, concentrations of the nonconservative elements (Sr^{2+}, SO_4^{2-}, Ca^{2+}, NH_4^+, and alkalinity) show changes that are related to local reactions such as the degradation of organic material and the recrystallization of carbonate minerals. Immediately below the flushed zone, the SO_4^{2-} concentration decreases slightly as a result of the local oxidation of organic material. This is accompanied by an increase in the concentration of methane. The concentration of SO_4^{2-} rises again to seawater values at 400 mbsf and then decreases to zero below 600 mbsf. The removal of sul-

fate marks the start of a third geochemical zone and corresponds to the appearance of concentrations of up to 10 ppm isobutane in the headspace samples postulated to be of thermogenic origin. The concentration of Sr^{2+} in this interval is strongly controlled by the solubility of celestite. Once the SO_4^{2-} has been completely removed from the pore waters, the Sr^{2+} increases to over 5 mM at a depth of 950 mbsf. A maximum in the Ca^{2+} concentration between 350 and 400 mbsf indicates a probable zone of carbonate dissolution in this area. Below this depth, Ca^{2+} concentrations decrease. When normalized to seawater Cl^- concentrations, this zone shows a net removal of Ca^{2+} from the pore waters.

Over the upper 900 mbsf the sediments consist of more than 90% carbonate. Below this depth, the concentration of carbonate decreases to between 60% and 80% with higher amounts of organic carbon (up to 1 wt%). Organic carbon is also higher in Subunit IVB. The hole is dominated by low-magnesium calcite (LMC), although Unit I consists mainly of aragonite with small amounts of dolomite and high-magnesium calcite (HMC). Throughout the remainder of the hole, dolomite is a minor constituent with concentrations of up to 40% in thin isolated intervals. Quartz is a ubiquitous component throughout the core and there are documented occurrences of pyrite and clay minerals.

Site 1007 completed the data set needed to address the questions in regard to sea-level changes and fluid flow. A foraminifer and nannofossil biostratigraphy provides the age control on the depositional changes that are related to sea-level fluctuations and the resulting sequence boundaries. This sedimentary record will add to the database that is needed to eventually establish the global synchrony of sea-level changes. Furthermore, the abundant well-preserved foraminifers in the Bahamas Transect give the unique opportunity to compare the sedimentary record with the oxygen isotope proxy for sea-level changes. This comparison will potentially allow assessment of the causal relationship between the stratal pattern and sea-level changes.

The geochemical profiles at Site 1007 indicate that there is active fluid flow in the upper part of the strata, as at the other sites. The occurrence of the change of gradients at similar depths along the transect gives strong evidence that flow is at least partially horizontal and related to stratigraphic boundaries. With increasing depth, diffusive processes become the dominant transport mechanism.

BACKGROUND AND OBJECTIVES

Site 1007, at the crossing of seismic Lines 106 and 102B, is located on the toe-of-slope of the western Great Bahama Bank (GBB) in 647 m of water depth (Fig. 1). The architecture of the strata at this location displays the interfingering of prograding clinoforms and the eastern portions of the drift deposit that forms a mound in the axis of the Straits of Florida. The three youngest sequences show westward-thinning clinoforms downlapping onto a thick wedge that onlaps and interfingers with the underlying clinoforms (Fig. 2). This thick, onlapping wedge could be either a drift deposit or an accumulation of mass-gravity flows that bypassed the upper slope. Below the wedge, the distal portions of the prograding clinoforms thin westward and interfinger with the drift deposits of Site 1006. Therefore, Site 1007 was the link between this basinal site and the proximal slope sites to the east.

Because Site 1007 is located in relatively deep water and in the distal portions of the prograding sequences, a higher content of microfossils with good preservation was expected than in the more proximal Sites 1005, 1004, and 1003. Therefore, the main objectives of this site in regard to sea level were to:

1. Precisely date the sequence boundaries,
2. Determine the facies in the distal portions of carbonate sequences, and
3. Assemble a data set suitable for comparing the sedimentary record with the oxygen isotope record of the Neogene to Holocene sea-level fluctuations.

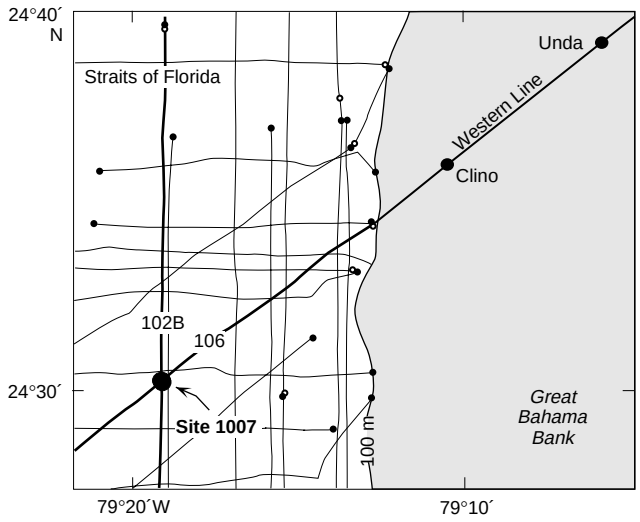

Figure 1. Location map of Site 1007. The site is located on the crossing of seismic Lines 106 and 102B, approximately 7 km to the southwest of Site 1003 at the toe-of-slope of the western Great Bahama Bank.

Site 1007 was also an intermediate site for the fluid-flow objectives. Interstitial water chemistry and in situ temperature measurements of this site were expected to provide information about the fluid flow in the lower slope and, by comparison with the three previously drilled proximal sites, assess lateral changes of the flow.

OPERATIONS

Transit

The 4.2-nmi transit from Site 1003 to Site 1007 was made in dynamic positioning mode while tripping pipe and handling the BHAs. A retrievable beacon was dropped at 0755 hr on the GPS coordinates for Site 1007 (24°30.26′N; 79°19.34′W).

Hole 1007A

An APC/XCB BHA similar to that used at previous sites was assembled and run to the seafloor. Hole 1007A was spudded at 1110 hr on 24 March. On Core 1H, the flapper core catcher remained open and some core fell out on the rig floor. The core had a good mudline and was archived as 6.65 m recovery; however, another mudline core was taken as a precaution. The water depth was 650.3 mbsl based on the core recovery.

Hole 1007B

Hole 1007B was initiated at 1135 hr on 24 March at the same location as Hole 1007A. Core 1H recovered 9.90 m, and the water depth was defined at 647.4 mbsl based on recovery. APC Cores 1H through 10H were taken from 0 to 91.7 mbsf with 97.1% recovery (Table 1). The interval between 38 and 40 mbsf was missed because the APC coring attempt after Core 4H refused to advance past 38.0 mbsf, presumably due to the presence of a hard layer. After drilling 2 m (38.0–40.0 mbsf), APC coring was resumed. Adara heat flow measurements were performed on Cores 4H through 10H. APC coring was terminated because of core disturbance from six successive partial strokes and high overpull (Cores 5H through 10H). XCB cores 11X through 41X (91.7–377.7 mbsf) were cut with 38.9% recovery. The WSTP was deployed after Cores 14X, 17X, 22X, and 27X. XCB coring was terminated when core recovery became unsatisfactory

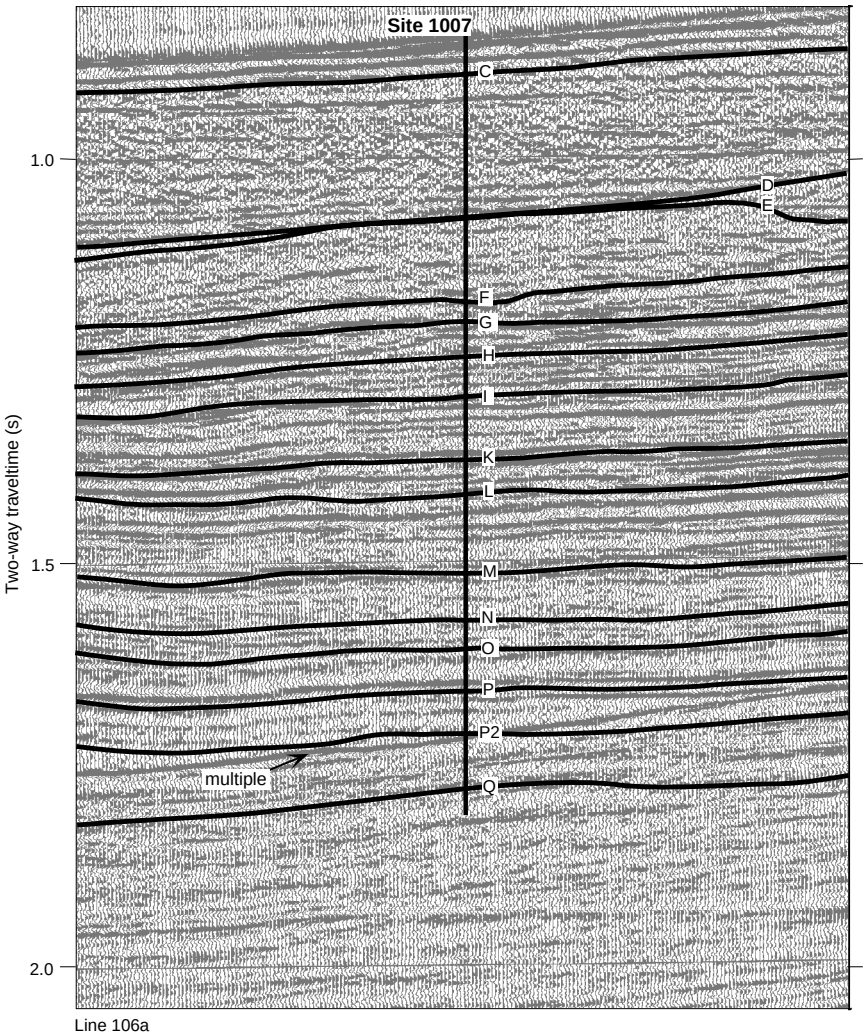

Figure 2. Portion of seismic Line 106 displaying the architecture of the strata at Site 1007. The Miocene Sequences *g* through *q* are the thin distal parts of prograding clinoforms. The package between C and D is an onlapping wedge that unconformably overlies sequence Boundary D. The Pleistocene package, above C, progrades over this wedge.

(13%) in the last nine cores. The hole was filled with 130 bbls of gel mud, and the bit cleared the rotary table at 2245 on 25 March.

Hole 1007C

The ship was moved 20 m to the southwest, and a RCB BHA similar to that used at the previous sites was run to the seafloor, which was tagged with the bit at 647.3 mbsl. Hole 1007C was initiated at 0340 hr on 25 March and drilled from 0 to 302.0 mbsf. RCB cores were cut from 302.0 to 1235.4 mbsf with 53.9% recovery. Three wiper trips were required to condition the hole while RCB coring. A short trip was made from 504 to 357 mbsf without incident. Below 750 mbsf, overpull and drag increased from 10,000 to 20,000 lb, requiring a second short trip. A third wiper trip was made at 821 mbsf, with 80,000-lb overpull noted at 277 mbsf. The drill string had to be backreamed out of the hole through numerous tight spots to 78.4 mbsf. No ledges or fill were noted in running pipe back to the bottom of the hole, and RCB coring continued from 821.4 to 1235.4 mbsf (total depth). Coring was terminated after penetrating the base of the Neogene. A gel mud sweep was circulated, and a conditioning trip was made to 76.2 mbsf, with overpull at 171, 159, and 102 mbsf (50,000 lb). The bit had to be reamed back to bottom from 1141.0 to 1235.4 mbsf. The bit was released, and the pipe was positioned at 111.5 mbsf. A Quad-combo log was run to 1158 mbsf. The FMS log was canceled because of the large hole diameter; and the WST was run to 1093 mbsf. The VSP tool (WST) could not be pulled back into the pipe even after 5000-lb overpull. As at Site 1005, the Kinley crimper and cutter were used to cut the logging line, and the WST was retrieved. The ship was under way to Site 1008 at 2018 hr on 3 April.

LITHOSTRATIGRAPHY

Introduction

A nearly continuous section of Pleistocene to upper Oligocene sediments was recovered at Site 1007, which was drilled near the toe-of-slope of the present-day GBB. Hole 1007A recovered 6.7 m of nannofossil ooze and unlithified foraminifer wackestone. Hole 1007B recovered 198.4 m of nannofossil ooze, unlithified to lithified foraminifer and peloidal wackestone and packstone, and foraminifer nannofossil chalk. Hole 1007C, the deepest of the three holes, penetrated 1235.4 m of foraminifer wackestone, foraminifer nannofossil chalk and limestone, bioclastic packstone to wackestone, mudstone, and thin clay- and organic-rich layers, for a total recovery of 53.9%. Carbonate contents in sediments recovered at Site 1007 average 91 ± 10 wt%, but range to less than 20% in thin clay- and organic-rich layers (see "Organic Geochemistry" section, this chapter).

Sediments at Site 1007 are divided into eight lithostratigraphic units on the basis of compositional and textural changes (Fig. 3). Methods used to describe the sedimentary succession at Site 1007 include visual core descriptions, determination of silt- to sand-sized allochems in wash samples, smear-slide analyses, and thin-section

Table 1. Site 1007 coring summary.

Core	Date (1996)	Time (UTC)	Depth (mbsf)	Length cored (m)	Length recovered (m)	Recovery (%)
166-1007A-						
1H	24 Mar	1615	0.0–6.6	6.6	6.7	101.0
Coring totals				6.6	6.7	101.0
166-1007B-						
1H	24 Mar	1645	0.0–9.5	9.5	9.9	104.0
2H	24 Mar	1720	9.5–19.0	9.5	9.9	104.0
3H	24 Mar	1745	19.0–28.5	9.5	6.8	71.1
4H	24 Mar	1830	28.5–38.0	9.5	9.1	95.9
5H	24 Mar	2015	40.0–49.5	9.5	10.1	105.8
6H	24 Mar	2055	49.5–57.5	8.0	7.5	94.1
7H	24 Mar	2155	57.5–67.0	9.5	9.7	102.0
8H	24 Mar	2230	67.0–76.5	9.5	8.7	91.1
9H	24 Mar	2320	76.5–84.7	8.2	8.4	102.0
10H	25 Mar	0020	84.7–91.7	7.0	7.1	102.0
11X	25 Mar	0110	91.7–101.2	9.5	6.1	64.1
12X	25 Mar	0150	101.2–110.6	9.4	1.3	14.1
13X	25 Mar	0215	110.6–120.0	9.4	0.6	6.5
14X	25 Mar	0335	120.0–129.5	9.5	0.3	3.0
15X	25 Mar	0405	129.5–138.5	9.0	8.7	96.3
16X	25 Mar	0445	138.5–147.4	8.9	6.8	75.9
17X	25 Mar	0605	147.4–156.8	9.4	7.8	83.4
18X	25 Mar	0640	156.8–166.1	9.3	2.0	21.7
19X	25 Mar	0710	166.1–175.4	9.3	1.5	15.8
20X	25 Mar	0740	175.4–184.7	9.3	0.5	4.9
21X	25 Mar	0820	184.7–193.9	9.2	0.4	4.1
22X	25 Mar	0930	193.9–203.1	9.2	0.0	0.1
23X	25 Mar	1020	203.1–212.4	9.3	8.8	94.4
24X	25 Mar	1045	212.4–221.5	9.1	9.5	104.0
25X	25 Mar	1110	221.5–230.6	9.1	8.7	95.8
26X	25 Mar	1135	230.6–239.8	9.2	9.3	101.0
27X	25 Mar	1250	239.8–249.1	9.3	8.8	94.2
28X	25 Mar	1335	249.1–258.4	9.3	6.0	64.1
29X	25 Mar	1415	258.4–267.7	9.3	3.8	40.3
30X	25 Mar	1450	267.7–276.9	9.2	6.9	75.4
31X	25 Mar	1525	276.9–286.0	9.1	0.5	5.6
32X	25 Mar	1610	286.0–295.1	9.1	2.6	28.0
33X	25 Mar	1705	295.1–304.3	9.2	1.0	10.3
34X	25 Mar	1740	304.3–313.6	9.3	1.7	17.8
35X	25 Mar	1820	313.6–322.8	9.2	0.4	4.2
36X	25 Mar	1855	322.8–332.0	9.2	0.7	7.6
37X	25 Mar	1945	332.0–341.1	9.1	1.0	11.3
38X	25 Mar	2040	341.1–350.2	9.1	2.3	24.8
39X	25 Mar	2130	350.2–359.4	9.2	1.6	17.0
40X	25 Mar	2240	359.4–368.5	9.1	1.4	15.4
41X	26 Mar	0000	368.5–377.7	9.2	0.7	7.3
Coring totals				375.7	198.4	52.8
166-1007C-						
1R	26 Mar	1820	302.0–311.6	9.6	1.4	14.9
2R	26 Mar	1840	311.6–321.2	9.6	0.4	3.9
3R	26 Mar	1905	321.2–330.8	9.6	2.4	25.4
4R	26 Mar	1930	330.8–340.4	9.6	1.9	20.2
5R	26 Mar	2020	340.4–350.0	9.6	2.7	27.8
6R	26 Mar	2055	350.0–359.6	9.6	3.5	36.2
7R	26 Mar	2155	359.6–369.3	9.7	3.3	34.0
8R	26 Mar	2255	369.3–378.9	9.6	3.8	39.3
9R	27 Mar	0000	378.9–388.5	9.6	3.8	39.9
10R	27 Mar	0045	388.5–398.1	9.6	3.6	37.8
11R	27 Mar	0125	398.1–407.7	9.6	3.5	36.5
12R	27 Mar	0220	407.7–417.4	9.7	4.5	45.9
13R	27 Mar	0315	417.4–427.0	9.6	3.5	36.2
14R	27 Mar	0410	427.0–436.7	9.7	4.0	41.0
15R	27 Mar	0455	436.7–446.3	9.6	6.5	67.8
16R	27 Mar	0610	446.3–455.9	9.6	3.8	39.9
17R	27 Mar	0745	455.9–465.5	9.6	8.4	87.1
18R	27 Mar	1025	465.5–475.2	9.7	7.0	71.6
19R	27 Mar	1215	475.2–484.8	9.6	7.4	76.5
20R	27 Mar	1355	484.8–494.4	9.6	2.7	28.0
21R	27 Mar	1555	494.4–504.1	9.7	7.1	73.4
22R	27 Mar	1915	504.1–513.7	9.6	5.7	59.4
23R	27 Mar	2030	513.7–523.3	9.6	8.3	86.9
24R	27 Mar	2135	523.3–532.9	9.6	8.7	90.8
25R	27 Mar	2245	532.9–542.5	9.6	9.5	98.5
26R	27 Mar	2355	542.5–552.1	9.6	8.7	90.4
27R	28 Mar	0045	552.1–561.8	9.7	8.3	85.5
28R	28 Mar	0145	561.8–571.4	9.6	4.9	51.0
29R	28 Mar	0245	571.4–581.0	9.6	8.7	90.7
30R	28 Mar	0340	581.0–590.6	9.6	6.1	63.8
31R	28 Mar	0445	590.6–600.2	9.6	8.1	84.3
32R	28 Mar	0615	600.2–609.8	9.6	1.8	18.9
33R	28 Mar	0800	609.8–619.4	9.6	0.2	1.9
34R	28 Mar	0915	619.4–629.0	9.6	4.4	46.2
35R	28 Mar	1020	629.0–638.7	9.7	4.6	46.9
36R	28 Mar	1135	638.7–648.3	9.6	3.1	32.6
37R	28 Mar	1255	648.3–657.9	9.6	5.2	53.8
38R	28 Mar	1415	657.9–667.5	9.6	4.0	41.5
39R	28 Mar	1530	667.5–677.1	9.6	3.8	39.5
40R	28 Mar	1655	677.1–686.8	9.7	7.0	71.8
41R	28 Mar	1805	686.8–696.4	9.6	6.0	62.4
42R	28 Mar	1910	696.4–706.0	9.6	4.8	49.7
43R	28 Mar	2020	706.0–715.6	9.6	4.2	43.9
44R	28 Mar	2155	715.6–725.2	9.6	4.3	45.2
45R	28 Mar	2330	725.2–734.8	9.6	6.4	67.1
46R	29 Mar	0105	734.8–744.4	9.6	5.1	52.6
47R	29 Mar	0235	744.4–754.1	9.7	5.8	59.3
48R	29 Mar	0355	754.1–763.7	9.6	6.1	63.1
49R	29 Mar	0515	763.7–773.3	9.6	5.5	57.0
50R	29 Mar	0620	773.3–783.0	9.7	5.2	53.5
51R	29 Mar	0745	783.0–792.6	9.6	5.3	55.0
52R	29 Mar	0935	792.6–802.2	9.6	4.6	47.6
53R	29 Mar	1130	802.2–811.9	9.7	5.1	52.9
54R	29 Mar	1305	811.9–821.5	9.6	4.3	44.4
55R	30 Mar	0145	821.5–831.1	9.6	3.3	34.8
56R	30 Mar	0220	831.1–840.7	9.6	4.3	44.3
57R	30 Mar	0450	840.7–850.3	9.6	4.5	46.5
58R	30 Mar	0635	850.3–859.9	9.6	4.7	49.3
59R	30 Mar	0830	859.9–869.5	9.6	2.4	25.3
60R	30 Mar	1000	869.5–879.1	9.6	3.9	40.8
61R	30 Mar	1140	879.1–888.7	9.6	1.7	17.8
62R	30 Mar	1330	888.7–898.3	9.6	2.7	27.6
63R	30 Mar	1515	898.3–907.9	9.6	4.6	47.9
64R	30 Mar	1635	907.9–917.6	9.7	0.9	8.8
65R	30 Mar	1810	917.6–927.2	9.6	6.1	63.4
66R	30 Mar	1925	927.2–936.9	9.7	7.8	80.7
67R	30 Mar	2045	936.9–946.5	9.6	2.3	23.4
68R	30 Mar	2210	946.5–956.1	9.6	2.6	27.1
69R	30 Mar	2330	956.1–965.7	9.6	7.5	78.3
70R	31 Mar	0055	965.7–975.3	9.6	8.6	89.4
71R	31 Mar	0250	975.3–985.0	9.7	2.4	24.2
72R	31 Mar	0525	985.0–994.6	9.6	5.0	52.5
73R	31 Mar	0710	994.6–1004.3	9.7	8.2	84.2
74R	31 Mar	0945	1004.3–1013.9	9.6	7.2	74.7
75R	31 Mar	1255	1013.9–1023.5	9.6	8.2	85.3
76R	31 Mar	1520	1023.5–1033.1	9.6	5.1	53.3
77R	31 Mar	1710	1033.1–1042.8	9.7	1.3	13.3
78R	31 Mar	1955	1042.8–1052.4	9.6	8.5	88.3
79R	31 Mar	2150	1052.4–1062.1	9.7	6.5	66.7
80R	01 Apr	0040	1062.1–1071.7	9.6	8.4	87.7
81R	01 Apr	0245	1071.7–1081.3	9.6	8.1	84.4
82R	01 Apr	0435	1081.3–1091.0	9.7	3.7	38.1
83R	01 Apr	0650	1091.0–1100.6	9.6	9.0	93.6
84R	01 Apr	0945	1100.6–1110.3	9.7	9.5	97.9
85R	01 Apr	1250	1110.3–1119.9	9.6	9.5	98.4
86R	01 Apr	1515	1119.9–1129.5	9.6	6.4	66.3
87R	01 Apr	1740	1129.5–1139.2	9.7	5.9	60.4
88R	01 Apr	2020	1139.2–1148.8	9.6	7.6	79.4
89R	01 Apr	2235	1148.8–1158.4	9.6	8.7	90.6
90R	02 Apr	0110	1158.4–1168.1	9.7	8.9	91.5
91R	02 Apr	0405	1168.1–1177.7	9.6	7.7	80.5
92R	02 Apr	0645	1177.7–1187.3	9.6	6.0	62.8
93R	02 Apr	0925	1187.3–1196.9	9.6	3.6	37.9
94R	02 Apr	1135	1196.9–1206.5	9.6	2.7	28.3
95R	02 Apr	1335	1206.5–1216.1	9.6	2.4	25.3
96R	02 Apr	1515	1216.1–1225.8	9.7	3.5	35.5
97R	02 Apr	1705	1225.8–1235.4	9.6	2.9	30.2
Coring totals				933.4	503.3	53.9

Note: An expanded version of this coring summary table that includes lengths and depths of sections, location of whole-round samples, and comments on sampling disturbance is included on CD-ROM in the back pocket of this volume.

analyses. Most unit boundaries correspond to (1) inferred periods of reduced deposition, expressed as firmgrounds, (2) changes in sediment composition, and (3) inferred periods of increased platform input, expressed as turbidites. The degree of lithification of deposits changes downhole (Fig. 3). Unit I consists of unlithified, partially lithified, and lithified sediments, Unit II is composed of partially lithified to lithified sediments, and Units III through VIII consist of lithified sediments.

Description of Lithologic Units

Lithologic Unit I

Intervals: 166-1007A-1H; 166-1007B-1H through 22X
Age: Pleistocene to late Pliocene
Depth: 0–203.1 mbsf

Unit I consists of a sequence of nannofossil ooze and variably lithified wackestones to packstones. Smear-slide analyses indicate that aragonite needles (5–10 mm) are an important but variable component in the silt-sized fraction of Unit I (Fig. 4). The X-ray data are compatible with the smear-slide data, and show that the aragonite content of the sediments decreases markedly at the base of Unit I from a maximum of 70–80 wt% to less than 5 wt% (Fig. 4). In addition, color reflectance data show a strong positive covariance with aragonite content (Fig. 4). Throughout this unit, silt- to fine sand-sized peloids are the dominant allochem. The abrupt disappearance of peloids (Fig. 4), a sharp decrease in aragonite needle abundance, and a lithologic change to nannofossil chalk at the top of Core 166-1007B-23X defines the contact between Units I and II (Fig. 3).

Unit I is divided into four subunits (IA–ID) on the basis of composition and the distribution of firmgrounds, hardgrounds, and gravity-flow and/or current deposits. Subunit IA is a sequence of nannofossil ooze, unlithified wackestone, and packstone that is interrupted by gravity-flow deposits. The contact between Subunits IA and IB is defined at the base of a series of centimeter-thick grainstone layers in Section 166-1007B-2H-1, 139 cm. Subunit IB is characterized by meter-scale alternations between intervals of silt- and clay-rich sediments and intervals of silt- and clay-free sediments. The contact between Subunits IB and IC occurs at the top of the lowermost of two hardgrounds in Section 166-1007B-2H-1, 139 cm. Subunit IC encompasses a sequence of faintly laminated, unlithified peloidal wackestone to packstone. This sequence is interrupted by an interval of partially lithified foraminifer wackestone (Section 166-1007B-11X-2, 132 cm, through Core 166-1007B-14X) and a slumped interval containing beds of unlithified packstone to floatstone (Core 166-1007B-15X through Section 166-1007B-16X-3, 135 cm). The contact between Subunits IC and ID is defined by a change in degree of lithification that coincides with a firmground in Section 166-1007B-19X-1, 24 cm. Subunit ID consists of slightly dolomitized wackestone and packstone. The details of Subunits IA–ID are outlined below.

Subunit IA

Intervals: 166-1007A-1H; 166-1007B-1H through 2H-1, 139 cm.
Age: Pleistocene
Depth: 0–10.9 mbsf

Subunit IA consists of an upper sequence of monotonous, white to light gray nannofossil ooze (Sections 166-1007B-1H-1 through 1H-2, 40 cm) that changes downhole into a sequence of white to pale yellow unlithified foraminifer packstone, unlithified foraminifer wackestone, and foraminifer nannofossil ooze that is interrupted by 10- to 30-cm-thick turbidites and centimeter-thick grainstones (Sections 166-1007B-1H-2, 40 cm, through 2H-1, 139 cm). Throughout the lower part of Subunit IA, little textural or compositional difference exists between intervals classified as either unlithified wackestone, unlithified packstone, or foraminifer nannofossil ooze. For example, foraminifer nannofossil ooze with a grain-supported texture occurs in Section 166-1007A-1H-1, 0–45 cm, whereas grain-poor unlithified foraminifer wackestone occurs in Section 166-1007A-1H-1, 45–150 cm. The base of Subunit IA is defined at the base of the lowermost centimeter-thick grainstone layer in Section 166-1007B-2H-1, 139 cm, and by a downhole change in the character of the sediments at this point to meter-scale intervals of clay- and silt-rich sediments that alternate with intervals of clay- and silt-poor sediments (Fig. 3).

The upper part of Subunit IA is composed of white to light gray nannofossil ooze that is characterized by moderate bioturbation, which is visible as color mottling or as distinct burrows filled with fine-grained sediment or concentrations of silt- to fine sand-sized skeletal grains. Allochems are primarily silt- to fine sand-sized planktonic foraminifers, benthic foraminifers, and pteropods. Some planktonic foraminifers are blackened as a result of either pyritization or phosphatization. Minor components include peloids, echinoderm spines, coral fragments, lithoclasts, sponge spicules, and ostracodes.

White to pale yellow unlithified foraminifer packstone, unlithified foraminifer wackestone, and foraminifer nannofossil ooze that make up the lower part of Subunit IA contain abundant planktonic and benthic foraminifers, pteropods, echinoderm spines, peloids, and shell fragments. As in the upper part of this subunit, some planktonic foraminifers are blackened and commonly concentrated within small burrows. In Sections 166-1007B-1H-2 and 2H-1, 10- to 30-cm-thick turbidites occur. Each turbidite is marked by a sharp basal contact that is overlain by an unlithified bioclastic grainstone that grades upward into unlithified wackestone. Within each turbidite interval, the basal unlithified grainstone often contains fine to medium sand-sized neritic carbonate grains, including shell fragments and *Halimeda.* The dominant allochem in unlithified wackestone is silt to fine sand-sized planktonic foraminifers. In some cases, the tops of turbidite sequences are partially lithified. Five grain intervals are present in Section 166-1007B-2H-1, 90–139 cm. These intervals occur as centimeter-thick, grain-supported laminae within an otherwise monotonous sequence of foraminifer nannofossil ooze. The base of the lowermost of these laminae marks the base of Subunit IA (Section 166-1007B-2H-1, 139 cm).

Subunit IB

Intervals: 166-1007B-2H-1, 139 cm, through 5H-3, 56 cm
Age: Pleistocene
Depth: 10.9–43.5 mbsf

Subunit IB consists of a sequence of nannofossil ooze (Section 166-1007B-2H-1, 139 cm, through Core 166-1007B-3H) that grades downhole into unlithified mudstone and wackestone (Core 166-1007B-4H through Section 166-1007B-5H-3, 56 cm). Silt- to fine sand-sized planktonic foraminifers are the dominant allochem in the nannofossil ooze, whereas silt- to fine sand-sized peloids are the primary components in unlithified mudstone and wackestone. Benthic foraminifers, pteropods, peloids, echinoderm spines, sponge spicules, and lithoclasts occur throughout the entire subunit in relatively minor amounts. Some grains are pyritized and appear blackened. Bioturbation is pervasive and decreases in intensity downhole. Bioturbation is visible as (1) indistinct color mottling; (2) round, structureless burrows filled with unlithified to partially lithified, fine-grained sediment or concentrations of skeletal material; and (3) concentrations of pyritized grains. Subunit IB is characterized by a cyclicity, manifest as an alternation between meter-scale intervals of light-colored, clay- and silt-poor sediment and intervals of dark-colored, clay- and silt-rich sediment. The base of Subunit IB is defined at the top of the lowermost of two hardgrounds that occurs in Section 166-1007B-5H-3, 56 cm, and by the disappearance of meter-scale cycles (Fig. 3).

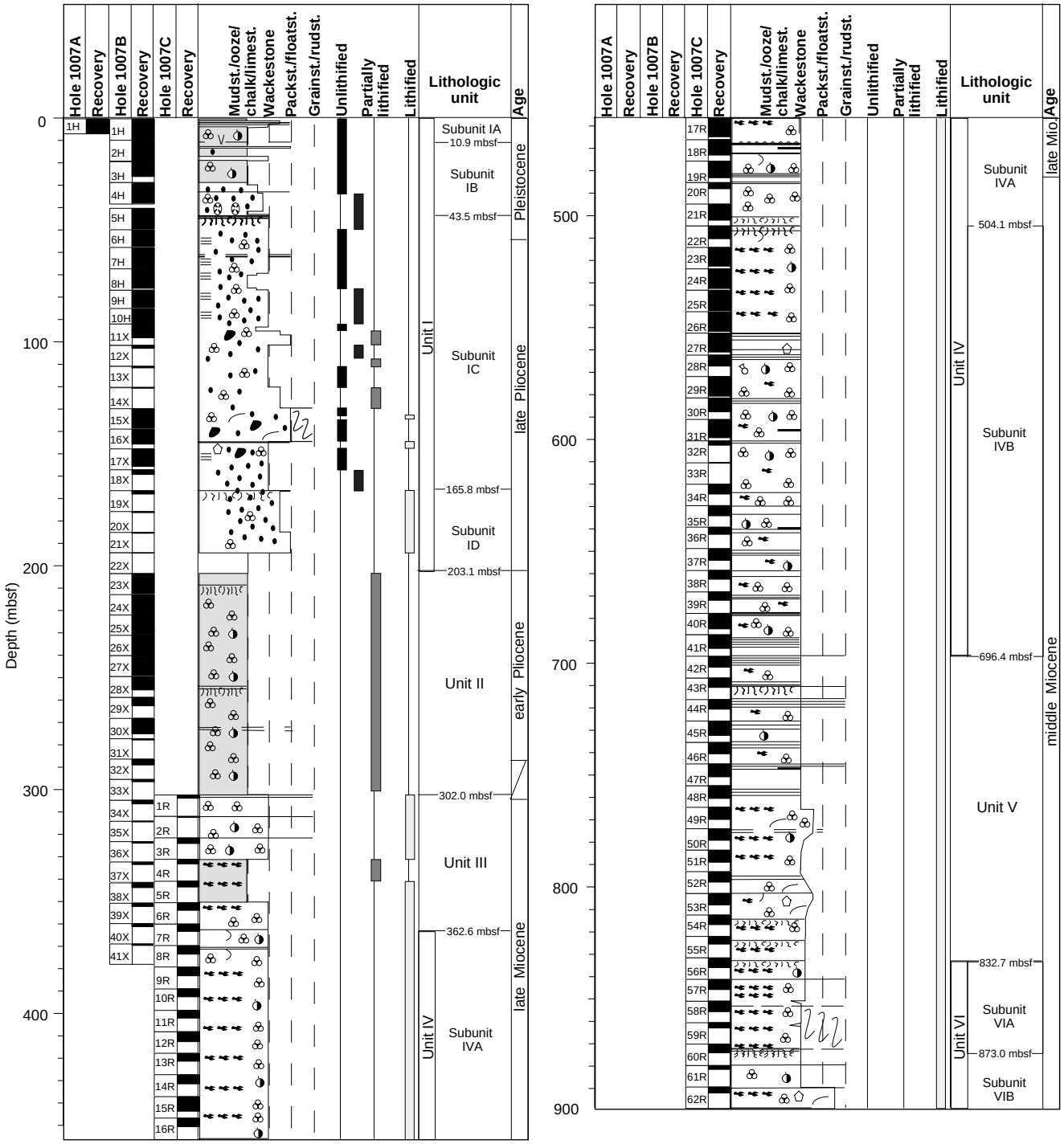

Figure 3. Synthesis of the dominant textures and components of the sedimentary succession at Site 1007.

In the upper part of Subunit IB (Section 166-1007B-2H-1, 139 cm, through Core 166-1007B-3H), light olive brown, silty peloidal wackestone alternates with white nannofossil ooze. Contacts between these lithologies are in all cases gradational. Smear-slide analyses indicate that olive brown wackestones contain as much as 30% silt and clay. The contrast in color and amount of silt and/or clay between the upper and lower parts of cycles decreases downhole from Core 166-1007B-2H through 3H, such that only slight differences are observed in Core 166-1007B-3H. In the lower part of Subunit IB (Core 166-1007B-4H through Section 166-1007B-5H-3, 56 cm), clay- and silt-poor sediment alternates with gray, clay- and silt-rich, unlithified mudstone. The gray mudstone is intensely bioturbated, such that it is difficult to determine the nature of transitions into clay- and silt-poor sediment. Clay- and silt-rich intervals in Core 166-1007B-4H are relatively thin and thicken downhole through the base of Subunit IB. Section 166-1007B-5H-1, 85 cm, to 5H-2, 81 cm, contains skeletal debris, including large fragments of coral (*Acroporidae*) and red algae.

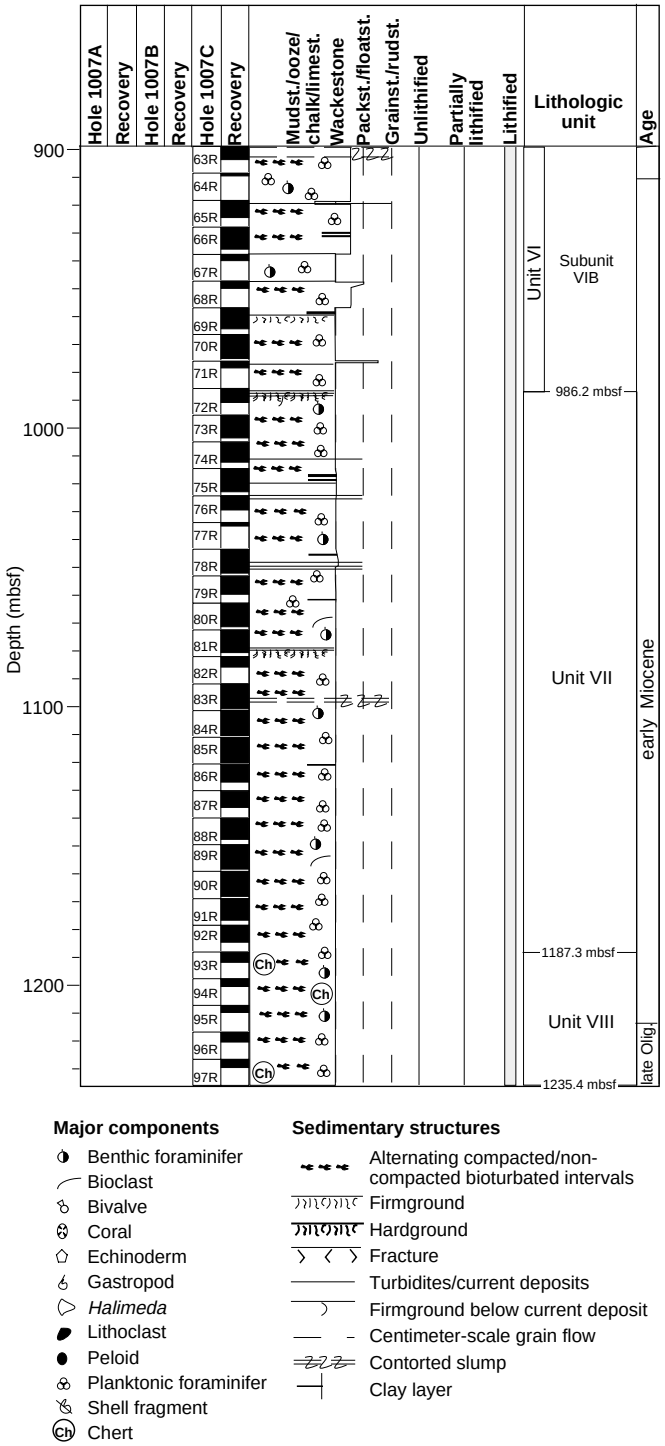

Figure 3 (continued).

Subunit IC

Interval: 166-1007B-5H-3, 56 cm, through 19X-1, 24 cm
Age: Pleistocene to late Pliocene
Depth: 43.5–165.8 mbsf

Subunit IC consists of peloid-rich, unlithified biowackestone in Sections 166-1007B-5H-3, 56 cm, through 5H-CC, 37 cm, which grades downhole into faintly laminated, pale yellow to white, unlithified peloidal wackestone to packstone. The sequence of laminated peloidal wackestone to packstone is interrupted by (1) partially lithified foraminifer wackestone in Section 166-1007B-11X-2, 132 cm, through Core 166-1007B-14X, and (2) a slumped interval in Core 166-1007B-15X through Section 166-1007B-16X-3, 135 cm. The base of Subunit IC is defined by the presence of a firmground that coincides with a change in degree of lithification in Section 166-1007B-19X-1, 24 cm (Fig. 3).

Throughout Subunit IC, silt to fine sand-sized peloids are the dominant component. With the exception of the interval of partially lithified foraminifer wackestone (Section 166-1007B-11X-2, 132 cm, through Core 166-1007B-14X), planktonic and benthic foraminifers are rare and poorly preserved. The entire subunit appears mottled as a result of bioturbation. Bioturbation obscures primary, centimeter-scale laminae of centimeter-scale alternations of yellowish, grain-supported sediment and whitish, mud-supported sediment. Compositional variation in the clay- to silt-size fraction in the color laminae is minimal, although qualitative smear-slide analyses suggest that whitish layers contain relatively higher proportions of calcareous nannofossils and clay, whereas yellowish, grain-rich laminae contain a higher proportion of aragonite needles. The grain-supported laminae and centimeter-scale, partially lithified layers containing abundant skeletal fragments in Section 166-1007B-7H-3 (10, 99, and 131 cm) are indicative of redeposition. Such features could represent winnowed current deposits.

Recovery in the interval containing gray, partially lithified, foraminifer wackestone (Section 166-1007B-11X-2, 132 cm, through Core 166-1007B-14X) was poor. Dominant allochems are silt- to fine sand-sized planktonic foraminifers, some of which are filled with pyrite and/or glauconite. Other components include benthic foraminifers, peloids, echinoderm spines, fish debris, and unidentifiable blackened grains.

The slumped interval (Cores 166-1007B-15X through Section 166-1007B-16X-3, 135 cm) contains highly contorted interbeds of gray unlithified foraminifer lithoclastic packstone to floatstone with laminated, pale yellow to white, unlithified peloidal wackestone to packstone. Gray unlithified packstone to floatstone contains lithoclasts (up to 1 cm in diameter), benthic foraminifers, shell fragments, and blackened grains. A lithified interval of packstone to floatstone occurs in interval 166-1007B-16X-3, 64–90 cm. Thin-section analysis (Sample 166-1007B-16X-3, 82–84 cm) shows that, although fine sand-sized planktonic foraminifers are the dominant allochem within the packstone to floatstone, echinoderm debris, micritized bioclasts, fish remains, and shell fragments are also present. Many grains are broken, filled with sediment, or micritized, suggesting that they were reworked. This interval is underlain by two graded turbidites with sharp basal contacts (intervals 166-1007B-16X-6, 61–114 and 114–150 cm). Unlithified to partially lithified packstone to floatstone, which composes the lower part of the turbidites, contains lithoclasts, coral debris, and benthic foraminifers. These intervals are underlain by gray, unlithified packstone to floatstone and pale yellow, unlithified peloidal wackestone to floatstone, which continue downhole into Section 166-1007B-17X-2, 100 cm. The lowermost part of Subunit IC consists primarily of laminated, unlithified peloidal wackestone to packstone. Toward the base of this subunit (interval 166-1007B-17X-4, 90–135 cm), faint, centimeter-scale color laminations disappear and particle abundance increases gradually downsection to the top of Subunit ID. Thin-section analysis of a bioclastic packstone that occurs in Sample 166-1007B-17X-CC, 28–33 cm, shows that this interval contains many reworked skeletal grains and minor fine sand-sized quartz grains and rock fragments.

Subunit ID

Intervals: 166-1007B-19X-1, 24 cm, through 166-1007B-22X
Age: late Pliocene
Depth: 165.8–203.1 mbsf

Subunit ID consists of a succession of slightly dolomitized wackestone to packstone. Dominant allochems are silt-sized peloids and

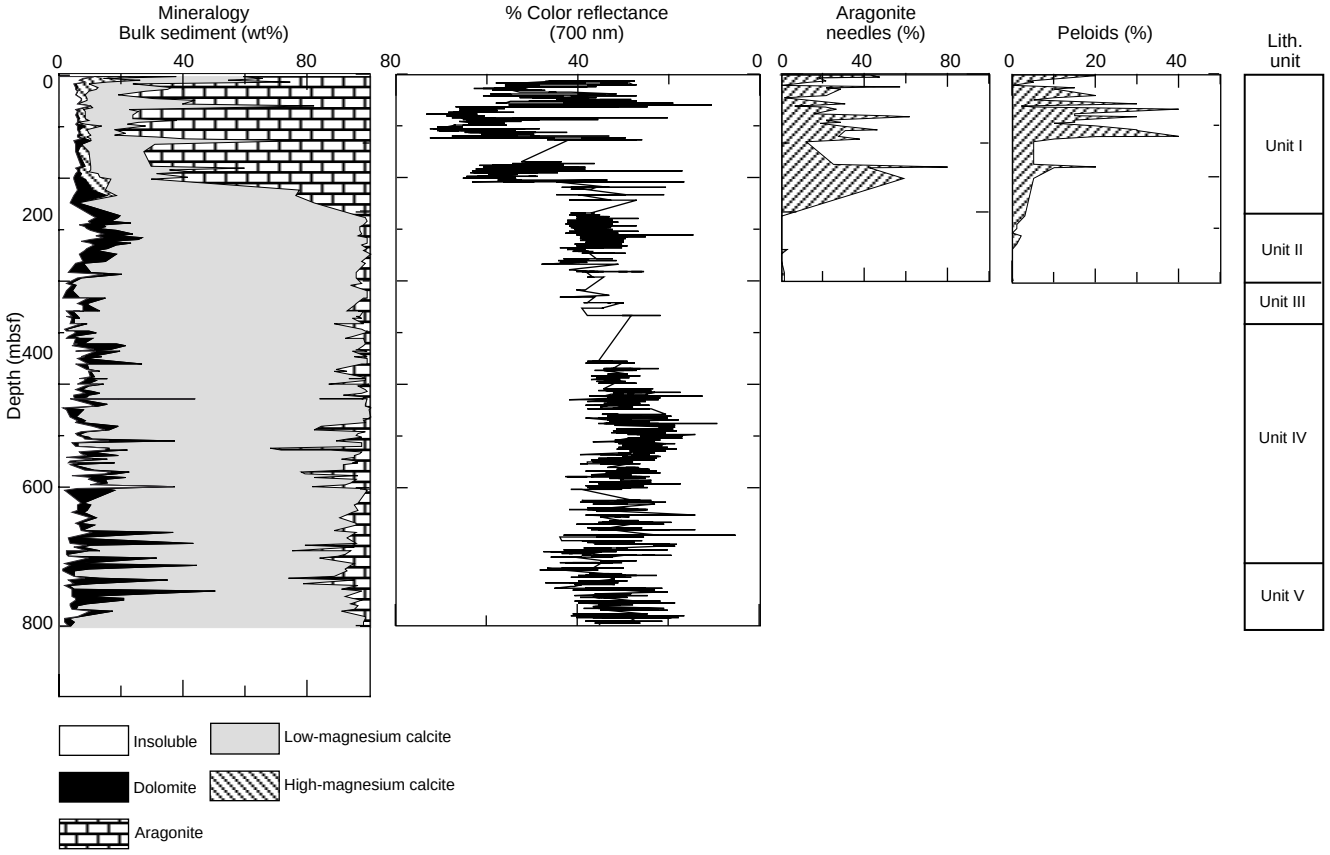

Figure 4. Comparison of mineralogy and color reflectance data with smear-slide estimates of aragonite needles and peloids vs. depth in sediments at Site 1007.

silt- to fine sand-sized planktonic foraminifers. The entire subunit is slightly to moderately bioturbated. Bioturbation is visible as round, structureless burrows (up to 1 cm in diameter) that are filled with peloidal packstone. Molds of bioclasts occur in the lowermost part of this interval (Cores 166-1007B-20X and 21X). The base of Subunit ID is defined by the disappearance of peloids at the top of Core 166-1007B-23X (Fig. 3).

Lithologic Unit II

Intervals: 166-1007B-23X through 33X
Age: early Pliocene
Depth: 203.1–302.0 mbsf

Unit II consists entirely of light gray to pale yellow foraminifer nannofossil chalk. Silt- to fine sand-sized planktonic foraminifers are the dominant allochem. Minor components include fine sand-sized benthic foraminifers, echinoderm spines, and occasional shell fragments. Some grains are pyritized. Throughout Unit II, sediments are pervasively bioturbated. Bioturbation occurs as (1) color mottles, (2) round, structureless burrows filled with fine-grained sediment or concentrations of skeletal material, (3) *Zoophycos*-type burrows, and (4) *Chondrites*-type burrows.

Compositional and textural variation within Unit II is minor. Sediments are marked only by alternating intervals of higher and lower grain abundance. Pyritized foraminifers, which are scattered throughout this unit, are more concentrated in intervals with higher grain abundance. The base of Unit II is defined at the top of the first of a series of coarse-grained turbidites that occur in Section 166-1007C-1R-1 (Fig. 3).

Lithologic Unit III

Intervals: 166-1007B-34X through 39X; 166-1007C-1R through 7R-2, 134 cm
Age: late Miocene
Depth: 302.0–362.6 mbsf

Unit III consists of a succession of light gray to light olive gray foraminifer wackestone, foraminifer nannofossil chalk, and nannofossil limestone. The upper part of Unit III (Sections 166-1007C-1R-1 through 3R-1, 40 cm) contains a series of coarse-grained turbidites. These turbidites typically have sharp, scoured basal contacts, which are overlain by poorly sorted, bioclastic packstones/floatstones to grainstones/rudstones that grade upward to foraminifer wackestones. In some cases, rip-up clasts from the underlying lithology occur within the basal packstone/floatstone to grainstone/rudstone (Fig. 5). Other components include blackened lithoclasts, shell fragments, benthic foraminifers, and planktonic foraminifers. In the foraminifer wackestone, foraminifer nannofossil chalk, and nannofossil limestone, which make up the bulk of Unit III, silt- to fine sand-sized planktonic foraminifers are the dominant allochems. Minor allochems include benthic foraminifers, echinoderm spines, and bioclasts. Some grains are pyritized and concentrated within small burrows. The background sediment of Unit III is, thus, a typical section of periplatform ooze, sensu Schlager and James (1978). Pervasive slight to moderate bioturbation appears as undefined color mottles, or as distinct burrows filled with whitish, grayish, and brownish sediment. The base of Unit III is defined at the top of a series of sharp-based intervals of fine-grained, laminated packstone in Section 166-1007C-7R-2, 134 cm (Fig. 3).

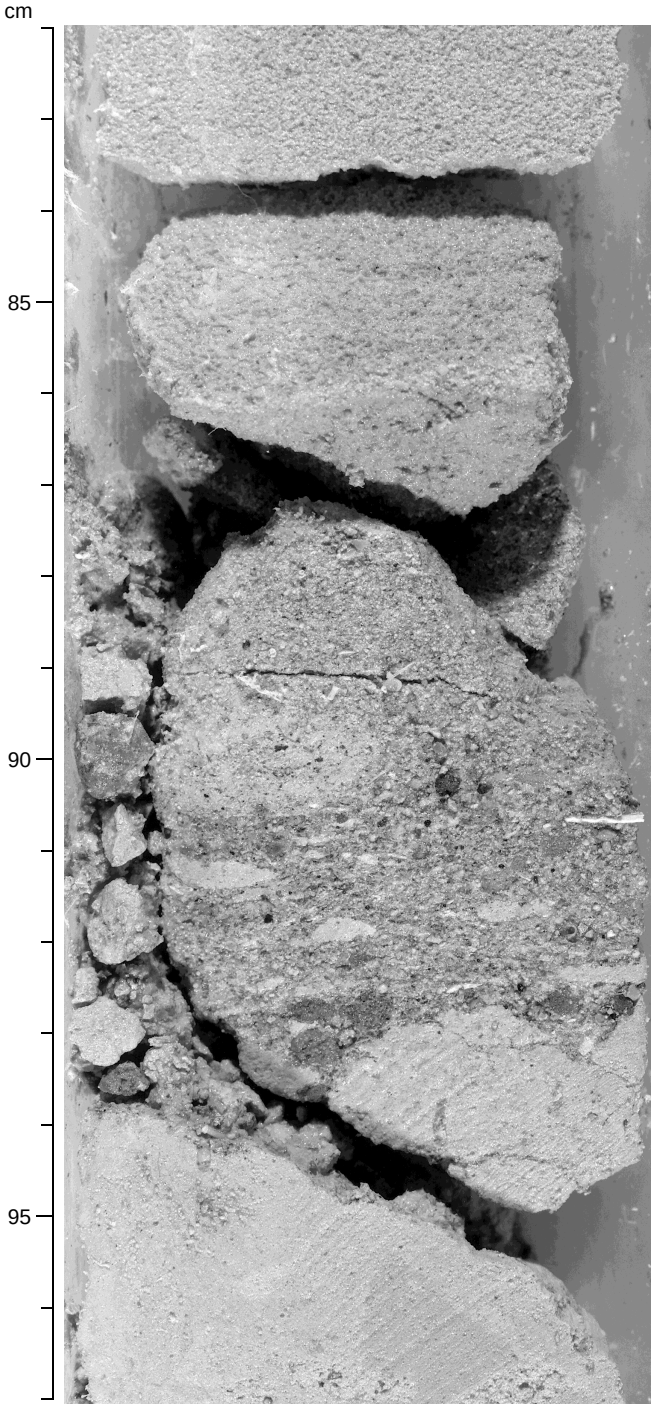

Figure 5. Detail of a turbidite that occurs in the upper part of Unit III in interval 166-1007C-1R-1, 82–97 cm. The basal contact is scoured and overlain by poorly sorted, bioclastic packstone/floatstone to grainstone/rudstone that grades upward to foraminifer wackestones. Note the occurrence of dark, rounded lithoclasts and light-colored rip-up clasts from the underlying lithology between 89 and 93 cm.

Lithologic Unit IV

Interval: 166-1007C-7R-2, 134 cm, through 43R-3, 50 cm
Age: late to middle Miocene
Depth: 362.6–696.4 mbsf

Unit IV consists of a sequence of light gray, gray, and olive gray foraminifer wackestone. Dominant allochems are silt- to sand-sized planktonic foraminifers. Minor components are benthic foraminifers, shell fragments, echinoderm spines, and micritized bioclasts. This unit is characterized by (1) the occurrence of 5- to 10-cm-scale intervals of yellowish, fine-grained packstone with millimeter-scale planar laminations (Fig. 6), and (2) an alternation between decimeter- to meter-scale intervals of densely cemented sediment with intervals of weakly cemented sediment that show evidence of compaction. The entire unit has been bioturbated to such a degree that other primary sedimentary structures are obscured. Bioturbation appears as (1) color mottling, (2) round, structureless burrows up to 3 cm in diameter and 50 cm in length, and (3) *Chondrites*-type burrows (in Subunit IVB). Celestite-filled fractures occur sporadically throughout Unit IV. The largest of these, which ranges up to 1 cm in width, occurs in Section 166-1007C-39R-2, 12–24 cm.

Unit IV is divided into two subunits on the basis of a series of firmgrounds and a hardground that occurs in Section 166-1007C-22R-1, 25 cm, and a subsequent downhole change in the character of the sediments. Above this contact, sediments show distinct alternations in color, and intervals of laminated packstone are relatively rare (or poorly preserved because of bioturbation). Below the lowermost firmground, color variation is minimal, and the occurrence of 5- to 10-cm-scale intervals of laminated packstones increases. The base of Unit IV is defined at the top of a series of turbidites in Section 166-1007C-42R-1, 0 cm (Fig. 3).

Subunit IVA

Interval: 166-1007C-7R-2, 134 cm, through 22R-1, 25 cm
Age: late to middle Miocene
Depth: 362.6–504.1

Subunit IVA consists primarily of light gray to gray foraminifer wackestone. Dominant allochems are silt- to sand-sized planktonic foraminifers. Minor components include benthic foraminifers, shell fragments, echinoderm spines, and micritized bioclasts. Some grains are pyritized. The silt- to clay-sized fraction consists of subequal proportions of micrite and nannofossils. Throughout Subunit IVA, aragonite needles constitute a very minor proportion of matrix constituents (<5%). The base of Subunit IVA is defined at the top of a hardground that occurs in Section 166-1007C-22R-1, 25 cm.

Cores 166-1007C-7R, 8R, 19R, and 20R contain 5- to 10-cm-scale layers of yellowish, fine-grained packstone with millimeter-scale planar lamination. Each of these layers is marked by a sharp basal contact and a gradational upper contact into foraminifer wackestone. Although sediments throughout the rest of Subunit IVA are generally uniform in appearance, several features suggest the presence of primary sedimentary structures that have been overprinted by bioturbation. Small lensoids of yellowish, grain-supported material occur scattered throughout this interval, which could represent the bioturbated remnants of planar-laminated intervals, small-scale gravity flow deposits, or winnowed layers of redeposited carbonate material. In Section 166-1007C-9R-3, 86 cm, a sharp contact occurs in association with distinctly neritic carbonate grains (*Halimeda*, serpulids, and bivalves). Section 166-1007C-18R, 50–75 cm, comprises a section of bioturbated, grain-supported sediments that are underlain by rotated beds. This interval may represent a slump block that is overlain by a fine-grained turbidite. A dark gray claystone occurs beneath this interval in Section 166-1007C-18R-3, 41–57 cm.

Subunit IVA sediments display gradual downhole trends in color, cementation, and compaction. Cores 166-1007C-7R through 10R are generally uniform in color and degrees of compaction and cementation. Beginning with Core 166-1007C-11R, Subunit IVA sediments are marked by alternating, decimeter- to meter-scale intervals of darker and lighter color. In Cores 166-1007C-11R through 14R, darker intervals are characterized by weak cementation and by an orientation of burrows and the long axes of grains parallel to bedding. In

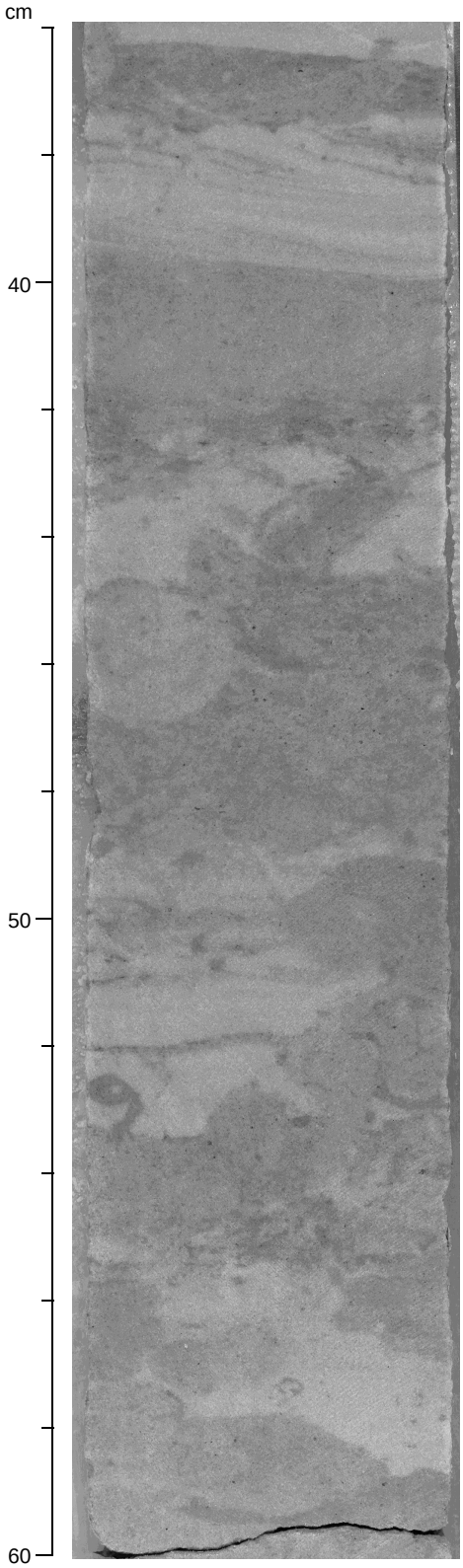

Figure 6. Detail of yellowish, fine-grained packstone with millimeter-scale planar laminae in interval 166-1007C-40R-1, 36–60 cm. Bioturbation partially obscures some laminated intervals (e.g., 50–53.5 cm).

lighter intervals, sediments are densely cemented and show no evidence of compaction; furthermore, the color contrast between burrow fill and the surrounding sediment is low. Cores 166-1007C-15R through 22R are characterized by stronger variations in color, cementation, and degree of compaction. Within these cores, darker intervals are strongly compacted, such that burrows are flattened and elongated parallel to bedding. Lighter intervals are identical to those in Cores 166-1007C-11R through 14R. Contacts between dark- and light-colored intervals are gradational in Cores 166-1007C-15R and 16R. In Cores 166-1007C-17R through 22R, gradational contacts separate dark intervals from overlying light intervals, whereas contacts between light intervals and overlying dark intervals are sharp.

Subunit IVB

Interval: 166-1007C-22R-1, 25 cm, through 42R-1, 0 cm
Age: middle Miocene
Depth: 504.1–696.4

Subunit IVB consists primarily of light gray, gray, and olive gray foraminifer wackestone, which contains 5- to 10-cm-scale layers of yellowish, fine-grained packstone with millimeter-scale planar laminae (Fig. 6). Some laminated packstones are bioturbated. The thickness and occurrence of these layers increase markedly in Cores 166-1007C-39R through 43R. Thin-section analysis shows that yellowish packstones are densely cemented and contain well-sorted, silt- to fine sand-sized phosphatic fish debris and a variety of micritized, replaced, and/or recrystallized carbonate skeletal fragments (Samples 166-1007C-30R-3, 57–59 cm, and 40R-1, 35–57 cm). Some spar-filled micritic envelopes were also observed.

Like Subunit IVA, Subunit IVB is made up of alternating, decimeter- to meter-scale intervals of densely and weakly cemented sediment. Two of the weakly cemented, compacted intervals are especially clay-rich and black in color (intervals 166-1007C-31R-5, 25–37 cm, and 36R-1, 7–10 cm). Subunit IVB sediments generally lack the sharp variations in color characteristic of sediments in Subunit IVA, but they are otherwise identical compositionally and texturally. The base of Subunit IVB occurs at the top of a series of turbidites in Section 166-1007C-42R-1, 0 cm.

Lithologic Unit V

Interval: 166-1007C-42R-1, 0 cm, through 56R-2, 29 cm
Age: middle Miocene
Depth: 696.4–832.7 mbsf

Unit V consists primarily of a sequence of light gray to light brownish or olive gray foraminifer wackestone with minor intervals of packstone and mudstone. Throughout this unit, silt- to sand-sized planktonic foraminifers are the dominant allochem. Although benthic foraminifers, bioclasts, and shell fragments occur in relatively minor amounts, they are more abundant than in Units III and IV. Pyritized grains are scattered throughout the interval. The entire unit is moderately to intensely bioturbated and occurs as described in Unit IV.

The upper part of Unit V contains a series of decimeter-scale turbidites (Section 166-1007C-42R-1 through Core 166-1007C-44R). Basal contacts are sharp and often scoured or rippled. These contacts are overlain by bioclastic packstone to grainstone/rudstone that grade upward to bioclastic foraminifer wackestone (Fig. 7). The lower parts of these layers typically show planar lamination. A firmground occurs within this turbidite sequence in Section 166-1007C-43R-3, 50 cm (Fig. 8). Within the turbidites below this firmground, there is a general downsection increase in (1) the thickness of laminated intervals within each turbidite, (2) the thickness of individual planar laminae, and (3) the grain size.

The remainder of Unit V (Core 166-1007C-45R through Section 166-1007C-56R-2, 29 cm) is characterized by an alternation of decimeter- to meter-scale, light- and dark-colored intervals. As in Unit

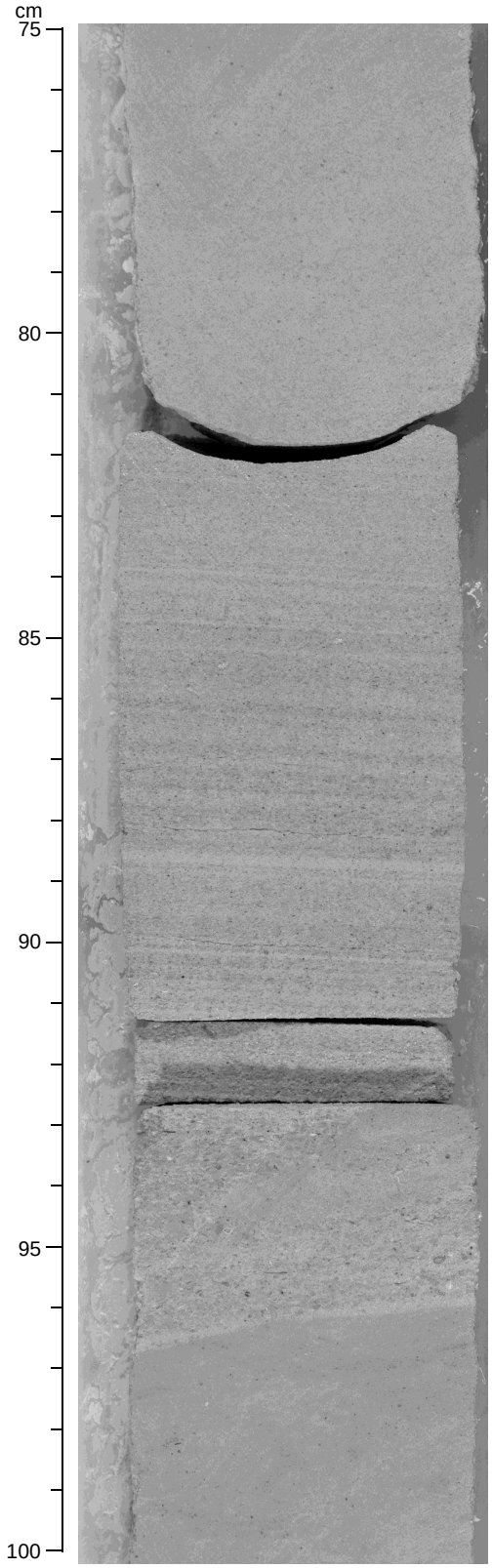

Figure 7. Detail of a decimeter-scale turbidite in interval 166-1007C-44R-1, 75–100 cm. The basal contact is sharp and overlain by bioclastic packstone to grainstone/rudstone that grades upward to bioclastic foraminifer wackestone. The lower and middle part of this sequence shows planar lamination (82–96 cm).

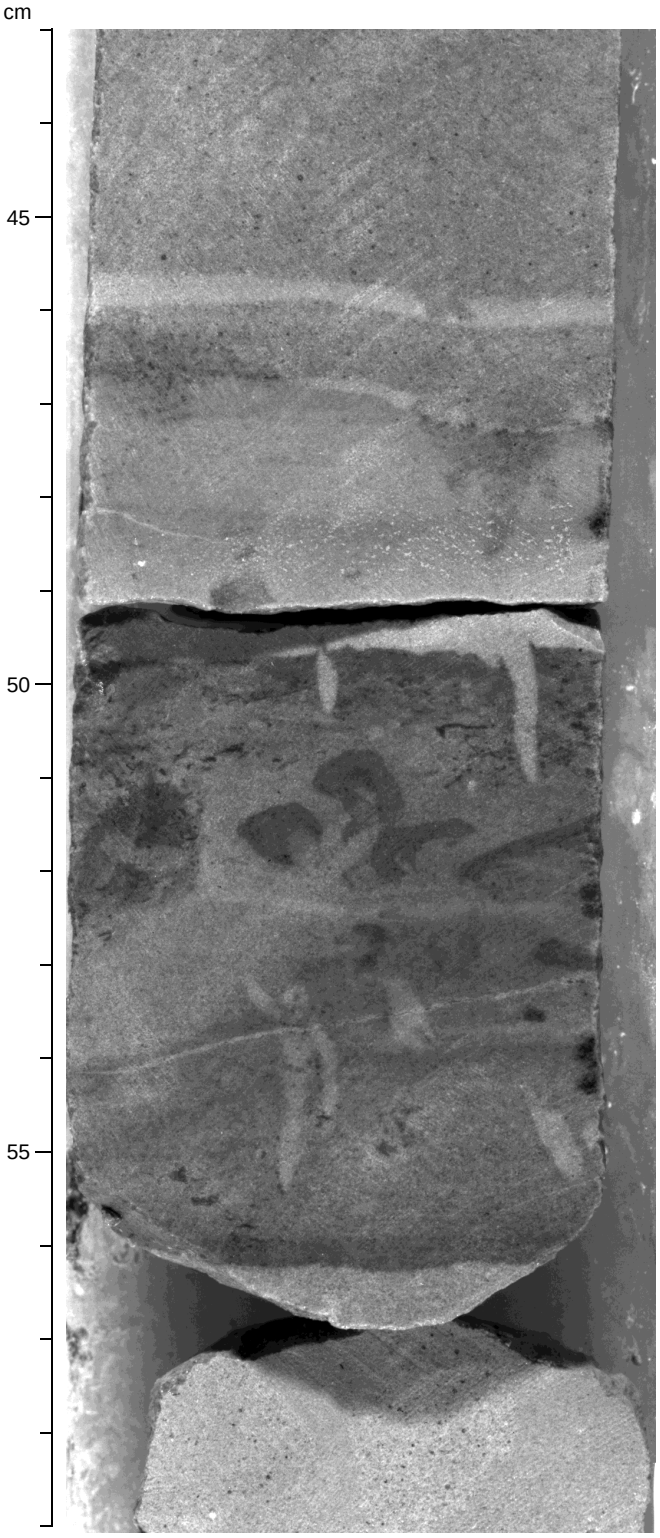

Figure 8. Detail of a firmground (interval 166-1007C-43R-3, 43–59 cm) that occurs within a sequence of turbidites in the upper part of Unit V.

IV, light-colored intervals are densely cemented and show little to no evidence of compaction. Darker intervals are weakly cemented and show evidence of compaction, including a flattening and elongation of burrows parallel to bedding, and a draping of primary sedimentary laminae around compacted burrows. In addition, thin-section analysis of a dark interval in 166-1007C-52R-2, 139–140 cm, suggests that (1) the long axes of grains tend to be oriented parallel to bedding; (2) some foraminifer tests and skeletal grains are compacted and broken; and (3) primary sediment laminae are draped around skeletal grains. Throughout Unit V, dark intervals often contain centimeter-scale, bioturbated layers or discontinuous lensoids of yellowish bioclastic packstone. Some of these layers show a faint parallel lamination. The base of Unit V occurs at the top of a firmground in Section 166-1007C-56R-2, 29 cm (Fig. 3).

Lithologic Unit VI

Interval: 166-1007C-56R-2, 29 cm, through 72R-2, 85 cm
Age: middle to early Miocene
Depth: 832.7–986.2 mbsf

Unit VI consists of a succession of light gray to light olive or brownish gray foraminifer wackestone with minor intervals of fine-grained bioclastic packstone and wackestone. Throughout this unit, silt- to sand-sized planktonic foraminifers are the dominant allochem. Toward the base of Unit VI, the sizes and sorting of the planktonic foraminifers generally become more variable, with grain sizes ranging from silt up to medium sand. Although benthic foraminifers, bioclasts, echinoderm debris, and shell fragments occur in minor amounts throughout Unit VI, they are most abundant in the bioclastic wackestone and packstone. Unit VI sediments are moderately to intensely bioturbated. Bioturbation is visible as (1) described above, and (2) as discrete *Zoophycos*-type burrows. The entire interval is characterized by an alternation between decimeter- to meter-scale intervals of light-colored, densely cemented sediment with decimeter-scale intervals of weakly cemented, dark-colored sediment that shows evidence of compaction.

Unit VI is divided into Subunits VIA and VIB on the basis of a series of firmgrounds in Section 166-1007C-60R, 92 cm, and the occurrence of thin, clay-rich layers below this interval. The contact between Subunits VIA and VIB is defined at the base of these firmgrounds (Section 166-1007C-60R-3, 92 cm). The base of Unit VI occurs at the base of another series of firmgrounds in Section 166-1007C-72R-2, 85 cm.

Subunit VIA

Interval: 166-1007C-56R-2, 29 cm, through 60R-3, 92 cm
Age: middle Miocene
Depth: 832.7–873.0 mbsf

Subunit VIA is characterized by an alternation of decimeter- to meter-scale, light-colored intervals and decimeter-scale, dark-colored intervals. As in Units IV and V, the light intervals are densely cemented and show little evidence of compaction, whereas the darker intervals are weakly cemented and show compaction features.

Sections 166-1007C-58R-2 through 59R-2, 107 cm, contain intervals of contorted bedding. This entire interval is interpreted to represent a slump deposit. A series of firmgrounds that occur below this slumped interval defines the base of Subunit VIA (Section 166-1007C-60R-3, 92 cm).

Subunit VIB

Interval: 166-1007C-60R-3, 92 cm, through 72R-2, 85 cm
Age: middle to early Miocene
Depth: 873.0–986.2 mbsf

The foraminifer wackestone sequence that composes Subunit VIB contains (1) isolated, fine-grained turbidite deposits in intervals 166-

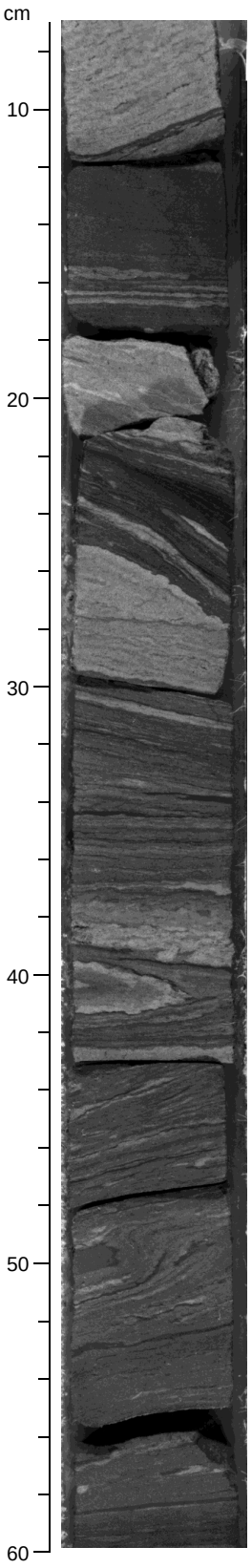

Figure 9. Section within the slumped interval 166-1007C-63R-1, 0 cm, through 63R-2, 108 cm (interval shown 166-1007C-63R-1, 7–60 cm). The composition of the slump is similar to the surrounding sediment, indicating a local source for the slump mass.

1007C-62R-1, 0–79 cm, and 65R-2, 0–36 cm; (2) a slumped interval (Fig. 9), identical to that noted in Subunit VIA, in Sections 166-1007C-63R-1, 0 cm, through 63R-2, 108 cm; and (3) thin intervals of dark, clay-rich nannofossil chalk in intervals 166-1007C-66R-2, 25–50 cm, 66R-3, 7–10 cm, and 69R-2, 11–13 cm. Beginning in Core 166-1007C-67R and continuing downhole through the base of Unit VI, sediments appear more crystalline. The base of Subunit VIB is defined at the base of a series of firmgrounds in Section 166-1007C-72R-2, 85 cm (Fig. 3).

Lithologic Unit VII

Interval: 166-1007C-72R-2, 85 cm, through 166-1007C-92R
Age: early Miocene
Depth: 986.2–1187.3 mbsf

Unit VII consists of a sequence of foraminifer wackestone with minor intervals of mudstone and foraminifer wackestone to packstone. Dominant allochems are fine to medium sand-sized planktonic foraminifers. Minor components include benthic foraminifers and skeletal fragments. Some grains are blackened. Disseminated pyrite crystals occur throughout Unit VII, but they are especially prevalent in Cores 166-1007C-75R through 93R. Moderate to intense bioturbation is pervasive and occurs as described above. The base of Unit VII is defined at the top of Core 166-1007C-93R on the basis of a change in sediment color, a decrease in grain abundance and grain size, and the occurrence of black chert nodules (Fig. 3).

Unit VII is also characterized by an alternation between well-cemented, decimeter- to meter-scale, light-colored intervals and decimeter-scale, dark-colored intervals that show evidence of compaction. There is a general downhole trend in the degree of compaction in the dark intervals and in the style of diagenetic alteration. The upper and lower contacts of the dark intervals show a downhole change from gradual to sharp, in which the bases of the dark intervals become sharp at slightly shallower depths than do the upper contacts. Beginning in Core 166-1007C-86R and continuing to the bottom of Unit VII, the lower parts of the dark intervals are cut by anastomosing or wispy solution seams (Fig. 10). In Core 166-1007C-77R, burrows are outlined by white reaction rims or halos up to 2 mm thick (Fig. 11). The intensity and thickness of the rims increase downhole through Core 166-1007C-82R, and decrease again downsection toward the base of Unit VII.

The foraminifer wackestones that comprise Unit VII contain numerous turbidites and clay-rich layers. Turbidites occur in Section 166-1007C-74R-6, 38 cm; in Sections 166-1007C-76R-1 through 76R-2, 19 cm; and in Sections 166-1007C-78R-4, 49 and 121 cm, and 78R-5, 83 cm. Components include planktonic foraminifers and bioclasts, some of which are blackened. The upper parts of these turbidites are dark and typically show evidence of postdepositional compaction. Some dark intervals in Subunit VIIB grade downward into soft, clay-rich sediment that contains abundant organic matter (see "Organic Geochemistry" section, this chapter). Such sediment occurs in intervals 166-1007C-75R-1, 30–62 cm; 75R-2, 72–90 cm; 78R-2, 8–18 cm; and 80R-3, 0–21 cm. The lowermost part of the interval 166-1007C-75R-1, 30–62 cm, contains an especially high amount of organic matter, as evidenced by a high fluorescence under UV light. A slumped interval occurs in Section 166-1007C-83R-4.

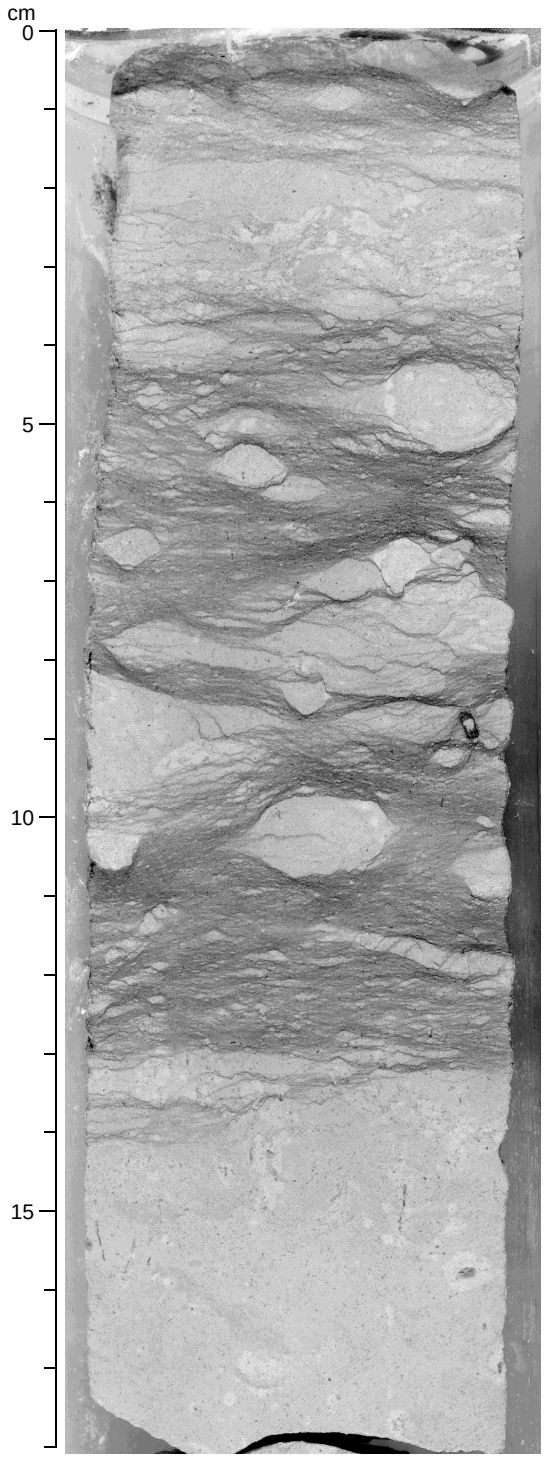

Figure 10. Anastomosing or wispy solution seams within a dark interval in Unit VII (interval 166-1007C-87R-3, 0–18 cm). Solution seams first occur in Core 166-1007C-86R and increase in intensity to the bottom of the hole.

Lithologic Unit VIII

Interval: 166-1007C-93R through 97R
Age: early Miocene to late Oligocene
Depth: 1187.3–1235.4

Unit VIII consists of pale yellow and light gray foraminifer wackestone and bioclastic wackestone. Primary allochems are fine sand-sized planktonic and benthic foraminifers, shell fragments, and bioclasts. Blackened (glauconized) grains, disseminated pyrite, and disseminated organic matter occur throughout this interval. Black chert nodules occur in intervals 166-1007C-93R-2, 44–49 cm; 94R-4, 110–118 cm; and 97R-2, 13–17 cm. Moderate to intense bioturbation is pervasive, and visible as indistinct, round, structureless burrows or as faint color mottles.

Unit VIII is characterized by an alternation of decimeter- to meter-scale, light- and dark-colored intervals that are generally sim-

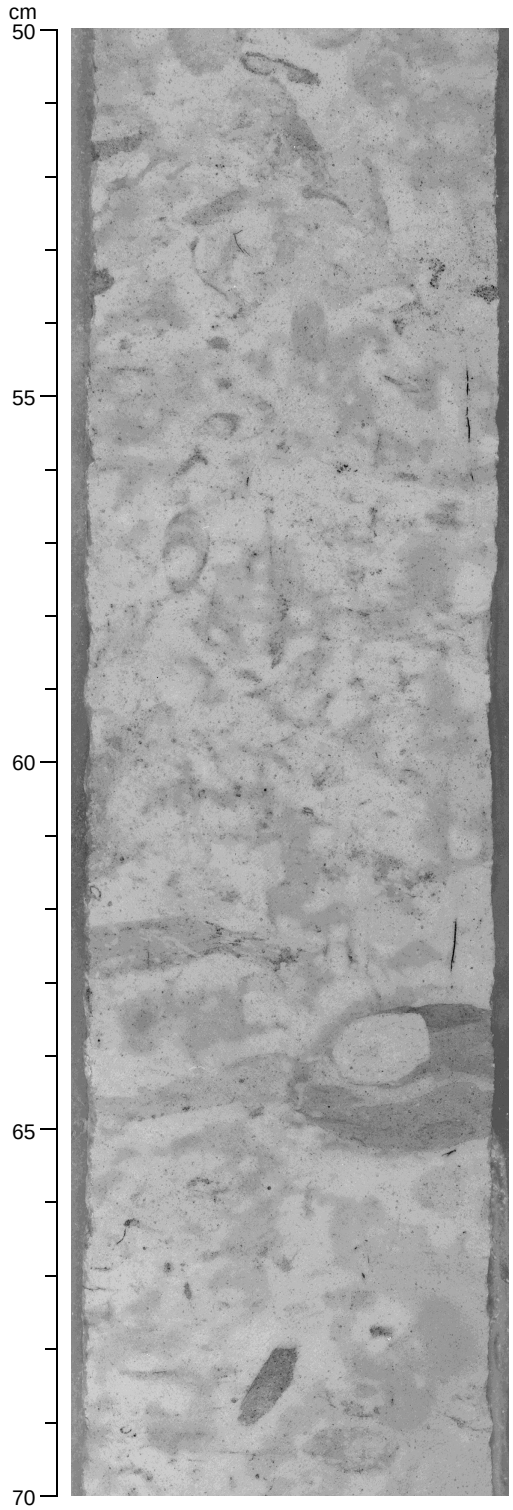

Figure 11. White reaction rims or halos that surround burrows in interval 166-1007C-79R-1, 50–70 cm. First appearance of such reaction halos is in Core 166-1007C-77R. The intensity and thickness of rims is greatest in Core 166-1007C-82R. Below this interval, intensity decreases toward the base of Unit VII.

ilar to those described in overlying units. Throughout this unit, dark intervals are crosscut by small, featherlike, compaction/dissolution cracks similar to the anastomosing or wispy solution seams described in Unit VII. Downcore, differences in color, degree of compaction, and cementation between light and dark intervals decrease.

Discussion

Deposits recovered at Site 1007 contain elements identified at more proximal Site 1003 and more distal Site 1006. This sedimentary succession is interpreted to record an interplay between (1) change in platform-to-basin morphology, (2) sea-level variation; (3) pelagic input, and (4) ocean currents. In contrast to other sites drilled during Leg 166, the section at Site 1007 is characterized by an increased occurrence of turbidites and slumped intervals, and by a relatively high amount of clay- and silt-sized siliciclastics in the upper Pliocene and Pleistocene parts of the section. In addition, below 1120 mbsf, sediments at Site 1007 are marked by the presence of compaction-dissolution features, namely, the anastomosing or wispy solution seams.

Sedimentary Succession

The high amount of turbidites and slump deposits probably reflects the position of Site 1007, near the toe-of-slope of the Great Bahama Bank, where the break in slope causes deposition of mass gravity flows. Intervals containing yellowish, fine-grained packstone with millimeter-scale planar laminae at Site 1007 (see “Unit IV” above) correlate roughly with intervals containing turbidites at Site 1003. For example, Subunit VA at Site 1003, characterized by a high abundance of turbidites, is temporally equivalent to Subunit IVB at Site 1007, which contains an abundance of 5- to 10-cm-thick layers of yellowish, laminated, fine-grained packstone. Petrographic analysis indicates that fine-grained packstone at Site 1007 contains a well-sorted abundance of phosphatic fish debris and carbonate skeletal grains that have been replaced, recrystallized, and/or micritized (see “Subunit IVB” above). Taken as a whole, sedimentologic and petrographic features suggest that laminated packstones at Site 1007 consist of ramp-derived carbonate sediment, which was reworked and redeposited by turbidity currents.

The lithology of slumped deposits suggests that slumped material is derived locally. Similar (middle Miocene) deposits drilled during Leg 101 were interpreted to have been deposited by gravity flows, such as debris flows and/or high-density turbidity currents (Fulthorpe and Melillo, 1988). Postulated causes for slumping include (1) sediment loading and subsequent gravitational instability during a rise in sea level, (2) slope failure during a fall in sea level, and (3) earthquake activity (Fulthorpe and Melillo, 1988).

The Pleistocene section at Site 1007 is characterized by a meter-scale alternation between (1) silt- and clay-rich sediment and (2) silt- and clay-poor sediment. These alternations are similar to the clay cycles observed in the Pleistocene section at Site 1006, and are interpreted to reflect erosion of continent-derived siliciclastics during sea-level lowstands and incipient sea-level rise, and a subsequent increase in neritic and pelagic input following flooding. At Site 1006, these cycles were characterized by sharp basal contacts overlain by clay, whereas cycles at Site 1007 are characterized by gradual contacts between intervals of clay/silt-rich and clay/silt-poor sediment. This difference probably reflects a larger Pleistocene neritic and/or pelagic input at this site relative to at Site 1006.

Pleistocene and upper Pliocene sediments at Site 1007 contain a higher abundance of silt- to fine sand-sized siliciclastic grains relative to Pleistocene and upper Pliocene deposits at other Leg 166 sites. Although the upper part of the Pleistocene is not present at Site 1007, seismic stratigraphic and biostratigraphic data suggest that the upper Pliocene section is thicker and characterized by a higher sedimentation rate relative to other Leg 166 sites (see “Seismic Stratigraphy” and “Biostratigraphy” sections, this chapter). This thickness variation

is caused by two processes: (1) an accumulation of mass gravity-flow deposits, which bypassed the upper slope and accumulated at Site 1007; and (2) an increase in the amount of current drift deposits. This latter increase could reflect a migration of the northward-flowing Santaren Channel Current toward the platform during the late Pliocene and earliest Pleistocene.

As at other sites drilled during Leg 166, the sedimentary succession at Site 1007 records an important change in the mode of neritic carbonate production. At the base of Unit I (base of upper Pliocene), there is a sudden increase in the occurrence of platform-derived material, including aragonite needles and peloids (Fig. 4). The turnover from skeletal-dominated to aragonite needle/peloid-dominated sediments probably reflects the coupled effects of (1) climate change and (2) the transition of the Bahama Bank from a carbonate ramp, characteristic of the Miocene, to the present-day, flat-topped carbonate platform (Eberli and Ginsburg, 1989).

The Miocene section at Site 1007 is nearly identical to the Miocene section recovered at Sites 1003, 1005, and 1006. It consists of alternating intervals of (1) well-cemented, decimeter- to meter-scale, light-colored, clay-free intervals that show no evidence of compaction; and (2) decimeter-scale, dark-colored, relatively clay-rich intervals that show evidence of compaction (see "Unit V" above). These alternations are interpreted to reflect changes in the rate of neritic carbonate input and the subsequent impact of these changes on the primary diagenetic potential of sediments. In this regard, light-colored, well-cemented intervals may reflect periods of higher neritic (aragonite and high-Mg calcite) input and the deposition of sediments with a higher diagenetic potential. In contrast, dark-colored, weakly cemented intervals may reflect (1) periods of decreased neritic input and (2) the deposition of sediments with higher amounts of low-Mg calcite.

Burial-Compaction Features

In the Miocene and upper Oligocene alternations between well-cemented intervals and clay-rich intervals, an increase in overall compaction is observed. Beginning in Core 166-1007C-86R and continuing to the bottom of Hole 1007, the lower parts of dark intervals are cut by anastomosing or wispy solution seams. Similar trends have been noted in Upper Cretaceous carbonate rocks from offshore Louisiana (Scholle et al., 1983). In these rocks, the primary alternation of carbonate-rich (light) and carbonate-poor (dark) lithologies has been accentuated by mechanical and chemical compaction, which has resulted in the export of carbonate from originally carbonate-poor zones to carbonate-rich zones. Similarly, at Site 1007, solution seams tend to be concentrated in carbonate-poor intervals, and networks of anastomosing solution seams initially isolate carbonate in whitish zones that are probably burrow fillings (Cores 166-1007C-86R and 87R). Whitish zones (burrows) are lost below this interval. The intensity and occurrence of anastomosing solution seams increase downcore in Unit VIII of Site 1007 to such an extent that differences in color, degree of compaction, and cementation between light and dark intervals decrease and the primary dark/light alternation is lost. These compaction-related dissolution trends were not observed in similar sediments recovered from identical depths at Site 1003.

BIOSTRATIGRAPHY

The sedimentary sequence recovered from the three holes cored at Site 1007 consists of a 1230-m-thick interval of Pleistocene to upper Oligocene sediments. The section includes a relatively condensed Pleistocene interval compared with Pleistocene successions at the other transect sites higher up the slope of the Great Bahama Bank. Pleistocene calcareous microfossils are abundant and moderately to well preserved. The expanded upper Pliocene section lies unconformably below the Pleistocene interval and yields varying abundances of microfossils. The preservation varies among poor, moderate, and good. Another unconformity separates the lower and upper Pliocene, and the lower Pliocene is a thick, continuous sequence. The Miocene/Pliocene boundary occurs between Cores 166-1007B-32X (289 mbsf) and 166-1007C-1R-1 (303 mbsf). It is impossible to locate the boundary more precisely owing to the poor preservation and absence of nannofossil and planktonic foraminiferal marker species. Several Miocene planktonic foraminiferal events occur between Samples 166-1007C-3R-CC (323.35 mbsf) and 4R-2, 9–10 cm, (332.39 mbsf), indicating the presence of an unconformity similar to those found at Sites 1003 and 1005. The abundance of calcareous microfossils in the upper Miocene sediments is highly variable, and they are generally poorly preserved, although scattered samples yield well-preserved faunas.

The middle/upper Miocene boundary is placed in between Samples 166-1007C-19R-1, 67–70 cm, (475.87 mbsf) and 20R-2, 121–123 cm (487.51 mbsf). A well-constrained biostratigraphy is provided by the nannofossils and planktonic foraminifers for the lower and middle Miocene interval. The lower/middle Miocene boundary occurs between Samples 166-1007C-63R-1 and 65R-3, 99–103 cm, at 910 mbsf. The lower–middle Miocene biostratigraphic sequence appears continuous. Three intervals of reduced sedimentation that occur within the sequence correlate to the time-equivalent hiatuses at Site 1003. The microfossils occur mainly within the clayey intervals (see "Lithostratigraphy" section, this chapter) and show varying states of preservation from poor to good. The base of the sedimentary sequence is assigned to the upper Oligocene calcareous nannofossil Zone NP25 and the planktonic foraminiferal Zone P22. In summary, the numerous biohorizons include most marker species for zonal assignment and provide sufficient detail to construct a reliable biostratigraphy for the sedimentary sequence recovered at Site 1007.

Site 1007 yields in situ upper–middle bathyal benthic foraminiferal faunas with diverse platform-derived taxa in the upper Pliocene to Pleistocene section and minor transported shallow-water benthic foraminifers in and below the lower Pliocene section. Deep-water planulinids are common in the Miocene to lower Pliocene section. The deep-water planulinids occur sporadically in the upper Pliocene, but they are absent from the Pleistocene section.

Calcareous Nannofossils

Calcareous nannofossils in Holes 1007A, 1007B, and 1007C are moderately to poorly preserved. Zonal boundaries at Site 1007 are listed in Table 2 and shown in Figure 12.

Calcareous nannofossils from Samples 166-1007A-1H-CC and 166-1007B-1H-CC are characterized by the presence of *Pseudoemiliania lacunosa* and *Reticulofenestra asanoi* and the absence of *Emiliania huxleyi* and *Gephyrocapsa parallela.* These two samples are between 0.95 and 1.16 Ma (between the base of *Gephyrocapsa parallela* and the base of *R. asanoi*) in the middle part of Zone NN19 at about the Jaramillo Event. Large-form *Gephyrocapsa* spp. (larger than 6 µm) was found in Samples 166-1007B-2H-CC and 3H-CC (19 to 26 mbsf), indicating an age range between 1.20 and 1.44 Ma. The first appearances of *Gephyrocapsa caribbeanica* and *Gephyrocapsa oceanica* mark the base of the Pleistocene and occur in Sample 166-1007B-4H-CC (38 mbsf). Samples 166-1007B-5H-CC through 22X-CC (50 to 200 mbsf) are characterized by *Pseudoemiliania lacunosa* and the absence of *G. caribbeanica* and are correlated to the upper Pliocene. Because discoasters define the upper Pliocene zonal boundaries NN16 through NN18 but are rare to absent in this interval, this interval cannot be subdivided. Abundant reworked specimens from the early Pliocene or older are also recognized in Samples 1007B-11X-CC through 14X-CC. Samples 166-1007B-23X-CC through 32X-1, 68–69 cm, (212–287 mbsf) contain abundant specimens of *Sphenolithus abies* and *Reticulofenestra pseudoumbilicus,* which define the NN15/16 boundary (3.66 Ma). As *Discoaster asymmetricus* was also found in these samples, this interval is assigned to the lower

Table 2. Calcareous nannofossil bioevents.

Event	Age (Ma)	Interval (cm)	Depth* (mbsf)
T *Gephyrocapsa* spp. (large)	1.20	1007B-1H-CC to 1007B-2H-CC	14.23
B *Gephyrocapsa* spp. (large)	1.44	1007B-3H-CC to 1007B-4H-CC	43.54
B *G. caribbeanica* (NN18/19)	1.72	1007B-3H-CC to 1007B-4H-CC	43.54
T *R. pseudoumbilicus* (NN15/16)	3.66	1007B-22X-CC to 1007B-23X-CC	202.98
B *C. rugosus*	4.7	1007B-32X-1, 68–69, to 1007B-32X-CC	287.60
T small *Reticulofenestra* int.	6.5	1007C-1R-CC to 1007B-34X-1, 102–104	304.30
B *D. quinqueramus* (NN10/11)	8.6	1007C-3R-CC to 1007B-37X-1, 35–37	327.99
T *D. hamatus* (NN9/10)	9.40	1007C-14R-2, 41–43, to 1007C-15R-1, 78–40	432.99
B *D. hamatus* (NN8/9)	10.7	1007C-19R-1, 67–70, to 1007C-20R-2, 121–123	481.68
B *C. coalitus* (NN7/8)	11.3	1007C-21R-4, 104–106, to 1007C-22R-3, 34–36	503.69
T *C. floridanus* (NN6/7)	13.2	1007C-49R-3, 109–111, to 1007C-50R-1, 70–72	769.40
T *S. heteromorphus* (NN5/6)	13.6	1007C -50R-1, 70–72, to 1007C-51R-3, 118–121	780.59
T *H. ampliaperta* (NN4/5)	15.6	1007C-58R-2, 112–114, to 1007C-59R-2, 67–71	857.50
T *S. belemnos* (NN3/4)	18.3	1007C-69R-CC to 1007C-70R-4, 106–109	967.44
B *S. belemnos* (NN2/3)	19.2	1007C-73R-3, 71–74, to 1007C-74R-3, 46–50	1003.04
B *D. druggii* (NN1/2)	23.2	1007C-85R-2, 150–151, to 1007C-86R-2, 100–102	1117.85
T *R. bisectus* (NP25/1)	23.9	1007C-95R-2, 32–33, to 1007C-96R-3, 0–1	1117.85

Notes: B = base, T = top. * = average depth for the interval; for actual interval depth, see coring summary on CD-ROM. Average depth was used for constructing Figure 12.

Pliocene Zone NN14 to NN15. Samples 166-1007B-32X-CC through 33X-CC contain rare and poorly preserved nannofossil specimens, which hampers zonal assignment.

Well-preserved specimens of *Discoaster quinqueramus* and *Discoaster berggrenii* were found in Samples 166-1007B-37X-1, 35–37 cm, 166-1007C-3R-1, 105–107 cm, and 166-1007C-3R-CC, which indicates Zone NN11 (5.6 to 8.6 Ma). The absence of the large form *R. pseudoumbilicus* confines this interval to the lower part of Zone NN11 (older than 6.5 Ma). *Discoaster neohamatus* and *Discoaster bellus*, which indicate the lower upper Miocene Zone NN10, were found in Samples 166-1007B-37X-1, 35–37 cm, through 41X-CC and 166-1007C-5R-2, 50–52 cm, through 13R-2, 41–44 cm. Samples 166-1007C-15R-1, 37–40 cm, through 19R-1, 67–70 cm, are correlated to the lowermost upper Miocene Zone NN9 on the basis of the presence of *Discoaster hamatus* and *Catinaster calyculus.* Samples 166-1007C-20R-2, 121–123 cm, and 166-1007C-21R-4, 104–106 cm, are characterized by the occurrence of *Catinaster coalitus*, the lowest occurrence of which defines the Zone NN8/7 boundary. *Cyclicargolithus floridanus*, which last appears at the Zone NN6/7 boundary, occurs below Sample 166-1007C-50R-1, 70–72 cm. The highest occurrences of *Sphenolithus heteromorphus, Helicosphaera ampliaperta*, and *Sphenolithus belemnos,* each of which defines the lower to middle Miocene Zones NN5, NN4, and NN3 are detected in Samples 166-1007C-51R-3, 118–125 cm, 59R-2, 67–71 cm, and 70R-4, 106–109 cm, respectively. The bases of NN3 and NN2, defined by the first appearances of *S. belemnos* and *Discoaster druggii*, respectively, were found in Samples 1007C-73R-3, 71–74 cm/74R-3, 46–50 cm, and 85R-2, 150–151 cm/86R-2, 100–102 cm.

Below the NN2/1 boundary to bottom sample, the abundance of calcareous nannofossils decreases, and *Braarudosphaera bigelowii*, which lives abundantly in the neritic environment, was found. The lowermost two samples, Samples 166-1007C-96R-3, 0–1 cm, and 97R-CC, contain the Oligocene species *Sphenolithus ciperoensis*, which defines the Zone NP25/NN1 boundary. This indicates that the bottom of Hole 1007C is correlated to the uppermost Oligocene Zone NP25.

Planktonic Foraminifers

Planktonic foraminiferal biostratigraphy of Site 1007 is based on core-catcher samples from three holes that were supplemented by discrete samples from the lower Pliocene to Oligocene section. Planktonic foraminifers are present throughout the record, although shells are rare in some intervals, and the preservation is highly variable, ranging from poor to good. Despite their rarity and poor preservation in some sections, almost all marker species are present, and a reliable Neogene planktonic foraminiferal biostratigraphy was established for Site 1007.

The planktonic foraminiferal assemblages of Holes 1007A and 1007B are typically abundant and well preserved in the Pleistocene and the upper Pliocene. Samples 166-1007A-1H-CC and 166-1007B-1H-CC through 5H-CC contain highly diverse assemblages typified by *Globorotalia truncatulinoides* and *Globorotalia tosaensis.* The presence of *G. tosaensis* in Sample 166-1007A-1H-CC indicates that the upper part of the Pleistocene is missing at this site, as the top of the *G. tosaensis* range is 0.6 Ma. The presence of *G. truncatulinoides* assigns this interval to Zone N22.

Samples 166-1007B-6H-CC through 22X-CC appear to represent an expanded sequence of upper Pliocene Zone N21. The planktonic foraminiferal assemblages are highly diverse and the preservation varies from moderate to good, although the preservation deteriorates somewhat in the lowest part of the upper Pliocene. Several samples contained abundant reworked Zone N19 planktonic foraminifers, making zonal assignment difficult. Most of the samples in this interval are characterized by the presence of *G. tosaensis, Globorotalia limbata, Globorotalia miocenica,* and *Globigerinoides extremus.* The last appearance of the latter three species occurs in Sample 166-1007B-6H-CC. According to the ages of their latest occurrences (2.3 Ma for *G. miocenica*, 2.4 Ma for *G. limbata,* and 1.8 Ma for *G. extremus*) and the juxtaposition with the first appearance of *G. truncatulinoides,* a hiatus is placed just below the Pliocene/Pleistocene boundary.

Samples 166-1007B-23X-3, 66–68 cm, through 31X-CC yield diverse lower Pliocene assemblages. The planktonic foraminifers are generally abundant and preservation is moderate to good in the upper part of this interval. Planktonic foraminifers in the lowest lower Pliocene of this section, comprising Samples 166-1007B-30X-CC and 31X-CC, are poorly preserved. The assemblages are characterized by *Dentoglobigerina altispira, Globorotalia margaritae,* and *Globigerina nepenthes.* The latest occurrences of *D. altispira* (3.1 Ma), *G. margaritae* (3.6 Ma), and *G. nepenthes* (4.18 Ma) are in Sample 166-1007B-23X-3, 66–68 cm. The first occurrences of *G. tosaensis* (3.2 Ma) and *G. miocenica* (3.6 Ma) occur in the next sample uphole, Sample 166-1007B-22X-CC, which indicates that the lower/upper Pliocene boundary is either unconformable, extremely condensed, or there is substantial reworking of lower Pliocene specimens.

Samples 166-1007B-32X-1, 68–69 cm, (286.68 mbsf) through 166-1007C-3R-CC, 5–7 cm, (323.35 mbsf) yield rare to abundant planktonic foraminifers with variable preservation. The first occurrence of *Globigerinoides conglobatus* in Sample 166-1007C-3R-CC, 5–7 cm, the lowermost sample of this sequence, indicates an age of

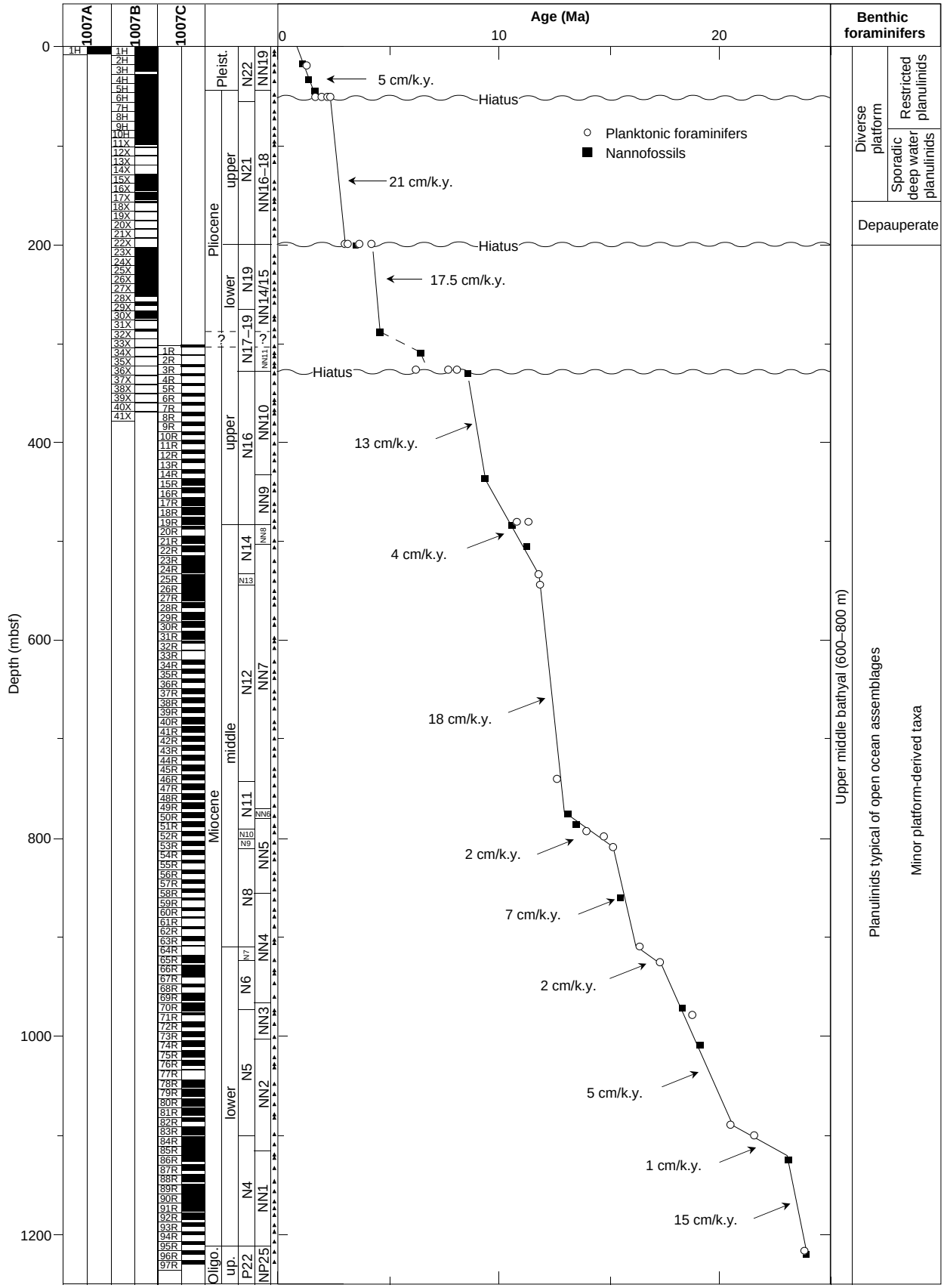

Figure 12. Calcareous nannofossil and planktonic foraminiferal zonation and benthic foraminiferal faunal changes for Site 1007. Recovery for each hole is adjacent to the cores. Solid triangles mark the position of samples examined for stratigraphy and benthic foraminiferal faunas. The age-depth plot is based on the biohorizons in Tables 2 and 3.

6.2 Ma for the lower boundary of this section. The last appearance of the nannofossil small *Reticulofenestra* spp. (6.5 Ma) occurs 20 m above this level. Either the first occurrence of *G. conglobatus* is older in this area or the latest occurrence of small *Reticulofenestra* spp. is younger. Nonetheless, this overlap between *G. conglobatus* and the small *Reticulofenestra* spp. indicates that the interval between 303 and 328 mbsf is uppermost Miocene. The Miocene/Pliocene boundary lies above this interval, between 287 and 304 mbsf (see "Calcareous Nannofossils," this section).

The first appearances of *Globorotalia cibaoensis* (7.7 Ma) and *G. extremus* (8.1 Ma) were found between Samples 166-1007C-3R-CC and 4R-2, 9–10 cm, at the same level as *G. conglobatus,* which indicates the presence of an unconformity. The interval between Samples 166-1007C-4R-2, 9–10 cm, and 19R-1, 67–70 cm, is characterized by upper Miocene species. The absence of *Neogloboquadrina humerosa* indicates that the sediments below the unconformity are assigned to Zone N16. The base of this zone is defined by the first appearance of *Neogloboquadrina acostaensis* (10.9 Ma), which occurs between Samples 166-1007C-19R-1, 67–70 cm, and 20R-2, 121–123 cm (482 mbsf). The appearance of this species also approximates the middle/upper Miocene boundary and is consistent with the nannofossil event used to place this boundary.

Middle Miocene Zone N14 is the concurrent range between *Globorotalia mayeri* and *G. nepenthes.* The last appearance of *Globorotalia mayeri* (11.4 Ma) at Site 1007 occurs between Samples 166-1007C-19R-1, 67–70 cm, and 20R-2, 121–123 cm, (482 mbsf) immediately below the base of N16. The first appearance of *G. nepenthes* (11.8 Ma) is between Samples 166-1007C-24R-6, 28–31 cm, and 25R-2, 2–5 cm (533 mbsf). Zone N13 is represented by Sample 166-1007C-25R-2, 2–5 cm, only. The top of the *Fohsella* lineage (11.9 Ma) and Zone N12 is in Sample 166-1007C-26R-6, 53–56 cm (550 mbsf). There is approximately 200 m of sediments within Zone N12, the base of which is marked by the first appearance of *Fohsella fohsi* (12.7 Ma), occurs between Samples 166-1007C-46R-3, 50–53 cm, and 47R-2, 0–2 cm, at a depth of 742 mbsf. The first appearance of *Fohsella praefohsi* and the base of Zone N11 occurs in Sample 1007C-51R-3, 118–125 cm (791 mbsf). Zones N10 and N9 are represented by only one sample each at Site 1007. The base of Zone N10 is defined by the first appearance of *Fohsella peripheroacuta* (14.8 Ma) between Samples 166-1007C-52R-3, 30–32 cm, and 53R-2, 80–87 cm (800 mbsf). The first appearance of *Orbulina universa* (15.1 Ma) and top of Zone N9 occur between Samples 166-1007C-53R-2, 80–87 cm, and 54R-1, 31–33 cm (808 mbsf). The lowermost zone in the middle Miocene is Zone N8, which is defined as the range from the first appearance of *Praeorbulina sicana* (16.4 Ma) to the first appearance of *O. universa.* The base of *P. sicana* occurs between Samples 166-1007C-63R-1, 60–64 cm, and 65R-3, 99–103 cm (910 mbsf).

The uppermost lower Miocene Zone N7 is the gap between the base of *P. sicana* and the last appearance of *Catapsydrax dissimilis* (17.3 Ma). At Site 1007, Zone N7 is represented only by Sample 166-1007C-65R-3, 99–103 cm (921 mbsf). Planktonic foraminifers are rare and not well preserved in this sample. However, samples above and below with similar abundances and preservation yielded several specimens of *P. sicana* and *C. dissimilis,* respectively, which indicates that this gap is real. The marker for the base of Zone N6 (18.8 Ma) is the first appearance of *Globigerinita insueta.* At Site 1007, the abundance of this species is rare at best, and its first occurrence was found between Samples 166-1007C-70R-4, 106–109 cm, and 71R-1, 25–28 cm (973 mbsf).

Zone N5 spans the interval from the first appearance of *G. insueta* to the last appearance of *Globorotalia kugleri* (21.5 Ma). At Site 1007, this interval occurs from Sample 166-1007C-71R-1, 25–28 cm, (975 mbsf) to the base of Zone N5, which was found between Samples 166-1007C-83R-3, 28–30 cm, and 84R-3, 136–137 cm (1100 mbsf). Within Zone N5, the first appearance of *Globigerinoides altiapertura* (20.5 Ma) is also a useful datum, and it is placed between Samples 166-1007C-81R-6, 22–24 cm, and 83R-3, 28–30 cm (1087 mbsf). Zone N4 is the total range of *G. kugleri* (21.5 to 23.8 Ma). At Site 1007, this zone ranges between Samples 166-1007C-84R-3, 136–137 cm, and 95R-1, 148–150 cm (1100 to 1214 mbsf). Zone N4 is not subdivided into Zones N4b and N4a because the marker species, *Globoquadrina dehiscens,* was found sporadically at this site. Below Zone N4, Samples 166-1007C-96R-3, 0–2 cm, and 97R-1, 130–133 cm, are dominated by *Globigerina ciperoensis, Globigerina angulisuturalis,* and *Globigerinoides primordius,* which are consistent with the upper Oligocene assignment indicated by the nannofossils (see "Calcareous Nannofossils," this section).

Benthic Foraminifers

The upper Pliocene to Pleistocene section at Hole 1007B yields diverse platform-derived taxa in and above Sample 166-1007B-18X-CC. Redeposited foraminifers originated from reefal (e.g., *Amphistegina lessonii, Asterigerina carinata, Tretomphalus* spp.; for others, see "Biostratigraphy" section, "Site 1003" chapter, this volume), shallow neritic (e.g., *Cibicides lobatulus, Elphidium* spp.), and upper bathyal (e.g., *Bulimina marginata, Planulina foveolata*) environments. Samples 166-1007B-19X-CC through 22X-CC contained rare benthic foraminifers with poor preservation. Below this, early Pliocene and older samples contain minor transported shallow-water benthic foraminifers, primarily *A. lessonii, A. carinata,* and *Elphidium* spp.

Below the Pliocene/Pleistocene boundary at Site 1006, the benthic foraminiferal assemblages contain planulinids that are more typical of an open-ocean setting, whereas the overlying Pleistocene section yields more restricted planulinids. There is a similar pattern at Site 1007, with sporadic occurrences of *Planulina wuellerstorfi* from Samples 166-1007B-9H-CC through 18X-CC and consistent deep-water planulinids in and below Sample 166-1007B-23X-CC (early Pliocene and older).

The paleobathymetric estimate for Site 1007 is upper middle bathyal (600–800 m), determined on the basis of the upper depth limit (approximately 600 m) of several taxa that are present at different levels, depending on the age of the section (e.g., *Anomalinoides capitatus, Anomalinoides globulosus, Anomalinoides pseudogrosserugosus, Anomalinoides semicribratus, Cibicidoides robertsonianus, Planulina rugosa, Pyrgo murrhina*), and the lower depth limit of *Planulina ariminensis* (~800 m). The global first occurrence of *P. ariminensis* is N16. Below this, the lower depth limit is constrained by several species generally found shallower than 1000 m (e.g., *Melonis pompilioides, Planulina ambigua,* and *Planulina dohertyi*). This does not necessarily reflect a paleobathymetric change within the middle bathyal zone; rather, it is an artifact of the age ranges of the paleobathymetric marker taxa.

Sedimentation Rates

Site 1007 was drilled at the toe-of-slope on the leeward side of the GBB. The stratigraphic section recovered at Site 1007 is 1230 m thick, representing the interval from the middle Pleistocene to the uppermost Oligocene. The sedimentation rates were determined on the basis of nannofossil and planktonic foraminiferal biostratigraphy. The age-depth relationship of these nannofossil and planktonic foraminifer datums from Holes 1007B and 1007C is plotted in Figure 12. Individual datums are listed in Tables 2 and 3.

The average sedimentation rate for the Pleistocene interval is reasonably well constrained; calcareous nannofossils and planktonic foraminifers are abundant, a prerequisite for reliable datum levels. A linear regression of the datum levels indicates that the long-term Pleistocene sedimentation rate is 5 cm/k.y. The zero-depth intercept is 0.95 Ma, indicating that the top of Hole 1007B is older than 0.95 Ma, which is consistent with the nannofossils. Current action along this part of the slope increased during the last 1 m.y., either through

Table 3. Planktonic foraminiferal bioevents.

Event	Age (Ma)	Interval (cm)	Depth* (mbsf)
T *G. obliquus*	1.3	1007B-2H-CC to 1007B-3H-CC	22.57
T *G. extremus*	1.77	1007B-5H-CC to 1007B-6H-CC	53.54
B *G. truncatulinoides* (N21/22)	2.0	1007B-5H-CC to 1007B-6H-CC	53.54
T *G. exilis*	2.2	1007B-5H-CC to 1007B-6H-CC	53.54
T *G. limbata*	2.4	1007B-5H-CC to 1007B-6H-CC	53.54
T *D. altispira*	3.09	1007B-22X-CC to 1007B-23X-3, 66–68	200.34
T *Sphaeroidinellopsis* spp.	3.12	1007B-22X-CC to 1007B-23X-3, 66–68	200.34
B *G. tosaensis* (N20/21)	3.2	1007B-22X-CC to 1007B-23X-3, 66–68	200.34
T *G. margaritae* (N19/20)	3.58	1007B-22X-CC to 1007B-23X-3, 66–68	200.34
T *G. nepenthes*	4.18	1007B-22X-CC to 1007B-23X-3, 66–68	200.34
B *G. conglobatus*	6.2	1007C-3R-CC to 1007C-4R, 9–10	327.87
B *G. cibaoensis*	7.7	1007C-3R-CC to 1007C-4R, 9–10	327.87
B *G. extremus*	8.1	1007C-3R-CC to 1007C-4R, 9–10	327.87
B *N. acostaensis*	10.9	1007C-19R-1, 67–70, to 1007C-20R-2, 121–123	481.69
T *G. mayeri* (N14/15)	11.4	1007C-19R-1, 67–70, to 1007C-20R-2, 121–123	481.69
B *G. nepenthes* (N13/14)	11.8	1007C-24R-6, 28–31, to 1007C-25R-2, 2–5	532.75
T *Fohsella* (N12/13)	11.9	1007C-25R-2, 2–5, to 1007C-26R-6, 53–56	542.48
B *Fohsella fohsi* (N11/12)	12.7	1007C-46R-3, 50–53, to 1007C-47R-2, 0–2	742.12
B *Fohsella praefohsi* (N10/11)	14.0	1007C-51R-3, 118–121, to 1007C-52R-3, 30–32	791.54
B *G. peripheroacuta* (N9/10)	14.8	1007C-52R-3, 30–32, to 1007C-53R-2, 80–87	800.20
B *O. universa* (N8/9)	15.1	1007C-53R-2, 80–87, to 1007C-54R-1, 31–33	808.39
B *P. sicana* (N7/8)	16.4	1007C-63R-1, 60–64, to 1007C-65R-3, 99–103	910.25
T *C. dissimilis* (N6/7)	17.3	1007C-65R-3, 99–103, to 1007C-66R-2, 40–43	925.35
B *G. insueta* (N5/6)	18.8	1007C-70R4, 106–109, to 1007C-71R-1, 25–28	973.41
B *G. altiapertura*	20.5	1007C-81R-6, 22–24, to 1007C-83R-3, 28–30	1086.75
T *G. kugleri* (N4/5)	21.5	1007C-83R-3, 28–30, to 1007C-84R-3, 136–137	1099.62
B *G. kugleri* (P22/4)	23.8	1007C-95R-1, 148–150, to 1007C-96R-3, 0–2	1213.71

Notes: B = base, T = top. * = average depth for the interval; for actual interval depth see coring summary on CD-ROM. Average depth was used for constructing Figure 12.

a shift in the current axis or an increase in velocity. This caused nondeposition and/or erosion to occur along the toe slope of the GBB. The base of this interval is bounded by a hiatus just below the Pliocene/Pleistocene contact (see "Planktonic Foraminifers," this section). The duration of this hiatus was approximately 0.4 m.y.

The upper Pliocene interval is highly expanded with an average sedimentation rate of 21 cm/k.y. This is much higher than in time-equivalent intervals at the other Great Bahama Bank slope transect sites, where sedimentation rates of about 2–3 cm/k.y. were found (i.e., pelagic sedimentation). The increased sedimentation rate at Site 1007 seems to be the combined result of deposition of platform-derived material that bypassed the upper slope and was deposited at the toe-of-slope and the accumulation of drift sediments. This interpretation is supported by the geometry of the package. The upper Pliocene interval appears to be a distinct seismostratigraphic unit that pinches out toward the upper slope of the platform (see "Seismic Stratigraphy" section, this chapter). This platformward termination of sediments can best be explained by the processes described above.

The lower Pliocene package is bounded by a hiatus at the top and a 16-m interval of undifferentiated sediments at the base. The duration of the hiatus spanning the lower/upper Pliocene boundary is approximately 1 m.y. (3.2 to 4.2 Ma; see "Planktonic Foraminifers," this section). The sedimentation rate below this hiatus is 17.5 cm/k.y. and is similar to the high rates at the slope sites located higher up the slope (Sites 1003 and 1005) or in the Straits of Florida (Site 1006). This indicates that the locus of deposition of platform-derived material extended from the upper flank down to the toe-of-slope. The base of this package at Site 1007 lies above a section (287 to 304 mbsf) of undetermined age because of poor preservation of the microfossils. The sample immediately above 287 mbsf contains *Ceratolithus rugosus,* indicating that it must be 4.7 Ma or younger. Below 304 mbsf, the presence of small *Reticulofenestra* spp. indicates an age of 6.5 Ma or older. Therefore, the interval of poor preservation represents either an interval of very low sedimentation (<1 cm/k.y.) or contains a hiatus that straddles the Miocene/Pliocene boundary. A lithologic break occurs at the base of this interval of poor preservation (304 mbsf), which indicates continuity with the overlying lower Pliocene sediments and is more consistent with the presence of a hiatus (see "Lithostratigraphy" section, this chapter).

A late Miocene hiatus was detected at approximately 328 mbsf that spanned approximately 2 m.y. (see "Planktonic Foraminifers," this section). Just above this unconformity, approximately 20 m of uppermost Miocene sediments were found. The sedimentation rate for this short section cannot be determined, but the planktonic foraminiferal events that occur at the unconformity require it to be much higher than 1 cm/k.y. This may provide evidence for some platform production and export to the basal slope during the uppermost parts of nannofossil Zone N11 and planktonic foraminiferal Zone N17 (Messinian), or it represents a lowstand wedge.

Although the number of upper Miocene planktonic foraminiferal and nannofossil datums is limited because of preservation of the fossils and rarity of marker species, those present suggest a high sedimentation rate (13 cm/k.y.) during this period. Sedimentation rates at the other Great Bahama Bank transect Sites 1003 and 1005 were similar. Site 1006, farther out in the basin, shows a much lower upper Miocene sedimentation rate (3 cm/k.y.; i.e., pelagic in nature). This sedimentation rate pattern shows that either the Great Bahama Bank platform was shedding to the gently dipping slope during the late Miocene or that the upper Miocene package records a shift in the position of drift deposition higher up the slope. The upper Miocene sequence outlined by the seismic stratigraphy supports the first interpretation (see "Seismic Stratigraphy" section, this chapter).

The middle and early Miocene sedimentation rates show four cycles with alternating low (<2 cm/k.y.) and high (>5 cm/k.y) rates. Periods marked by lower rates of sedimentation occurred from 9.5 to 11.5, 13 to 15, 16.5 to 17.5, and 20.5 to 23 Ma and correlate to hiatuses of similar duration at Site 1003. Periods of faster deposition occurred from 11.5 to 13, 15 to 16.5, 17.5 to 20.5, and older than 23 Ma, which correspond to intervals at Site 1003 with similarly high sedimentation rates. These cycles represent the turning off and on of platform production in response to changes in relative sea level.

PALEOMAGNETISM

Shipboard paleomagnetic measurements were conducted at Holes 1007B and 1007C. Whole-core cryogenic measurements were conducted on APC and XCB cores from Hole 1007B. As a result of polarity uncertainties, unrecovered intervals, and limitations in reliability of directional data from the shipboard cryogenic magnetometer, correlation to the geomagnetic polarity time scale (GPTS) was limited. Only tentative reversal zones could be identified in the shallow

part of Hole 1007B. In the upper portion of Hole 1007B, archive-half cores were analyzed at 20-cm intervals at NRM and 15-mT AF demagnetization level, and in deeper parts at only the NRM level. As a result of weaker intensities with depth and measurement problems associated with lower intensities, Holes 1007A (failed mudline) and 1007C (rotary drilled core) were not analyzed for magnetostratigraphic purposes. As with Sites 1003 through 1006, the reliability of both the inclination and declination data were suspect (see "Explanatory Notes" chapter, this volume).

The magnetic intensities of Holes 1007B ranged from about 10 to about 1.0 mA/m at the NRM level. After 15-mT AF demagnetization, intensity values usually fell to between about 1 and 0.3 mA/m (Fig. 13). Split-core measurements in Hole 1007C failed to have sufficient NRM intensities to overcome the axial bias problem with the cryogenic magnetometer. The low magnetic intensities throughout most of the core, the generally diamagnetic character of the whole-core susceptibility measurements, and several saturation isothermal remanent magnetization (SIRM) acquisition tests (Fig. 14) suggest that the remanence is carried by magnetite. In unconsolidated sediments from Hole 1007B, the remanence is likely carried by single-domain magnetite. In deeper, more indurated sediments from Holes 1007B and 1007C, magnetic remanence is held by either slightly coarser grained magnetite or perhaps highly interacting, single-domain magnetite (Fig. 14).

Directional data collected from the cryogenic magnetometer at Site 1007 should be viewed with caution, given the problems with the cryogenic magnetometer. The NRM inclination data in APC cores (below about 10 mbsf) from Hole 1007B show a strong grouping of values that are 60° or greater (Fig. 15). After 15-mT AF demagnetization, much of the upper 35 mbsf moves to lower inclination angles, and several portions show reverse polarity (Fig. 15). Below a zone of drilling disturbance (Core 166-1007B-5H), the inclination data also show several zones that had reverse polarity or inclination angles that had dropped significantly from the NRM values.

Although the inclination data in Hole 1007B had several 2- to 3-m-thick intervals with reverse polarity, the shipboard data could not definitively constrain a reversal stratigraphy. The top 2 mbsf in Hole 1007B had normal polarity after 15-mT AF demagnetization and was underlain (~2–18 mbsf) by inclinations that trend toward reverse polarity. Two zones of normal polarity were indicated by higher positive inclination at about 18–21 and 28–32 mbsf. The interval from about 60 mbsf to the base of the APC cores (91.7 mbsf) showed several normal polarity zones separated by zones trending toward reverse polarity.

Magnetostratigraphically, no definitive polarity zones could be identified for correlation with the GPTS. The trend toward predominantly reverse polarity in the upper part of Hole 1007B is consistent with shipboard biostratigraphy, which suggested that the base of Core 166-1007B-1H is approximately 1 Ma, somewhere in the C1r Matuyama Chron (i.e., the C1n Brunhes Normal Chron is missing). The normal polarity at the very top of the core may perhaps be correlative with the Jaramillo Subchron (C1r.1n). The other normal polarity zones at about 20 and 30 mbsf, if confirmed, may be correlative with short polarity events above the Olduvai Subchron (Sample 166-1007B-4H-CC has a calcareous nannofossil age of between 1.44 and 1.66 Ma; see "Biostratigraphy" section, this volume).

Whole-core magnetic susceptibility was measured in Holes 1007B and 1007C by the MST. For the most part, susceptibility was diamagnetic (negative) in the APC cores of Hole 1007B (Fig. 16). This diamagnetism is characteristic of carbonate-rich sediments (Shipboard Scientific Party, 1991). Several positive susceptibility peaks and variations in the degree of diamagnetism are also seen in the APC magnetic susceptibility data (Fig. 16). An exceptionally high positive susceptibility was measured in the top several meters of Hole 1007B, near the seafloor. This high susceptibility might be related to a nondepositional surface and/or to an interval of increased detrital magnetic material (lag), consistent with the middle Pleistocene age

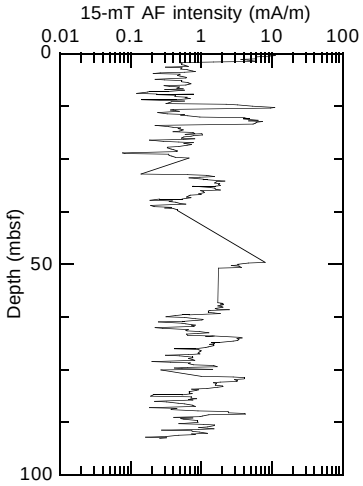

Figure 13. Remanence intensity after 15-mT AF demagnetization in APC split cores from Hole 1007B.

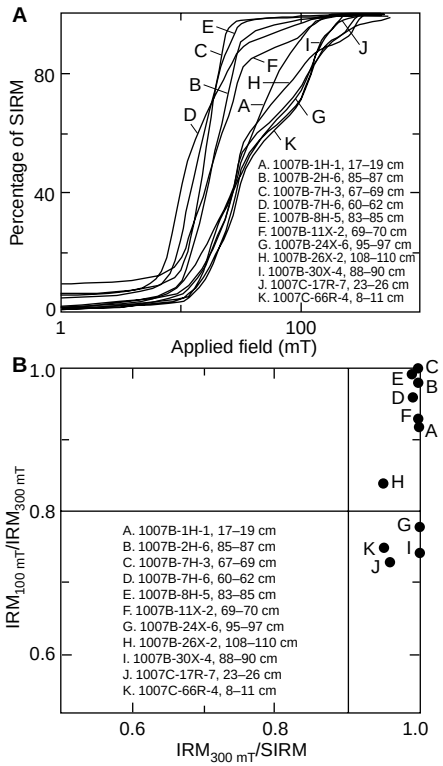

Figure 14. **A.** Isothermal remanent magnetization acquisition curves for several samples from Site 1007, representing differing lithologies and degrees of cementation. Most of the samples from unconsolidated sediment (A–F) show acquisition patterns similar to that of single-domain magnetite. Several samples (G–K) show slightly greater saturation levels, which may indicate either partial oxidation to maghemite, highly interacting single-domain magnetite, or perhaps a coarser grained magnetite component. **B.** Comparison of ratios from the IRM acquisition data. The upper right portion of the plot is used to define a single-domain magnetite mineralogy. The Site 1007 data from cemented limestone and clay-bearing samples (G–K) suggest that magnetic remanence is carried by magnetite, which is coarser grained than the single-domain type found in the overlying, unconsolidated sediments.

proposed for the seafloor sediments (see "Biostratigraphy" section, this volume). A proposed fine-grained magnetite remanence carrier in the section cored with the APC is also consistent with these predominantly diamagnetic susceptibility results, as susceptibility is grain-size dependent in magnetite (Maher, 1988) and does not usually show positive susceptibilities with a carbonate matrix. Downcore, the sections of Holes 1007B and 1007C cored with the XCB and the RCB also show a mainly diamagnetic signal. Several short, positive susceptibility spikes are prominent in the lower portions of Hole 1007B. Examination of the susceptibility data and the cores in this interval seems to suggest a least-partial contamination related to XCB coring. Many of the positive susceptibility peaks were only single points and were tentatively correlated with zones of inflow from drilling. In Hole 1007C, a similar, generally diamagnetic susceptibility was encountered, although several intervals between 1000 and 1200 mbsf had slightly positive susceptibilities (Fig. 17), perhaps related to greater amounts of siliciclastic input.

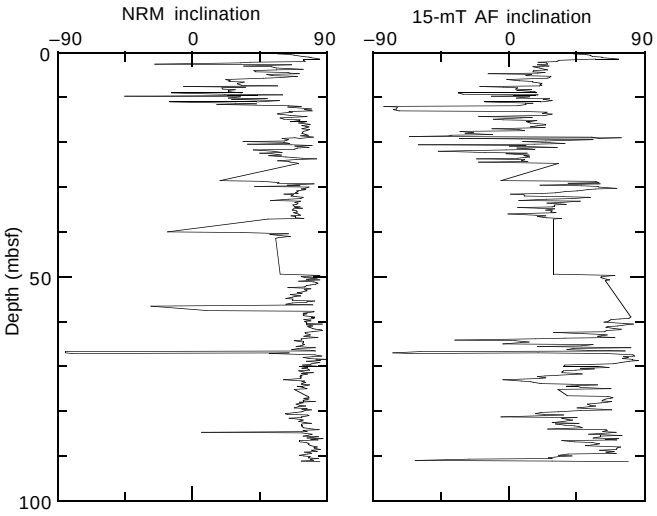

Figure 15. Inclination data from the shipboard cryogenic magnetometer in split-cores from Hole 1007B. Inclination angles after 15-mT AF demagnetization show several zones of reverse polarity in the upper 30 mbsf and a strong trend toward reverse polarity for much of the data. From about 60 to 90 mbsf in Hole 1007B, the figure also shows intervals that trend toward reverse polarity after 15-mT AF demagnetization. Unfortunately, correlation to the GPTS was hindered by the incomplete removal of an overprint component after 15-mT AF demagnetization. See text for further discussion of the directional data and measurement problems encountered at this site.

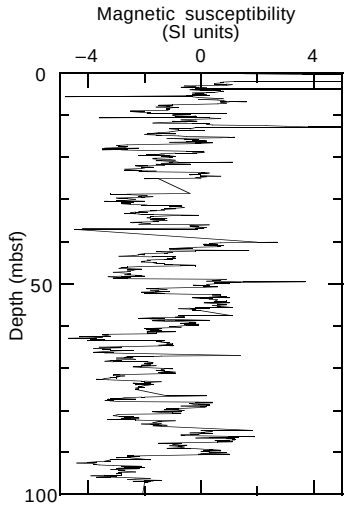

Figure 16. Whole-core magnetic susceptibility data from the MST at Hole 1007B for the APC section. Susceptibility is mostly diamagnetic as a result of the high carbonate content, but several positive susceptibility intervals or spikes occurred. These positive susceptibility intervals may be a result of greater detrital input correlative with the darker color, low carbonate lithologies.

ORGANIC GEOCHEMISTRY

At Site 1007, the shipboard organic geochemistry program included determinations of inorganic carbon, total carbon, total nitrogen, and total sulfur in addition to safety monitoring for hydrocarbon gases. The analytical procedures are described in the "Explanatory Notes" chapter (this volume).

Volatile Hydrocarbons

At Site 1007, low methane (C_1) concentrations (3–4 ppm) were observed between 0 and 22.0 mbsf. Below this depth, methane shows a steady increase from 13 to 178 ppm at 479.1 mbsf (Table 4 on CD-ROM; Fig. 18). Between 479.1 and 600 mbsf, methane concentrations increase to 1000 ppm after which they stabilize to approximately 1000 ppm. Ethane (C_2) was first detected at 47.5 mbsf (Table 4 on CD-ROM). The C_1/C_2 shows only minor variation (10–20), except for an interval (600–1000 mbsf) where the C_1/C_2 ranges between 20 and 40 (Fig. 18).

Higher weight hydrocarbons (C_{2+}) were first detected at 350.2 mbsf at Site 1007 (Table 4 on CD-ROM). The distribution of the higher weight hydrocarbons is illustrated by the plots of isobutane and *n*-butane in Figure 18. Isobutane and *n*-butane concentrations increase from trace levels (<1 ppm) at 350.2 mbsf to greater than 10 ppm in an interval from 540 to 850 mbsf. Below this interval, concentrations decrease to low levels (<1 ppm) at 1200 mbsf (Fig. 18). At the base of the section, high butane concentrations (>10 ppm) are again observed at 1207.2 mbsf. Hydrogen sulfide (H_2S) was detected at 54.0 mbsf and shows large variation (41–4113 ppm) in the upper 245 mbsf (Table 4 on CD-ROM). At greater depths H_2S concentrations vary between 20 and 40 ppm.

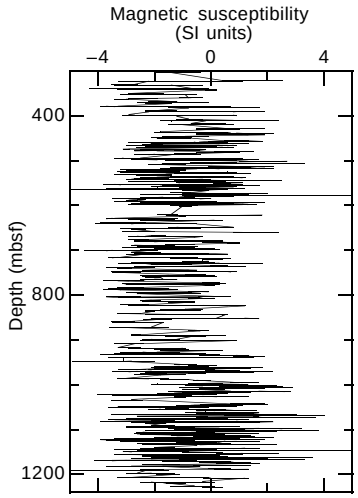

Figure 17. Magnetic susceptibilities for Hole 1007C. Although mainly diamagnetic, several intervals with more frequent positive susceptibilities may correspond to greater relative detrital input associated with clay layers and contourite deposits.

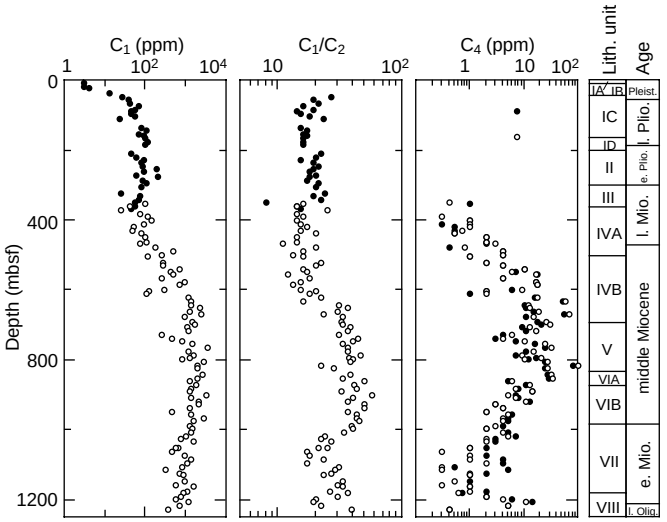

Figure 18. Concentration of methane (C_1) and methane/ethane (C_1/C_2) in Hole 1007B (solid circles) and Hole 1007C (open circles), and iso- and *n*-butane (I-C_4 and *n*-C_4) concentrations of headspace gases from Site 1007. For C_4, solid circles = isobutane and open circles = *n*-butane.

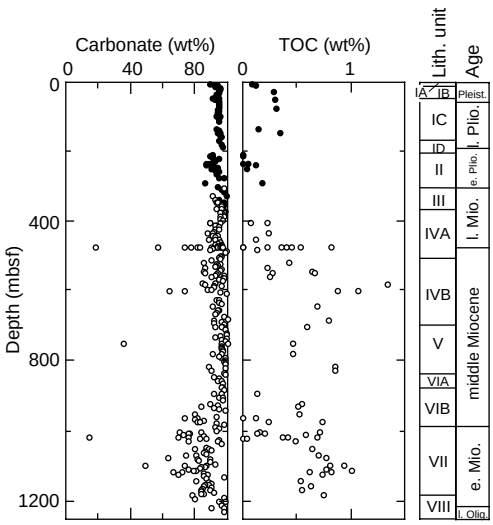

Figure 19. Concentration of carbonate and total organic carbon (TOC) at Site 1007. Solid circles = Hole 1007B, and open circles = Hole 1007C.

Inorganic and Organic Carbon, Total Sulfur, and Total Nitrogen

Carbonate data for Site 1007 are presented in Figure 19 and in Table 5 on CD-ROM. Carbonate contents vary from 18 to 100 wt% (Fig. 19). In the upper 900 mbsf of the section, carbonate content usually ranged between 85 and 100 wt%. Samples that deviate from this range (468.2–468.9 mbsf, 595.0–595.3 mbsf, and 746.2 mbsf) are confined to dark-colored clay-rich intervals (see "Lithostratigraphy" section, this chapter). The carbonate content below 900 mbsf displays a larger variation (70–100 wt%), with the fluctuations becoming smaller at the base of the hole (Fig. 19).

Seventy-seven samples with low carbonate contents were selected for total organic carbon (TOC), total sulfur (TS), and total nitrogen (TN) analyses. TOC at Site 1007 varied from 0.0 to 1.3 wt% (Fig. 19). Low TOC concentrations (<0.5 wt%) are restricted to the upper 450 mbsf of the section, whereas higher concentrations (>1.0 wt%) are observed in lithologic Subunit IVB (576.8 mbsf, and 595.0 mbsf) and Unit VII (1110.7 mbsf) in dark-colored intervals. Within lithologic Unit V and Subunit IVA, a decrease in TOC content occurs with depth (Fig. 19). TS concentrations at Site 1007 are generally high (0.0–2.5 wt%), which is in accordance with the abundant pyrite observed in the core (see "Lithostratigraphy" section, this chapter). One sample (1096.0 mbsf), however, contains 29.8 wt% sulfur (Table 5 on CD-ROM). This sample probably represents the in-filling of a void in the sediment by pyrite (1 cm × 1 cm) (see "Lithostratigraphy" section, this chapter). TN concentrations are low (0.00–0.11 wt%) and are generally below detection limits (<0.1 wt%) (Table 5 on CD-ROM).

Discussion

The low C_1/C_2 (<100) in the headspace gases below 350.2 mbsf at Site 1007 lies within the abnormal range defined by Emeis and Kvenvolden (1986), which indicates that the hydrocarbon gases are of thermogenic origin. However, no Rock-Eval analyses were conducted at this site; thus the maturity of the organic matter cannot be evaluated. The low T_{max} values (<430°C) observed at Site 1003 and 1006 (see "Organic Geochemistry" section, "Site 1003" chapter, and "Organic Geochemistry" section, "Site 1006" chapter, this volume) make it reasonable to assume that the organic matter at Site 1007 is immature with respect to petroleum genesis and that the hydrocarbons were not produced in situ, but rather migrated from deeper sources. The marked increase in the concentration of the heavyweight hydrocarbons in headspace gases below 540 mbsf in Hole 1007C (lithologic Units IVB through VIA) occurs in a sequence characterized by large acoustic velocity changes (see "Physical Properties" section, this chapter). However, the top of this interval does not coincide with any major changes in the acoustic velocity of the sediment (see "Physical Properties" section, this chapter) as seen at Site 1003 and 1006.

INORGANIC GEOCHEMISTRY

Inorganic chemical analyses were conducted on 54 interstitial water samples squeezed from whole-round samples at a frequency of one every other section in the first three cores and one per core thereafter. Below 300 mbsf, the hardness of the sediments necessitated taking samples intermittently from soft layers when they were recovered. Below 800 mbsf, only small volumes of interstitial water could be extracted (<3 mL), and not all of the standard shipboard analyses could be completed. Analytical methods are detailed in the "Inorganic Geochemistry" section of the "Explanatory Notes" chapter (this volume).

The mineralogy of the carbonate fraction of the sediments at Site 1007 was quantified by X-ray diffraction (XRD) on 314 samples selected at frequencies ranging from one per section to one per core (Fig. 20). In addition, a 1-m interval centered at 468 mbsf was analyzed at a frequency of one sample every 10 cm to look at high-resolution mineralogical variation across one distinct lithologic cycle. All carbonate mineralogy data were adjusted to include the weight percent noncarbonate fraction as determined by coulometric analysis of total carbonate (see "Organic Geochemistry" section, this chapter) and were corrected for the dolomite content within sediments.

Interstitial Waters

Salinity, Chloride, Sodium, and Potassium

At Site 1007, the salinity and major conservative elements show a significant increase in concentration with depth, reaching a maximum near 928 mbsf (Fig. 21; Table 6). The major characteristics of the chloride (Cl^-) profile are summarized as follows: (1) no measurable change in the shallow portion of the sediments (0–24.9 mbsf); (2) a sharp, continuous increase from 562 to 905 mM between 24.9

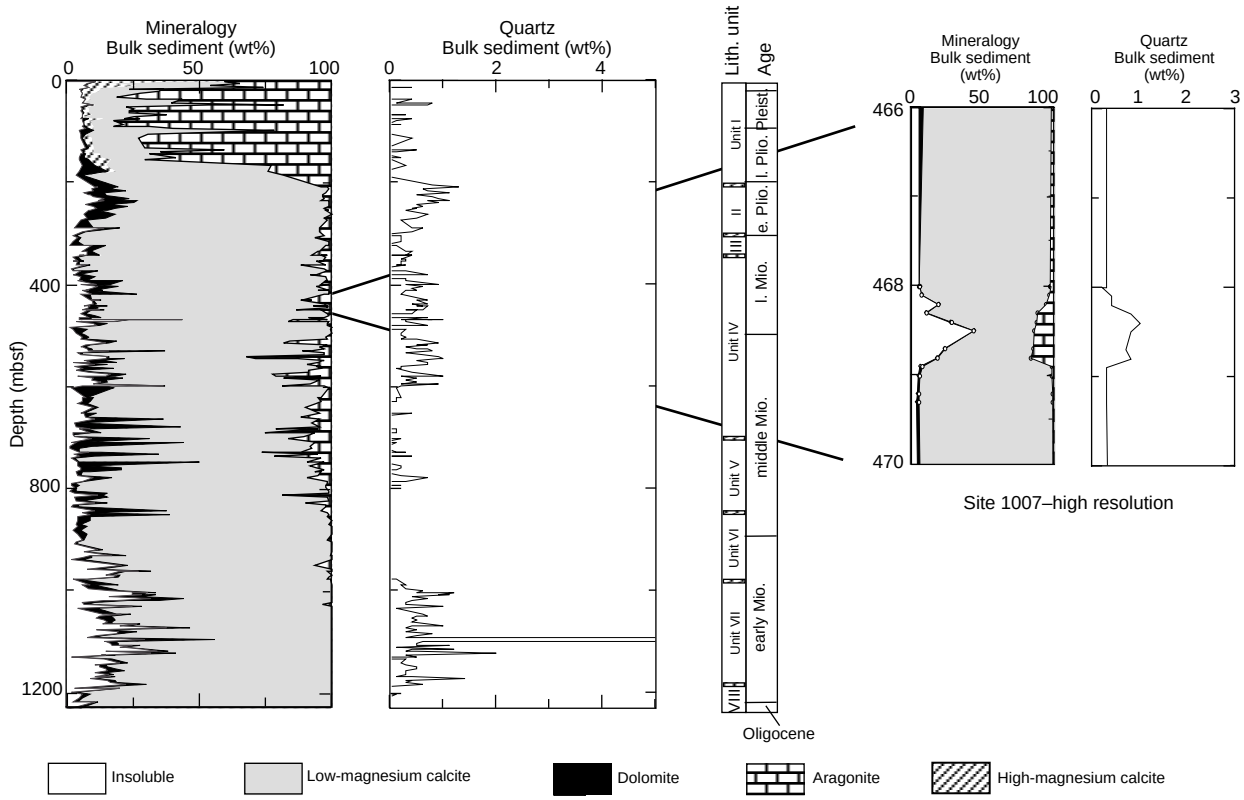

Figure 20. Quantitative X-ray mineralogy of sediments from Site 1007.

and 287.3 mbsf; (3) flattening of the profile between 287.3 and 928 mbsf, punctuated by several localized increasing/decreasing trends; and (4) a drop in Cl^- concentration below 928 mbsf. The sodium (Na^+) profile shows an identical trend and remains conservative with respect to Cl^- throughout the hole at near the seawater Na^+/Cl^- of 0.84. The potassium (K^+) concentration also shows a similar conservative behavior with respect to Cl^- to a depth of 842 mbsf, after which the K^+/Cl^- decreases from a normal seawater ratio of 0.018–0.012.

Alkalinity, Sulfate, Ammonium, and Phosphate

The titration alkalinity increases from bottom-water concentrations (2.87 mM) in the upper 21.9 mbsf, to a shallow maximum of 24 mM between 96 and 137 mbsf. Farther downhole, the alkalinity profile flattens, gradually decreasing to a concentration of 11.7 mM at 300 mbsf (Fig. 21; Table 7 on CD-ROM). Over the same interval, the sulfate (SO_4^{2-}) concentration mirrors the alkalinity profile, decreasing to a concentration of 19 mM at 96 mbsf, then increasing back to 29.4 mM near 300 mbsf. Below 300 mbsf, there is a noticeable decoupling of the alkalinity-SO_4^{2-} relationship observed in the upper part of the hole. The titration alkalinity remains within a concentration window of 9 to 16 mM down to the 900 mbsf (deepest alkalinity sample measured), with several distinctive decreasing trends at 368, 620, and 794 mbsf. In contrast, the SO_4^{2-} concentration decreases sharply below 368 mbsf and is nearly completely depleted by a depth of 670 mbsf. The SO_4^{2-} concentration in the lower portions of the hole remains very low (1–3.5 mM).

At Site 1007, the concentrations of ammonium (NH_4^+) and phosphate (HPO_4^{2-}) range from 1 to 12.5 mM and 0.36 to 15 µM, respectively. Both profiles increase sharply below 21.9 mbsf and reach shallow maxima coinciding with the alkalinity peak between 96 and 130 mbsf. Farther downhole, the NH_4^+ concentration decreases to 2.1 mM at 368 mbsf, then increases gradually to 12.5 mM at 900 mbsf with several sharp decreases in the profile, as observed in the alkalinity profile. The concentration of HPO_4^{2-} in the lower portions of the hole (below 368 mbsf) is below 4 µM with the exception of one spike to 15 µM at 620 mbsf.

Calcium, Magnesium, Strontium, and Lithium

The calcium (Ca^{2+}) and magnesium (Mg^{2+}) profiles at Site 1007 display a roughly inverse relationship in the upper 368 mbsf. The Ca^{2+} concentration decreases from 10.89 mM at 5.9 mbsf to 9.3 mM at 96.1 mbsf, and then increases to 26.4 mM at a depth of 368 mbsf. Over the same interval, Mg^{2+} increases from 53.6 to 62 mM at a depth of 158 mbsf, and then gradually decreases to 59.3 mM at 368 mbsf. Below 368 mbsf, Ca^{2+} and Mg^{2+} covary and, (1) decrease to 11.5 and 26.3 mM, respectively, at 682 mbsf, and (2) remain near these concentrations to 928 mbsf. On a normalized basis, the Mg^{2+} concentration is always depleted, whereas the Ca^{2+} concentration is enriched only between 200 and 368 mbsf. Dissolved strontium (Sr^{2+}) increases from a bottom-water concentration of 120 to 794 µM at a depth of only 47.4 mbsf. Below this depth, Sr^{2+} concentrations remain between 700 and 1000 µM to a depth of 368 mbsf, and then increase sharply, reaching a maximum concentration of 4780 µM at 928 mbsf. Dissolved lithium (Li^+) concentrations generally track Sr^{2+} concentrations down to 368 mbsf, but display a smaller increase over the interval from 368 to 928 mbsf. Below 928 mbsf, the Li^+ concentrations increase sharply and part substantially from the decreasing trend observed in the Sr^{2+} profile at this depth.

Silica, Fluoride, pmH, and Iron

Silica (H_4SiO_4) concentrations are between 40 and 50 µM in the upper 24.9 mbsf, increasing to 300 µM at 96.1 mbsf (Fig. 21). Farther downcore, dissolved silica decreases gradually to 235 µM at a depth

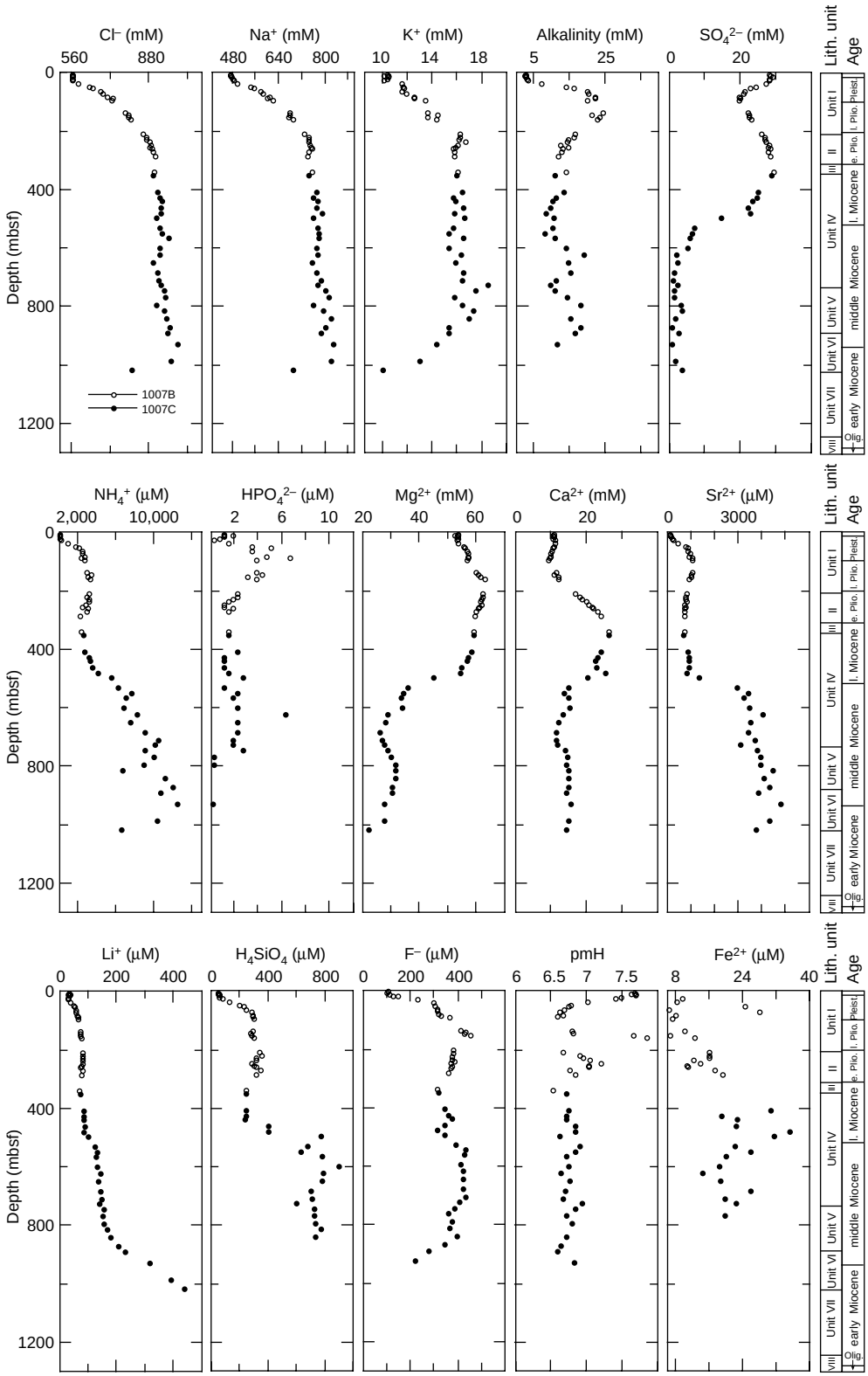

Figure 21. Depth profiles of interstitial water constituents at Site 1007.

Table 6. Composition of interstitial waters from Site 1007.

Core, section, interval (cm)	Depth (mbsf)	pmH	pH	Alkalinity (mM)	Salinity	Cl^- (mM)	Na^+ (mM)	Mg^{2+} (mM)	Ca^{2+} (mM)	SO_4^{2-} (mM)	HPO_4^{2-} (µM)	NH_4^+ (µM)	H_4SiO_4 (µM)	K^+ (mM)	Li^+ (µM)	Sr^{2+} (µM)	F^- (µM)	Fe^{2+} (µM)
166-1007B-																		
1H-4, 140–150	5.9	7.68	7.61	2.87	35.5	562	475	53.6	10.9	28.2	1.2	47	50	10.3	33	129	104	6
1H-6, 145–150	9.0	7.62	7.57	2.84	36.0	564	472	53.7	10.7	28.4	1.2	44	44	10.1	31	130	97	4
2H-2, 140–150	12.4	7.69	7.58	2.55	35.0	561	474	52.6	10.6	28.4	1.9	50	56	10.5	37	128	100	2
2H-4, 140–150	15.4	7.69	7.56	2.73	35.5	562	479	53.3	11.0	29.2	1.2	57	58	10.4	33	145	112	2
3H-2, 140–150	21.9	7.49	7.36	3.03	35.5	564	481	53.8	10.5	28.0	0.8	83	58	10.4	28	190	126	5
3H-4, 140–150	24.9	7.40	7.39	3.52	35.5	565	485	53.2	11.0	28.3	0.4	134	75	10.0	30	240	145	10
4H-5, 140–150	35.9	7.02	7.35	7.19	36.0	585	496	53.7	11.1	27.3	1.5	920	125	11.6	37	469	230	8
5H-5, 140–150	47.4	6.78	8.00	14.19	39.5	631	544	55.6	11.0	24.5	3.5	1,718	197	11.6	48	794	300	4
6H-3, 140–150	53.9	6.75	7.98	16.24	40.5	649	553	56.1	10.5	23.0	5.1	2,033	228	11.7	51	863	303	24
7H-5, 140–150	64.9	6.68	8.07	19.93	41.0	679	576	56.8	10.2	21.4	3.5	2,369	242	11.6	55	860	311	6
8H-4, 135–150	72.8	6.63	8.08	20.47	42.5	689	585	57.1	10.0	20.9	15.8	2,390	286	11.9	57	968	313	28
9H-4, 140–150	82.4	6.66	8.00	22.14	43.5	706	607	57.3	9.8	19.6	4.7	2,684	294	12.5	60	937	317	8
10H-2, 140–150	87.6	6.59	7.01	22.33	44.0	729	600	57.0	9.7	19.9	6.7	2,327	294	12.5	65	1,078	331	5
11X-3, 140–150	96.1		8.00	20.00	44.5	727	619	56.9	9.3	19.8	3.9	2,684	300	13.4	66	1,050	365	7
15X-5, 140–150	136.9	6.80	7.01	24.46	48.5	782	676	60.0	11.4	22.1	3.9	2,852	294	13.6	72	1,071	414	10
16X-3, 135–150	142.8	6.81	8.02	21.34	49.0	796	676	60.9	10.9	22.4	4.3	3,335	278	14.4	74	999	435	
17X-4, 135–150	153.2	7.66	8.05	23.63	49.5	796	674	61.3	12.1	22.5	3.1	2,999	286	13.6	73	1,004	428	7
18X-2, 0–15	158.3	7.84	8.05	22.88	49.5	803	689	63.0	12.0	23.1	3.9	3,188	297	14.3	77	898	456	12
23X-4, 135–150	209.0	6.66	6.94	16.45	53.5	858	729	62.5	16.8	26.1	2.3	3,167	339	16.2	79	824	381	16
24X-5, 135–150	219.8	6.90	7.53	16.42	54.0	870	744	62.3	18.2	26.9	2.3	2,894	350	16.2	79	765	383	16
25X-5, 135–150	228.8	6.95	7.49	14.76	54.0	871	743	61.8	18.8	27.0	1.9	3,146	317	16.1	79	789	378	16
26X-5, 135–150	238.0	7.05	7.64	14.35	54.0	88	742	61.5	19.9	27.4	1.6	3,167	317	16.7	79	806	378	12
27X-5, 135–150	247.2	7.20	7.41	12.46	55.0	888	748	62.0	20.5	28.2	1.2	2,747	286	16.1	83	747	386	14
28X-3, 135–150	253.4	7.03	7.26	14.57	54.5	882	752	61.0	21.5	28.0	1.2	2,432	300	15.9	76	755	373	11
29X-1, 135–150	259.8	7.03	7.27	13.03	55.0	894	754	60.6	21.7	28.4	1.9	3,020	312	15.7	74	721	377	11
30X-2, 135–150	270.6	6.76	7.98	12.68	55.5	897	742	60.0	23.1	27.9	1.6	2,873	343	15.8	79	754	370	17
32X-1, 135–150	287.4	6.85	7.82	11.75	55.0	905	738	59.4	24.0	28.4		2,159	318	15.8	75	723	361	19
38X-1, 0–11	341.1	6.53	7.95	13.92	55.0	901	755	59.2	26.3	29.4	1.6	2,285	242	16.0	71	708	311	
166-1007C-																		
6R-2, 0–10	351.4	6.71	7.01	11.07	55.0	897	745	59.3	26.4	28.7	1.6	2,495	241	16.0	73	704	316	
12R-2, 123–135	409.8	6.75	7.00	13.52	56.5	917	771	58.5	24.1	25.1	2.3	2,663	247	16.4	83	869	347	31
14R-1, 112–122	428.1	6.71	7.67	11.29	56.0	923	759	57.1	23.1	24.8	1.2	3,083	245	15.7	86	917	361	19
15R-3, 83–94	440.4	6.71	6.88	10.31	56.5	934	773	56.7	22.5	23.3	1.2	3,272	235	15.9	86	941	374	23
17R-6, 99–114	463.3	6.85	7.65	9.80	56.0	932	769	54.8	22.9	22.2	1.2	3,524	403	16.5	87	935	346	23
19R-3, 134–145	479.1	6.85	6.94	8.39	56.0	931	788	54.6	25.5	22.8	1.6	4,049	401	15.8	84	843	313	35
21R-2, 130–142	497.0	6.63	7.02	10.50	54.5	912	760	44.8	20.4	14.8	2.7	5,435	769	16.6	99	1,347	344	31
24R-5, 136–144	530.4	6.90	7.26	10.21	53.5	926	773	35.9	14.8	7.1	1.2	6,170	674	15.7	123	2,960	389	22
26R-6, 105–121	549.4	6.85	7.12	8.18	53.0	934	780	34.2	13.8	6.4	2.3	7,598	630	15.4	130	3,401	435	26
28R-3, 103–116	565.3	6.71	7.65	10.79	53.0	961	779	33.6	14.8	5.7	1.9	7,031	779	16.5	129	3,237	429	20
31R-6, 105–121	597.5	6.75	7.69	13.96	54.0	925	772	33.8	15.4	5.3	2.3	6,842	895	15.3	134	3,462	414	18
34R-1, 135–152	620.8	6.64	7.38	19.06	54.0	925	776	29.0	13.4	2.1	6.3	8,228	786	16.3	143	4,030	423	14
37R-1, 0–12	648.3	6.76	7.11	14.74	52.0	899	754	27.9	12.1	2.2	2.3	7,472	775	15.8	137	3,504	424	19
40R-4, 139–150	682.2	6.70	7.06	15.35	52.0	914	772	26.3	11.5	1.5	2.3	8,984	698	16.5	145	3,443	424	26
43R-2, 79–92	708.3	6.66	7.00	11.20	52.5	920	785	27.0	11.5	1.2	1.9	10,433	705	16.4	147	3,725	431	20
45R-2, 0–12	726.7	6.93	7.23	9.58	52.5	930	774	27.6	11.8	2.2	1.9	10,139	599	18.5	141	3,095	405	23
47R-2, 0–14	745.7	6.85	7.28	10.94	54.0	945	803	28.7	14.1	1.3	2.7	9,068	725	17.6	154	3,802	388	
49R-2, 112–124	766.3	6.71	7.09	14.43	54.0	951	811	29.9	14.7	1.3	0.4	10,034	723	15.8	152	3,960	358	20
52R-2, 31–44	794.4	6.80	7.18	18.05	54.0	911	760	31.7	14.4	3.2	0.4	8,879	731	16.5	154	3,920	377	
54R-3, 9–16	814.8				54.0	943	793	31.4	15.0	3.5		6,632	771	17.3	168	4,465	364	
57R-2, 0–10	842.1	6.71	7.11	15.35	54.5	955	820	31.4	15.0	1.7		11,131	729	17.0	180	4,095	395	
60R-1, 98–113	870.5	6.64	7.04	18.21	55.5	968	801	30.3	14.9	0.8		12,015		15.4	208	4,330	347	
62R-2, 0–13	890.1	6.59	6.97	16.68	55.0	957	786	30.3	14.2	2.5		10,655		15.4	232	3,830	277	
66R-2, 28–39	929.0	6.83	7.04	11.48	56.5	1,001	827	27.6	15.5	0.7	0.3	12,491		14.3	317	4,780	218	
72R-2, 0–5	986.4				55.5	971	820	27.6	15.1	1.8		10,281		12.9	391	4,300		
75R-1, 50–60	1014.4					809	688	22.3	14.2	3.5		6,592		10.0	439	3,740		

of 463 mbsf, after which there is a sharp increase to a maximum concentration of 895 µM at 597 mbsf. The concentration of dissolved fluoride (F^-) reaches a high of 456 µM between 158 and 209 mbsf. Below 209 mbsf, F^- remains between 311 and 423 µM, before decreasing sharply below 950 mbsf.

The pmH decreases from 7.68 to 6.6 in the upper 100 mbsf at Site 1007 and remains between 6.5 and 7.1 throughout the lower part of the hole. Two samples at 153 and 158 mbsf have anomalously high pmH values of 7.66 and 7.85, respectively. Iron concentrations (Fe^{2+}) are highly variable at Site 1007. With the exception of two samples at 53 and 73 mbsf, Fe^{2+} remains fairly low within the upper 200 mbsf (5–14 µM). There is a noticeable increase in Fe^{2+} concentrations between 200 and 500 mbsf, where it reaches the highest concentration (31 µM) at 409 mbsf. During the squeezing of this interval, a black precipitate was observed to form in the syringes within several minutes after interstitial water entered the syringe. The precipitate, which went back into solution when acidified, is thought to be an iron-sulfide precipitate of some type.

Discussion of Pore-Water Chemistry

The upper 22 m of Site 1007 shows no significant changes in any of the dissolved constituents, which is consistent with the zone of active flushing observed at Sites 1003–1006. The more conservative ions (Cl^-, Na^+, and K^+) all increase downhole at Site 1007, suggesting that a salt source such as halite (NaCl) may be located at some deeper depth below the platform margin. The lowermost two samples collected (Samples 166-1007C-72R-2 and 75R-5 at depths of 986 and 1014 mbsf, respectively) show a sharp decrease in Cl^- and Na^+ that was not observed at any of the other sites. As a result of the small volumes of interstitial water collected from these samples (<2 mL), it is not unreasonable to expect some contamination from drilling fluids. However, the low SO_4^{2-} concentration (1.77 and 3.5 mM, respectively) does not indicate substantial contamination by drilling fluids (SO_4^{2-} = 28.9 mM). Two other possible explanations for the decrease in Na^+ and Cl^- at these deeper depths are (1) horizontal fluid movement above and/or below the 1000 mbsf boundary carrying different formation fluids, or (2) a major increase in the compaction pressure across this boundary that moves Cl^- and Na^+ out of the lower sediments. Compaction fractures have been observed in the deeper sediments at Site 1007 (see "Lithostratigraphy" section, this chapter). A compaction mechanism that alters pore-fluid salinity has been documented in shales and sands (Chilingar and Rieke, 1975), but not to our knowledge in marine carbonates.

Changes in alkalinity, SO_4^{2-}, NH_4^+, HPO_4^{2-}, and pmH profiles between 30 and 150 mbsf are interpreted to be caused by the microbial consumption and oxidation of primary organic matter. The lower amounts of sulfate reduction observed at Site 1007 probably result from the lower amounts of organic material buried in these more distal sediments (see "Organic Geochemistry" section, this chapter). There is a major change in the sulfate profile below 368 mbsf. The sharp loss of SO_4^{2-} below 368 mbsf also coincides with an increase in the dissolved pore-water Fe^{2+}, possibly derived from the numerous clay layers present throughout these upper and middle Miocene sediments (see "Lithostratigraphy" section, this chapter). Reactive iron has a major influence on sulfur pathways, and most commonly reacts with microbially generated HS^- to produce pyrite and other iron sulfides, such as mackinawite and greigite (Berner, 1970). Similarly, the low amount of dissolved Fe^{2+} measured in the upper 368 mbsf at Site 1007 allows reduced sulfur compounds to be oxidized to elemental sulfur or sulfate (Canfield, 1989).

The changes in Ca^{2+} and Mg^{2+} at Site 1007 are also influenced by the lithostratigraphic boundary at 368 mbsf. In the upper sediments, the relatively small changes in the elements indicate lower amounts of carbonate diagenesis than observed at the more proximal sites, Sites 1004 and 1005. Below 368 mbsf, the changes in Ca^{2+} and Mg^{2+} are more pronounced, suggesting that significant dolomite may be forming in this lower interval (see "Inorganic Geochemistry" section, "Site 1004" chapter, this volume). Significant amounts of dolomite are present in these lower sediments (see following mineralogy discussion). However, the amount of dolomite formed by the pore fluid is difficult to assess because of a charge imbalance that seems related to the Mg^{2+} deficiency (see the following discussion).

The Sr^{2+} concentrations measured in pore fluids are controlled by the dissolution and alteration of aragonite, and the precipitation of calcite and celestite as discussed for Site 1005 (see "Inorganic Geochemistry" section, "Site 1005" chapter, this volume). In the upper zone, the high concentration of SO_4^{2-} limits the pore-water Sr^{2+} concentration as a result of the formation of $SrSO_4$. Below 368 mbsf, the decrease in SO_4^{2-} allows Sr^{2+} to build up in pore fluids. The Li^+ in the upper 368 mbsf is probably derived from the dissolution of biogenic aragonite. Below 900 mbsf, the increase in Li^+ is interpreted to be caused by an increased abundance of insoluble residues and clays (see the following discussion on mineralogy).

Charge Balance of Pore Fluids

Preliminary inspection of the charge balance of pore fluids at Site 1007 (and other transect sites as well) indicates that the balance is largely negative, ranging from 1 to 85 meq excess negative charge (Fig. 22A). This is outside of the expected range based on the analytical precision of each of the analyses conducted (see "Inorganic Geochemistry" section, "Explanatory Notes" chapter, this volume). At this time we have no explanation for the large imbalance. The extent of the negative charge imbalance increases downcore, suggesting that it may be related to an unidentified ion or ion-pair rather than a systematic underestimation of a single cation, such as sodium. An interesting observation is that the charge imbalance covaries with the normalized Mg^{2+} concentration of the solution (Fig. 22B). In other words, for each millimole/liter of Mg^{2+} removed from the system (normalized decrease of 1 mM), there is an associated negative charge imbalance of 1 meq. This correlation suggests that Mg^{2+} may be forming an ion pair that satisfies the demands of neutral charge within the solution, but is somehow not measured by our analytical

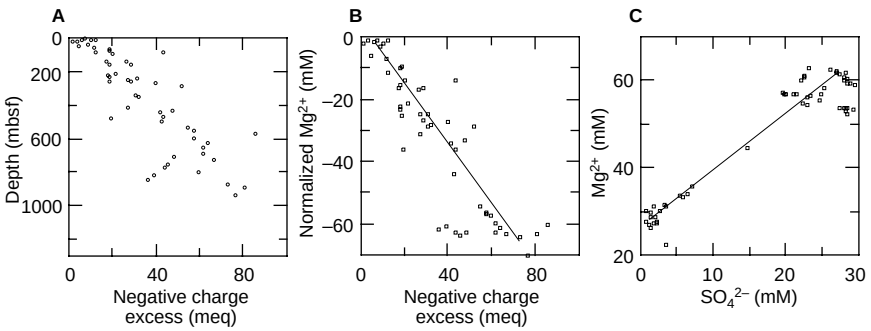

Figure 22. **A.** Profile of charge balance at Site 1007. **B.** Relationship between normalized Mg^{2+} concentration of pore fluids and charge balance (see text for explanation). **C.** Relationship between Mg^{2+} and SO_4^{2-}.

methods. The correlation of normalized Mg^{2+} and SO_4^{2-} within the interstitial waters also suggests that SO_4^{2-} may be involved in this charge imbalance phenomenon (Fig. 22C).

Mineralogy

The carbonate mineralogy at Site 1007 shows similar patterns to those observed in the four other transect sites (Table 7 on CD-ROM). Aragonite is abundant in the upper 180 mbsf, averaging 65–70 wt% and shows several pronounced cycles, but drops sharply below 200 mbsf, to less than 7 wt%. This drop coincides with the lower/upper Pliocene boundary at 203.1 mbsf (see "Biostratigraphy" section, this chapter). Deeper downhole (>203 mbsf), the aragonite content varies within distinctive lithologic cycles from 0 to 40 wt%. This cyclicity continues down to a depth of 1000 mbsf, below which aragonite was not detected in the sediments.

High-magnesium calcite (HMC) is present only in the upper 180 m of sediment at Site 1007, ranging from 0 to 27 wt%. Overall, the amount of HMC observed at Site 1007 is substantially lower than in sediments of comparable age in the more proximal transect Sites 1003–1005. This difference probably reflects lower inputs of platform-derived biogenic HMC and the decreased influence of HMC marine-floor cementation at Site 1007. The transition from HMC to low-magnesium calcite (LMC) seafloor cements occurs as a function of decreasing temperature and increasing pressure (Schlager and James, 1978; Videtich, 1985). Present-day bottom-water temperature measurements at Site 1007 are substantially lower (~10°C) than at Sites 1003–1005 (~15°–18°C) because of the differences in water depth (see "In Situ Temperature Measurements" section, this chapter). The current bottom-water conditions, therefore, may favor the formation of LMC cements over HMC cements at Site 1007.

Trace amounts of dolomite (<3 wt%) were detected throughout the upper 150 mbsf at Site 1007, with a notable peak of 5 wt% at 90.6 mbsf. Below 180 mbsf, the dolomite content increases to 3–14 wt%, with a peak occurring around the lower/upper Pliocene boundary at 203.1 mbsf. Farther down in the hole, the dolomite content ranges from 0 wt% to 40 wt% and is distributed in distinctive cycles down to a depth of 900 mbsf. There is a 40-m-thick sequence of partially dolomitized rocks beginning at 600 mbsf, which corresponds to a major change in the gamma-ray and acoustic velocity signals recorded in the downhole logs (see "Downhole Logging" section, this chapter). Below 900 mbsf, dolomite decreases in abundance to the base of the hole.

Quartz abundance varies greatly at Site 1007. From 0 to 200 mbsf, quartz content is very low (0–0.5 wt%). Between 200 and 600 mbsf, the concentration of quartz increases up to 1.2 wt%, showing several distinctive cycles. Below 600 mbsf, quartz decreases below 0.5% to a depth of 1000 mbsf, after which it increases to 1–3 wt% to 1181 mbsf. A particularly high quartz peak that occurs at 1094 mbsf may be associated with the presence of cherts. No quartz was detected below 1181 mbsf, though several large chert nodules were recovered within the cores (see "Lithostratigraphy" section, this chapter). The distribution of quartz at Site 1007 agrees well with the insoluble residue measurements, indicating that the majority of the quartz is associated with clay-rich intervals, and is detrital in origin. Other diagenetic minerals observed at Site 1007 include small amounts of pyrite, celestite, and glauconite (see "Lithostratigraphy" section, this chapter).

The high-resolution XRD analysis conducted on a 1-m-thick clay-rich cycle in Section 166-1007C-18R-3 (467–468 mbsf) shows several interesting features. Most noticeably, the aragonite content increases within the dark, clay-rich interval, as do the contents of quartz and insoluble material (Fig. 20). Conversely, the dolomite content decreases through the layer. This pattern is interpreted to reflect cyclic changes in the rate of neritic carbonate input, and the subsequent impact on the diagenetic potential of the sediments. In addition, clays and organic matter present within the darker layers (see "Organic Geochemistry" section, this chapter) may reduce the permeability enough to minimize reactant exchange with the ambient fluid. These layers also display a low acoustic velocity and a lack of cements, which is consistent with the low degree of diagenetic alteration observed (see "Physical Properties" section, this chapter).

PHYSICAL PROPERTIES

Measurements of physical properties at Site 1007 were conducted following the procedures described in the "Physical Properties" section of the "Explanatory Notes" chapter (this volume). Three discrete *P*-wave velocity measurements, two shear strength measurements, and one index property sample were taken in every section of unconsolidated core at Hole 1007A and down to Core 6H (57 mbsf) at Hole 1007B. In semilithified cores, the sampling interval for the velocity measurement was increased to approximately five per section. Thermal conductivity was measured at Hole 1007B on unconsolidated whole-round cores with a frequency of one per section down to Core 27X (247 mbsf).

The following describes the downhole variation in petrophysical properties and their correlation with lithostratigraphy. Variations in magnetic susceptibility are described within the "Paleomagnetism" section (this chapter).

Index Properties, GRAPE Density, and *P*-Wave Velocity

Tables 8 through 13 on CD-ROM summarize the measurements of index properties, discrete DSV velocity, GRAPE density, PWL velocity, magnetic susceptibility, and NGR at Site 1007.

Petrophysical properties at Site 1007 show a general downhole trend of increasing velocity and bulk density and decreasing porosity (Fig. 23). Baseline *P*-wave velocity increases downcore from 1.5 to 3.0–3.5 km/s, and bulk density increases from 1.75 to 2.3–2.4 g/cm^3, whereas porosity shows an overall downcore decrease from 55% at the seafloor to approximately 20% at 1228 mbsf. Natural gamma ray has a baseline radiation that remains nearly constant at 10 cps to total depth at Site 1007. Superimposed on these trends are strong positive deviations that usually coincide with downhole changes in lithology.

Comparison of DSV velocities with the velocity data obtained from the sonic log (Fig. 24) shows a pattern similar to that recognized at previous Leg 166 sites. Measured velocities of consolidated rocks show excellent agreement between the two methods, whereas DSV values of low-velocity zones (baseline) show negative departures from the log values. This velocity difference increases with depth until the base of petrophysical Unit IV. This pattern may be partially explained by the lack of effective pressure during DSV measurements, whereas the in situ effective pressure at 1000 mbsf assuming hydrostatic conditions is approximately 10 MPa. However, the fact that DSV velocities agree well with sonic log velocities below 1000 mbsf in homogeneous, low-velocity petrophysical Unit VI could indicate that most of the discrepancy observed is related to the limited resolution of the logging tool, which cannot recognize the lowest velocities of the thin cycles in the middle to upper Miocene sediments.

On the basis of deviations from the baseline trends of velocity, bulk density, porosity, and gamma ray, seven petrophysical units were defined. Petrophysical Unit I (0–360 mbsf) shows a narrow overall range in V_p, with a downcore baseline increase from 1.5 to approximately 2.0 km/s. Superimposed on this increase are several sharp peaks in velocity (up to 4 km/s). Bulk density increases in the same interval from 1.75 to 2.2 g/cm^3, whereas porosity decreases from 55% to 35%. The peaks in V_p coincide with several intervals of higher bulk density to 2.3 g/cm^3, which alternate with intervals of lower bulk density and velocity. On the basis of this alternation, petrophysical Unit I was divided into nine subunits (Fig. 25). Subunit Ia (0–1.8 mbsf) has low bulk density (GRAPE density) of 1.65 to 1.7 g/cm^3 and velocity of 1.5 to 1.55 km/s, which sharply increase down-

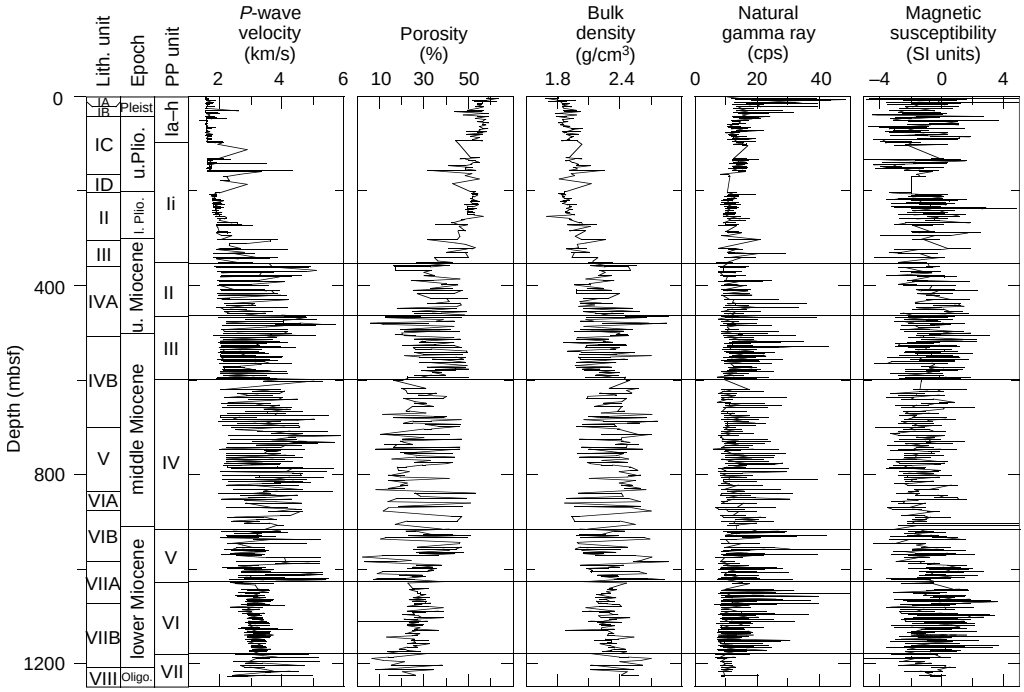

Figure 23. Combined plot of *P*-wave velocity, porosity and bulk density from discrete measurements, natural gamma ray, and magnetic susceptibility from the MST from Site 1007. Lithologic and petrophysical units are indicated along with age.

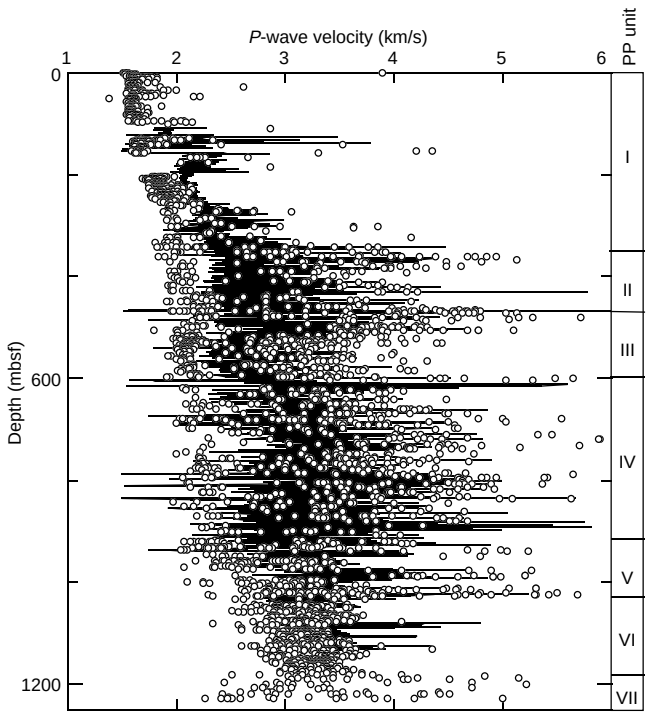

Figure 24. Combined plot of discrete *P*-wave velocity measurements on split core (points) and sonic velocity from well logs at Site 1007.

core in Subunit Ib to values of 1.9 g/cm^3 and 1.55 to 1.6 km/s, respectively. In addition, Subunit Ia has low gamma ray, close to background levels, and high magnetic susceptibility. Petrophysical Subunits Ib through Ih show a downcore increase in thickness, or distance, between layers of high bulk density and velocity. Peaks in velocity and bulk density commonly coincide with elevated gamma-ray values (up to 30–50 cps). Color reflectance data show an inverse correlation with velocity and bulk density (Fig. 25) that refines the high-frequency rhythmic variation in petrophysical properties in this unit. Petrophysical Subunit Ii (94–360 mbsf) has two intervals of poor recovery that are most likely more indurated layers with elevated velocities. Near the bottom of the unit, at approximately 300 mbsf, there is a significant increase in the velocity range from 1.9 to nearly 4.0 km/s. The boundary between petrophysical Units I and II shows an abrupt downcore increase in velocity and bulk density.

Petrophysical boundaries within petrophysical Unit I correlate well with lithologic boundaries. The transition between petrophysical Subunits Ib and Ic corresponds with the boundary between lithologic Subunits IA and IB at a thin floatstone layer. The transition between petrophysical Subunits If and Ig corresponds with the boundary between lithologic Subunits IB and IC, marked by a change from foraminifer mud to wackestone and a hardground, and with the Pliocene/Pleistocene boundary. The abrupt downcore increase in velocity and bulk density observed at 300 mbsf corresponds to the boundary between lithologic Units II and III. This boundary coincides with the appearance of turbidites and a lithologic change from nannofossil chalk to wackestone and is presumed to be close to the Miocene/Pliocene boundary.

Petrophysical Unit II (360–465 mbsf) has a high range in physical properties measurements superimposed on a nearly constant base level. Velocity shows a downcore decrease from 2.0 to 5.0 km/s to 2.0 to 3.5 km/s. Bulk density and porosity have values between 1.95 and 2.5 g/cm^3 and 20% and 45%, respectively. Natural gamma ray and magnetic susceptibility show a large range in values, but no clear trend with depth. The boundary with the underlying petrophysical

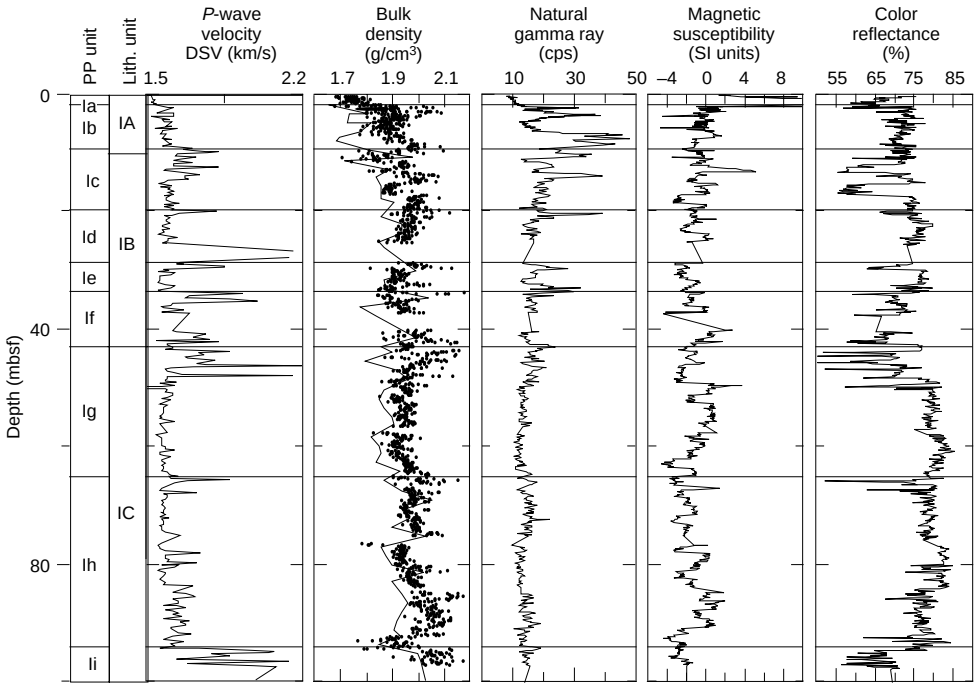

Figure 25. Summary of *P*-wave velocity from the DSV, bulk density from discrete measurements (points) and GRAPE density (line), natural gamma ray, magnetic susceptibility, and color reflectance for the interval to 100 mbsf. Petrophysical and lithologic units are indicated.

Unit III shows a sharp downcore increase in velocity and bulk density and a decrease in porosity. It does not correspond to a lithostratigraphic boundary, but is only 17 m above the middle/upper Miocene boundary.

Petrophysical Unit III (465–600 mbsf) is similar in character to Unit II, but as a result of higher recovery it has better-defined petrophysical trends. Velocity decreases downcore from values between 2.0 and 5.0 km/s to values between 2.0 and 3.5 km/s. Bulk density shows a decrease from 2.1 to 2.5 g/cm^3 to values between 1.95 and 2.3 g/cm^3. Porosity changes from between 15% and 40% to between 30% and 50%. The large range in petrophysical properties reflects the alternation between light- and dark-colored foraminiferal wackestone to packstone intervals (see "Lithostratigraphy" section, this chapter). Light-colored intervals have higher acoustic velocities and lower gamma-ray emissions than do dark-colored intervals.

To investigate the cyclicity within this unit, high-resolution sampling for V_p, calcium carbonate content, aragonite content, and color reflectance was conducted for the length of one cycle (Fig. 26). Results show that within the darker clay-rich intervals (indicated by low color reflectance), *P*-wave velocities and calcium carbonate contents decrease, whereas the aragonite content increases. These differences between light and dark intervals may: (1) record a preservational signal, wherein the clay acts as a seal preventing diagenetic alteration of the aragonite; or (2) reflect differences in the primary diagenetic potential of the sediments (see "Lithostratigraphy" section, this chapter). The transition into the clay layer within one of these cycles shows a sharp lower boundary for both *P*-wave velocity and aragonite content, with a more gradual change at the top of the clay unit (Fig. 26).

The transition to petrophysical Unit IV is marked by a slight increase in the average velocity and bulk density and a subsequent decrease in porosity. There is no corresponding change in lithology or age. The range in petrophysical properties within petrophysical Unit IV (600–920 mbsf) remains fairly constant throughout this unit, but still shows the cyclicity of Units II and III. Velocity has values between 2.0 and 4.5 km/s, bulk density ranges from 1.95 to 2.45 g/cm^3, and porosity varies between 10% and 40%. Unit IV spans most of lithologic Subunit IVB, Unit V, and Subunit VIA, which consist mostly of alternating dark- and light-colored foraminifer wackestone to packstone. The lower boundary with petrophysical Unit V, which is marked by a decrease in average velocity, has no equivalent lithostratigraphic transition and is close to the dated lower/middle Miocene boundary (910 mbsf).

Although displaying considerable scatter, petrophysical Unit V (920–1025 mbsf) shows a gradual downcore increase in velocity and bulk density and a decrease in porosity. In addition, the range in velocity is slightly reduced. Velocity increases downcore from values between 2.2 and 3.0 km/s to between 2.6 and 5.0 km/s, whereas bulk density and porosity remain fairly constant and range between 1.95 and 2.45 g/cm^3 and 10% and 50%, respectively. The transition to petrophysical Unit VI is an abrupt downcore change to a narrow and confined range in velocity, porosity, and bulk density. No changes in lithology or age correspond to this boundary.

Compared with the units above, velocity and bulk density within petrophysical Unit VI (1025–1180 mbsf) show monotonous values with a gradual downcore increase within a narrow range; velocity increases from between 2.5 and 3.0 km/s to 2.8 and 3.3 km/s, whereas bulk density increases from 1.95 to 2.25 g/cm^3 to values from 2.1 to 2.4 g/cm^3. Porosity gradually decreases to values between 15% and 25%. Unit VI corresponds to an alternation of grayish foraminifer packstone and thin, decimeter-scale, clay-rich (up to 50% noncarbonate matter) layers that form most of lithologic Subunit VIIB. However, the clear and sharp transition at the top of petrophysical Unit VI has no equivalent lithologic boundary. The sediments within lithologic Subunit VIIB are monotonous in structure, as seen in the physical property data. In contrast, the transition to petrophysical Unit VII coincides with the boundary between lithologic Subunit VIIB and Unit VIII, which is marked by the appearance of black chert nodules.

Petrophysical Unit VII (1180–1230 mbsf) indicates a downcore return to a larger range in velocity, bulk density, and porosity. Velocity ranges between 2.5 and 4.5 km/s, bulk density varies between 2.1 and 2.6 g/cm^3, and porosity ranges from 10% to 35%. This sharp petrophysical and lithologic change is located some 35 m above the Oligocene/Miocene boundary (1214 mbsf).

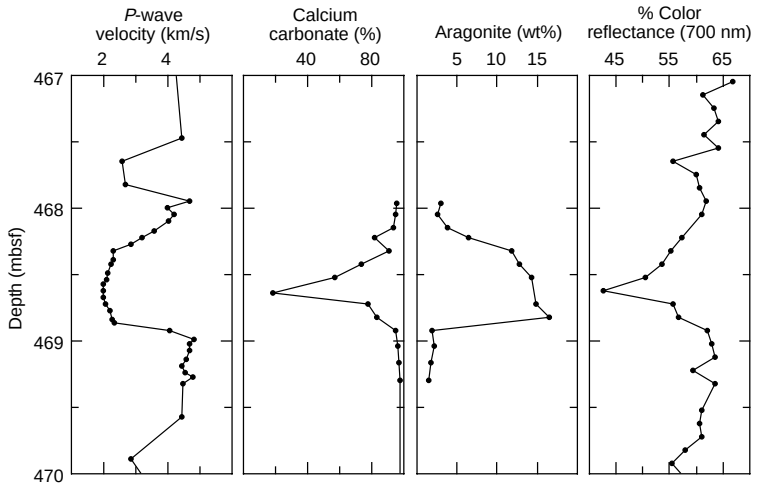

Figure 26. Combined plot of sonic velocity from the DSV, carbonate content, aragonite content, and color reflectance for the interval between 467 and 470 mbsf at Hole 1007C. See text for discussion.

Shear Strength

Shear strength was measured on cores from Holes 1007A and 1007B down to a depth of 14 mbsf (Table 14 on CD-ROM; Fig. 27). Below this depth the sediment is partially lithified, with shear strength values exceeding 150 kPa, and subsequently shear-vane measurements were discontinued. Shear strength at Site 1007 remains fairly constant down to 14 mbsf and has values between 2 and 30 kPa. Similarly, the S_u/P_o' has values below 0.4 and does not display any trend with depth.

Thermal Conductivity

A total of 104 thermal conductivity measurements were made on the sediments of Hole 1007B from 0 to 247 mbsf. Results of the individual measurements are shown in Table 15 on CD-ROM and Figure 28. The thermal conductivity values in the upper 30 mbsf vary between 0.95 and 1.25 W/(m·K). Below this depth, the baseline value of the thermal conductivity increases linearly with depth from 1.05 to 1.15 W/(m·K) at about 220 mbsf. This probably reflects downcore compaction of the sediments. The number of measurements from 100 through 130 mbsf and from 160 through 200 mbsf is limited because of poor core recovery. The average conductivity (1.27 W/[m·K]) is greater than that of any of the previous sites, as is the standard deviation (0.14 W/[m·K]).

DOWNHOLE LOGGING

Logging Operations

During the drilling and coring of Hole 1007C, bentonite mud sweeps were injected into the hole to help clean out the cuttings. Three such wiper trips were performed during drilling (see "Operations" section, this chapter). After drilling operations ended, the borehole was prepared for logging by performing another wiper trip, but no mud was used, and only seawater was circulated in the hole to clean out cuttings (see "Operations" section, this chapter). The lower limit of the bottom-hole assembly (BHA) was placed at 111 mbsf. We deployed two tool strings in the following order: Quad-combo and the well seismic tool (WST) (Fig. 29). The wireline heave compensator was employed to offset the ship's heave, which was of the order of 1 m full amplitude.

The decision to run the Quad-combo instead of the integrated porosity-lithology tool (IPLT) and induction-sonic strings was based on time constraints. The tool logged from 60 m above the total drilled depth and through pipe to the seafloor. The BHA was lifted 15 m during the final check-shot stations to reduce acoustic noise and to attempt clamping the tool at as shallow a depth as possible. Unfortunately, the tool did not clamp above 330 mbsf because of the enlarged hole diameter. At the end of the logging run, the WST tool would not reenter the pipe, requiring crimping and cutting the wireline above the tool head. The tool was retrieved with damage to the mechanical parts. Mud lodged inside the caliper mechanism had prevented it from closing fully.

Data Quality

The caliper log (Fig. 30) shows that the borehole was enlarged several centimeters beyond the bit size (25.1 cm) through most of the interval logged. The enlarged borehole prevented us from logging with the Formation MicroScanner tool and degraded the quality of the logs acquired with the Quad-combo tool string. Above 350 mbsf, the HLDT caliper remained constant at its maximum value (18 in or 45.7 cm), and the hole diameter must have been greater than 48 cm above 330 mbsf, because we were unable to clamp the WST tool in this interval.

Bulk-density data above 320 mbsf read consistently below the index property values measured on core samples. These log data, together with the photoelectric effect measurements, are probably not valid because of poor pad contact with the borehole wall. The data have been omitted from Figure 30. Further processing and analysis will be required to fully evaluate the quality of the density tool data.

Neutron porosity was measured with the compensated neutron tool (CNT-G), which uses a chemical source of neutrons instead of the minitron in the accelerator porosity sonde (APS) used at the other sites logged during Leg 166 (see "Explanatory Notes" chapter, this volume). Comparison with physical property measurements indicates that these porosity data are probably of good quality (Fig. 30). Although we do not have a direct comparison between the two porosity tools in the same hole, data from the APS tool in enlarged holes (e.g., see Fig. 28 of "Downhole Logging" section, "Site 1003" chapter, this volume, above 250 mbsf) read significantly lower than index property measurements. Over the enlarged section above 300 mbsf in Hole 1007C, neutron porosity values from the CNT-G are comparable to values measured in core. Tool contact with the borehole wall above 350 mbsf may have been maintained if the borehole was slightly deviated, resulting in good porosity measurements even in the enlarged section. Alternatively, the CNT-G tool, with sensors central-

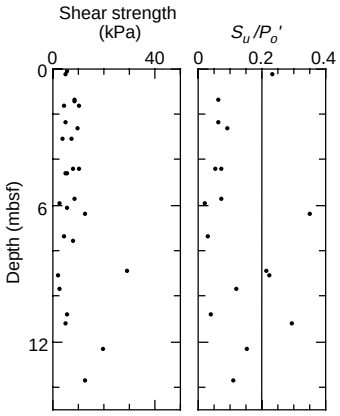

Figure 27. Shear strength and S_u/P_o' calculated from shear strength and overburden stress for cores from Hole 1007A.

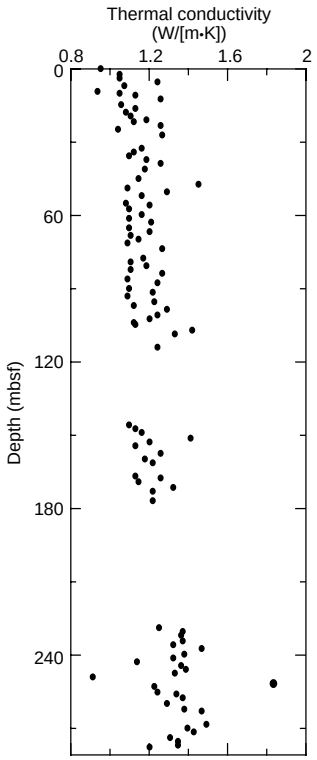

Figure 28. Thermal conductivity for Hole 1007A.

ized in the tool housing (vs. the focused sensors in the APS), may be less sensitive to poor borehole conditions.

The gamma-ray data require correction for borehole diameter variations before detailed analysis is possible, but changes observed in the unprocessed logs, such as the pronounced spikes through most of the logged interval, are clearly independent of changes in borehole diameter (Fig. 30).

Induction resistivity measurements are somewhat less sensitive to borehole diameter variations (Schlumberger, 1989). Some correlation with caliper variations can be clearly noted, but the broad changes in hole diameter (smaller diameter = more resistive intervals) are also likely related to lithification, porosity, and lithologic changes in the formation.

The sonic log displays a large number of invalid measurements, resulting from cycle skipping and noisy traces. The log shown in Figure 30 was edited for both very low and very high values. Comparison with measurements in core plugs and unconsolidated cores shows that low values in the cores are probably too low because of core disturbance and decompaction. The high values in the core data agree well with the log values, probably because in lithified and cemented samples the effect of decompaction and core disturbance is minimal (see "Physical Properties" section, this chapter).

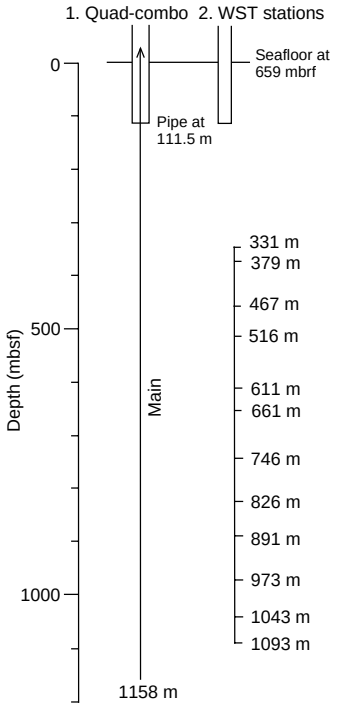

Figure 29. Summary of the logging runs in Hole 1007C. The logging speed for the Quad-combo tool string was 275 m/hr. Sonic traveltime was recorded with the WST at 12 stations. See "Explanatory Notes" chapter (this volume) for description of the tool strings.

Twelve check-shot stations were recorded with the WST (Fig. 29). About five air gun shots were stacked in each station, the stacked traces show good consistency and little noise. The results are discussed in the "Seismic Stratigraphy" section (this chapter).

Preliminary Observations

Geophysical and geochemical data acquired during the logging of Hole 1007C in the interval from 111 to 1155 mbsf provide detailed information on the sedimentary properties and structure of the strata that is especially important for intervals of poor core recovery. As sediment recovery below 111 mbsf was variable, averaging about 50%, the logs can provide additional information about Site 1007 that can be correlated with data gleaned from the core record. Log-to-core correlation permits significant interpretation about variation in the sedimentation patterns adjacent to the Great Bahama Bank from the earliest early Miocene (approximately 23.2 Ma) to the present. The changes recorded in the logs can be traced west and eastward to the GBB along the seismic sequence boundaries, providing a tie of the sedimentation patterns at Site 1007 to other drill sites across the platform margin and on the platform top.

Figures 30 and 31 contain compilations of the logged data plotted against depth in the section and related to core recovery, biostratigraphic age, lithologic units, and physical property laboratory data measured in discrete samples and whole-core sections. The general compatibility of the discrete points with the data obtained from the total logged interval supports the integrity of the data sets, apart from

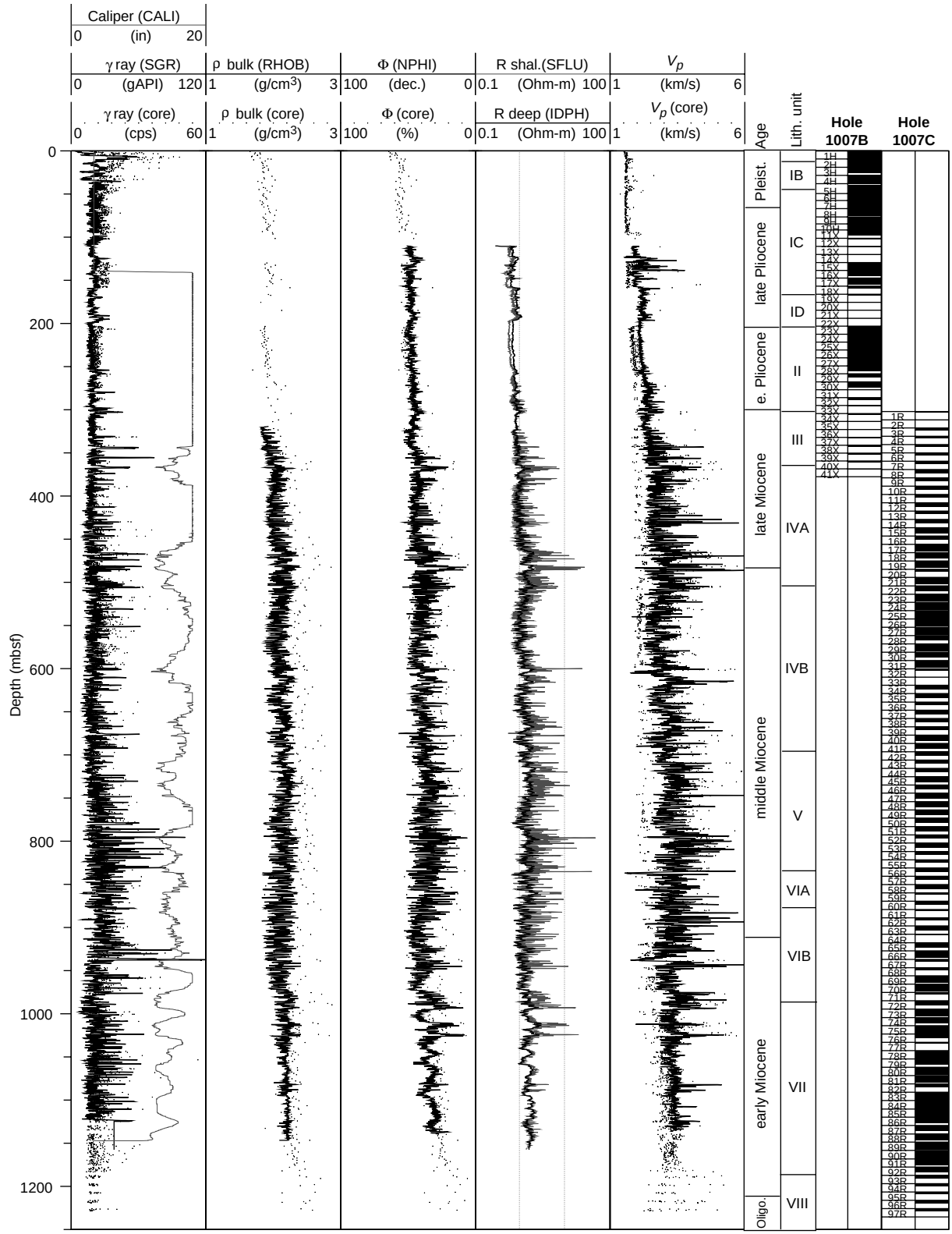

Figure 30. Summary of key geophysical logs acquired with the Quad-combo tool string. From left to right, columns are gamma ray and caliper, bulk density (ρ bulk), porosity (**Φ**), shallow and deep resistivity (R), sonic velocity (V_p), age, lithologic units, and core recovery. The points represent core measurements from the MST (natural gamma ray) and index properties (bulk density, porosity, and velocity) from the DSV instrument.

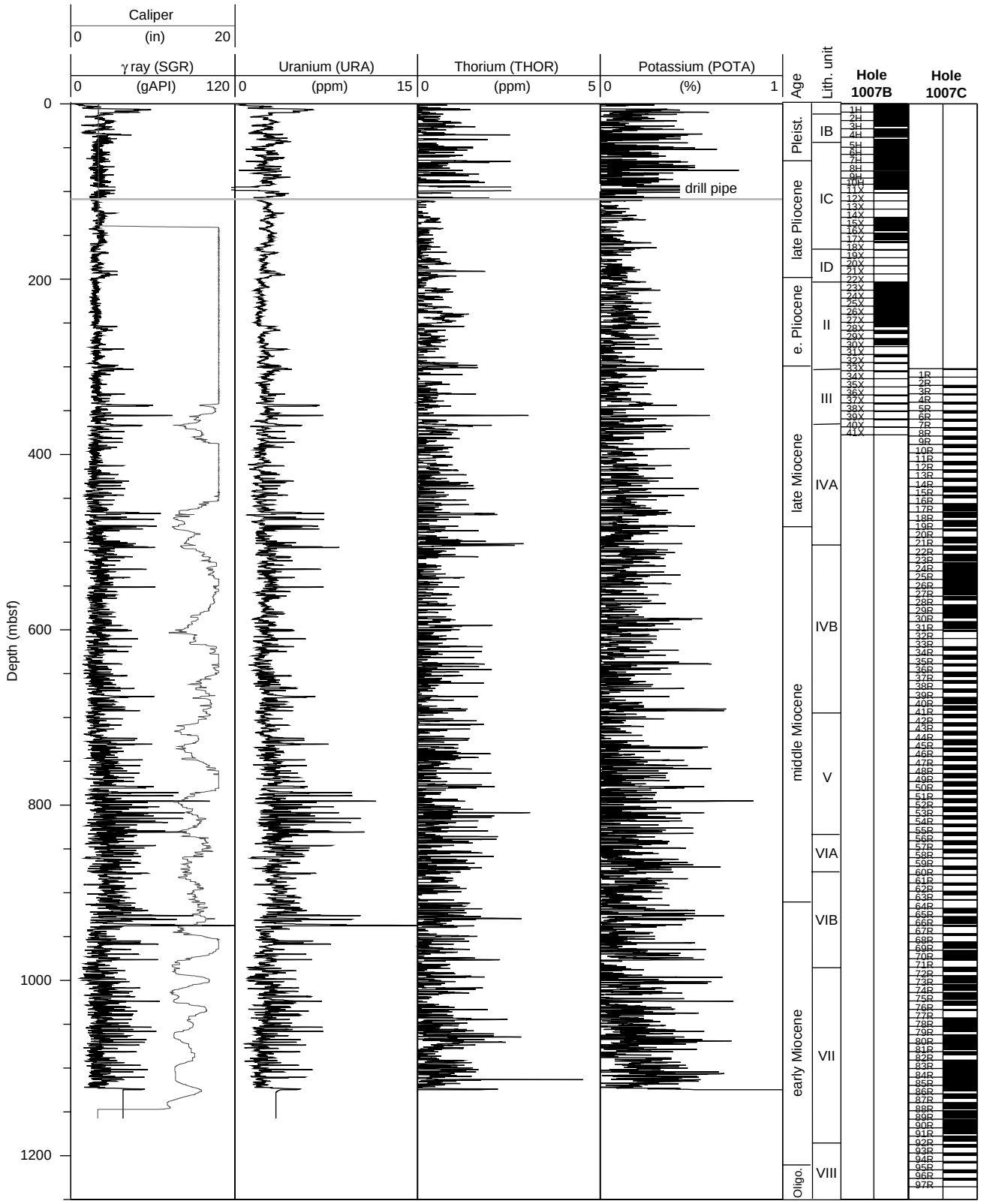

Figure 31. Spectral gamma-ray results using the NGT tool. The curves between 0 and 111 mbsf were corrected for the attenuation of the gamma-ray spectra caused by measurement in the drill pipe following empirical correction constants obtained by comparing logging runs in Holes 1005A and 1005C (correction factor = 4.0 within the BHA, 1.8 within 5 1/2-in drill pipe, and 1.7 within 5-in drill pipe).

the exceptions outlined previously. The extreme fluctuations in the values for discrete samples from the lower portion of the section are constrained by wide variability in the logged curves for the same interval.

In general, there is a downhole trend of increasing resistivity and sonic velocity that probably results from sediment compaction (Fig. 30). Small-scale fluctuations, as well as longer term excursions, are superimposed on this general trend. These variations show different patterns over different intervals, which are best expressed in the resistivity and sonic logs.

Between the base of the logged interval and 960 mbsf, which includes most of the lower Miocene, the logs display broad, low-amplitude excursions. In contrast, from 960 to 600 mbsf, comprising the sequences deposited between 18 and 12 Ma, the record contains about 10 units of higher amplitude, finer scale fluctuations, each characterized by upward-increasing resistivity and sonic velocity. The top of each unit terminates with a sharp decrease to lower values, which precedes the following bundle of steadily increasing values, with the shape of the resistivity curve resembling stacked, funnel-shaped sequences. Upsection, the thickness of a single unit greatly increases, and the character of the record changes to a pattern with lower amplitude fluctuations between 600 and 380 mbsf (deposition from 12 to 9 Ma). This interval contains two units separated by a section showing three areas of relatively higher resistivity and velocity between 508 and 465 mbsf, which is centered at about 10.7 Ma. Higher resistivity and velocity readings can be correlated approximately with sediments described as firmgrounds, hardgrounds, or turbidites (see "Lithostratigraphy" section, this chapter). In addition, the depths of the more resistive tops of these units can be correlated with the major sequence boundaries at Site 1007 (see "Seismic Stratigraphy" section, this chapter).

In the interval consisting of the uppermost Miocene-lower Pliocene (380 and 200 mbsf), the logs have a distinctive pattern that was observed at the other logged sites on the Bahamas Transect (Sites 1003, 1005, and 1006). At Site 1007, this interval contains two major hiatuses that bound the lower Pliocene sediments; the lower one is at 328 mbsf and the upper one is at 200 mbsf (see "Biostratigraphy" section, this chapter). Below the hiatus at 328 mbsf, the resistivity and sonic velocity logs show a series of four intervals with upward-increasing values marked by a sharp return to lower values at the top (Fig. 30). The top is also associated with a sharp gamma-ray peak. This serrated funnel shape is characteristic of coarsening-upward deposits (Serra, 1986), which may be related to current deposits or prograding turbidite lobes. In the core, firmgrounds associated with current deposits (reworked turbidites?) were observed in this interval (see "Lithostratigraphy" section, this chapter). The log pattern of the lower Pliocene sediments has a rather monotonous resistivity and sonic velocity signature and a relatively low gamma-ray signal. These sediments consist of nannofossil chalks and represent primarily pelagic sedimentation. Based on the lower Pliocene sediments recovered at all sites on the transect, pelagic sedimentation was pervasive and could account for the distinctive log pattern appearing at the sites. With the renewal of the platform carbonate input to the margin deposits in the late Pliocene, there is increased structure in the geophysical logs above 200 mbsf, with a number of small-scale peaks in the resistivity and sonic logs.

The gamma-ray logs (Fig. 31) indicate that the signal is related to a variable combination of U, Th, and K. The Th and K contents are relatively enriched throughout the sequence, probably reflecting a steady, but variable, detrital clay contribution to the sediments. The background U content is usually low in the sequence, particularly above 340 mbsf. This low U content may be related to the predominance of pelagic sediments. There is also a high U variability, with intervals containing significant U spikes. For example, an extremely large peak occurs at 937 mbsf near the lower/middle Miocene boundary or sequence Boundary O. Also, a pronounced U-rich interval occurs between 830 to 780 mbsf, corresponding to an interval of reduced sedimentation rate across sequence Boundary M.

These high-U intervals probably reflect diagenesis with incorporation of U into the firmgrounds and/or hardgrounds or an association with organic matter (Serra, 1986). The gamma-ray signal within the drill pipe shows increased U values in the upper Pleistocene, with a sharp decrease to an essentially null value for the uppermost sediments. This phenomenon was recognized at the other logged sites on the Bahamas Transect (Sites 1003, 1005, and 1006), implying that the incorporation of U into the periplatform ooze occurs after deposition.

IN SITU TEMPERATURE MEASUREMENTS

Introduction

At Site 1007, 11 in situ temperature measurements were made using three sets of Adara tools and one unit of downhole water sampler, temperature, and pressure probes (WSTP). Nine of the measurements were considered successful. In Core 166-1007A-6H, the advanced hydraulic piston corer (APC) could not penetrate a highly lithified layer. In Core 166-1007A-22X, the measurement was probably made in the bottom hole infill. The measurements and errors (Table 16) are described in the "In Situ Temperature Measurements" section of the "Explanatory Notes" and "Site 1003" chapters, this volume. The temperature at the seafloor (10.6°C) has been obtained from the mudline stops.

Geothermal Profile

The geothermal profile at Site 1007 is shown in Figure 32. The shallowest temperature measurement at 38 mbsf is approximately the same as the mudline temperature. The penetration temperature record (Fig. 33) for this measurement is of high quality and the equilibrium temperature determination is considered to be fairly reliable. From this depth, temperature increases downhole in a semi-linear fashion to about 60 mbsf where the slope of the geothermal profile changes. This concave downward profile below 40 mbsf resembles that of Site 1006, but it occurs at a shallower depth. The general geothermal profile resembles that of Site 1005, which is situated upslope on the bank margin. The temperature measurements below fall on a more or less straight line with a gradient of 36.8°C/km.

As discussed in the previous sites, either historical fluctuation of the bottom-water temperature or influx of seawater into the shallow zone of the sediments could explain the occurrence of lower geothermal gradient in shallow sediments than in the deeper sediments. At this site, the chemically inferred "flush zone" exists in the upper 30 mbsf (see "Inorganic Geochemistry" section, this chapter). The thickness of this zone is comparable to that of the zone of near-zero geothermal gradient.

Heat Flow

The lower linear part (below 48 mbsf) of the geothermal profile at Site 1007 gives a geothermal gradient of 36.8°C/km. The average of the thermal conductivities measured below 70 mbsf is 1.27 W/(m·K), yielding a heat flow value of 46.7 mW/m^2. This value is comparable to the heat flow at Site 1006 (44.4 mW/m^2).

SEISMIC STRATIGRAPHY

Introduction

Site 1007 penetrated through 17 late Cenozoic seismic sequences and drilled from 1208 to 1227.3 mbsf into 19.3 m of Oligocene sediments (Fig. 34; Table 17). By reaching the Oligocene at Site 1007, a complete record is in hand for the sequence stratigraphic architecture

Table 16. In situ bottom-hole sediment temperatures measured at Site 1007.

Core	Depth (mbsf)	Temperature (°C)	Error (°C)	Mudline (°C)	Tool	Notes
166-1007B-						
4H	38.0	9.91	0.23	10.92	Adara14	
5H	49.5	10.85	0.06	10.76	Adara18	
7H	67.0	12.12	0.06	10.56	Adara18	
8H	76.5	12.05	0.18	10.78	Adara11	
9H	84.7	12.60	0.10	10.32	Adara18	
10H	91.7	12.61	0.14	10.55	Adara11	
14X	120.0	13.35	0.12	10.35	WSTP201	
17X	147.4	14.91	0.08	10.63	WSTP201	
22X	193.9	15.24	0.02	10.48	WSTP201	Anomalous, poor recovery
27X	239.8	18.24	0.01	10.17	WSTP201	

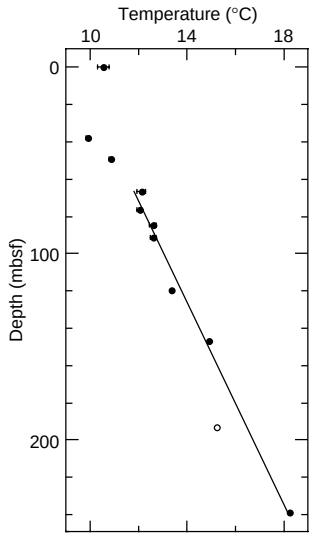

Figure 32. Geothermal profile at Site 1007. Solid circles = reliable temperature measurements, and open circles = unreliable measurements.

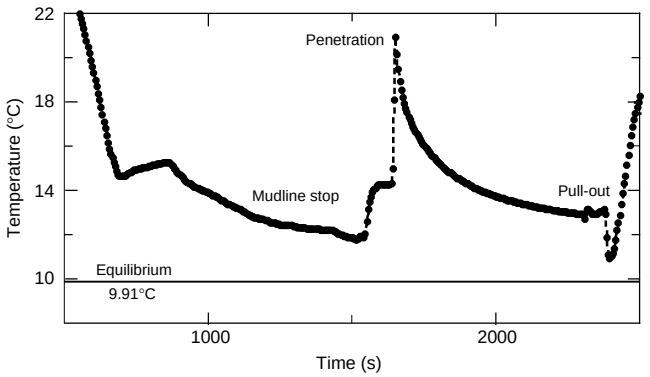

Figure 33. Adara penetration temperature record from Core 166-1007-4H. The equilibrium temperature is shown by the horizontal solid line.

of the Neogene along the Bahamas Transect (see Frontispiece and "Leg Synthesis" chapter, this volume). In the following paragraphs we discuss the depth-seismic traveltime relation, the location and geometries of the seismic sequences, and their signatures in lithology, physical properties, and log response.

Time-Depth Conversion

A check-shot survey was conducted at Site 1007 to provide an accurate time-depth conversion for translating the two-way traveltime of seismic reflection events into depth below seafloor (Fig. 35). During this VSP experiment, the well seismic tool (WST) was lowered to a depth of 1093 mbsf into Hole 1007C. Twelve stations recorded the traveltime of an acoustic signal from the air gun next to the drillship to the hydrophone within the borehole up to a depth 323.3 mbsf. No measurements could be made above 323 mbsf because of the large hole diameter (see "Downhole Logging" section, this chapter). Consequently, the time-depth curve for Site 1007 is linear between that depth and the seafloor. Because this shallow depth usually is characterized by strong velocity gradients that normally would not be linear, we used the time-depth values from Site 1003 for the upper 323 mbsf. Figure 35 and Table 18 display the resulting time-depth curve compared to the other Leg 166 sites and to the traveltimes derived from the integrated sonic log at Site 1007. The comparison of the VSP traveltimes with the integrated sonic log shows that, analogous to Sites 1003 and 1005, the sonic log values are, in general, too high and result in a depth error of 70 m at the bottom of the hole (for a discussion of possible causes, see "Seismic Stratigraphy" section, "Site 1005" chapter, this volume).

The VSP experiment at Site 1007 is the fourth survey performed in the Bahamas Transect and completes the information on the lateral variability of time-depth curves. The four time-depth curves of Sites 1003, 1005, 1006, and 1007 plotted in one graph (Fig. 35) show that the poorly consolidated drift deposits at Site 1006 comprise the slowest formation velocities. The two sites in the middle of the transect (Sites 1003 and 1007) display higher overall velocities than Site 1005, which is closest to the modern bank margin. This difference can be explained by the geometry of the Holocene-Pleistocene package. At Site 1005, the unconsolidated Holocene-Pleistocene section amounts to 180 m in thickness, but thins westward to 35 m thickness at Site 1007 (Sequences *a–c* in Fig. 6 of "Leg Synthesis" chapter, this volume.). The wedge-like geometry of this relatively low-velocity interval causes the higher traveltimes observed Site 1005. The precise time to depth conversion at this site enabled the correlation between the lithostratigraphy, seismic stratigraphy, and biostratigraphy summarized in Table 17 and in Figure 36.

Holocene-Pleistocene Sequences

At Site 1007, the upper Pleistocene is only approximately 14 m thick. As a result, the two seismic Sequences *a* and *b* are not resolvable on the seismic line. Seismic Sequence *c* extends to 40 milliseconds below seafloor (msbsf [TWT]) or 35 mbsf. This correlates to the first occurrence of *Gephyrocapsa caribbeanica* and *G. oceanica* (38 mbsf) marking the base of the Pleistocene. Thus, sequence Boundary C (SSB C) coincides with the Pleistocene/Pliocene boundary (Table 17). The same age for SSB C is found at the other sites of the Bahamas Transect (1003–1006), as well as in Holes Unda and Clino on the platform top (Eberli et al., this volume). At Site 1007, this boundary is characterized by a clay- and silt-rich mudstone with large skeletal debris including fragments of corals. The enrichment of clay and silt clearly indicates that sea level was low during the formation of the sequence boundary. In addition, the skeletal debris indicates that erosion of the reefal margin occurred at the same time. Petrophysically,

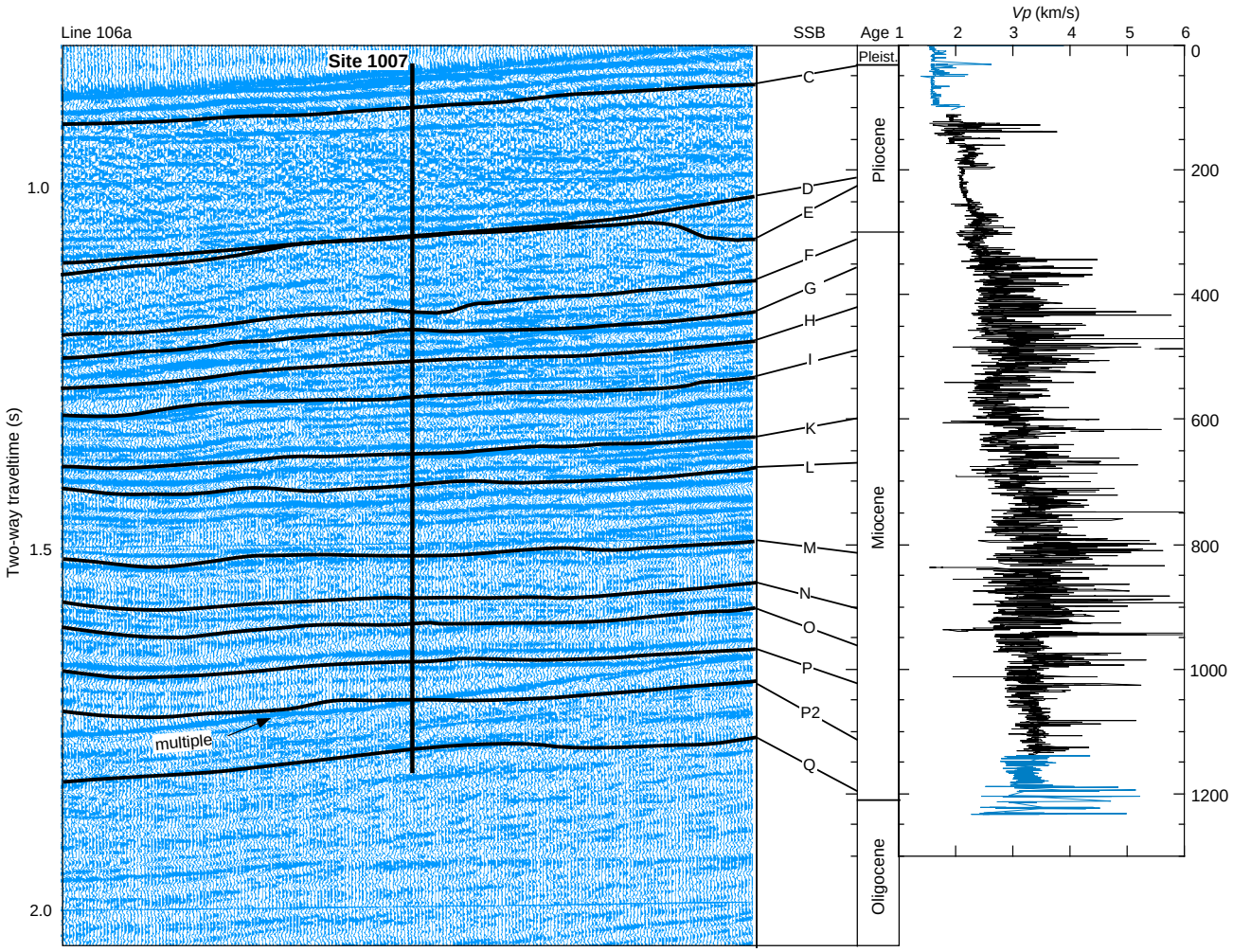

Figure 34. A portion of seismic Line 106a showing location of Site 1007 (full line in "Leg Synthesis" chapter, this volume). The major sequence boundaries have been traced and converted to depth. Origin of seismic reflections can be identified in the sonic log shown to the right. The shipboard DSV-velocity measurements are displayed in intervals in which no sonic log data are available (0–100 and 1140–1240 mbsf).

Table 17. Time-depth conversion and tentative age assignments of seismic sequence boundaries.

Seismic sequence boundary	TWT below seafloor (msbsf)	Depth (mbsf)	Nannofossil zone	Foraminifer zone	Age	Age* (Ma)
A	Not resolvable					
B	Not resolvable					
C	40	35	NN19	N22	Pleistocene/Pliocene	1.5–1.7
D	220	210	(NN16)/NN15	(N21)/N19	late/early Pliocene	3.2–4.2
E	220	210	(NN16)/NN15	(N21)/N19	late/early Pliocene	3.2–4.2
F	310	310	NN11/?	N17–19	Messinian	6.4-5.5
G	350	365	NN10	N16	late Miocene	8.8
H	390	420	NN9/10	N16	late Miocene	9.4
I	440	490	NN9/(NN8)	N16/(N14)	late/middle Miocene	10.9–11.4
K	520	600	NN7	N12	middle Miocene	12.2
L	570	670	NN7	N12	middle Miocene	12.5
M	660	810	NN5	N9/8	middle Miocene	15.1
N	720	900	NN4	N8/(N7)	middle Miocene	16.2–16.4
O	760	960	NN4	N6	early Miocene	18.2
P	800	1020	NN2	N5	early Miocene	19.4
P2	860	1115	NN2/1	N4	early Miocene	23.2
Q	910	1190	NN1	N4	earliest Miocene	23.7
R	1080	Not reached				

Note: * = ages are preliminary and based on shipboard biostratigraphy (see "Biostratigraphy" section, "Explanatory Notes" chapter, this volume).

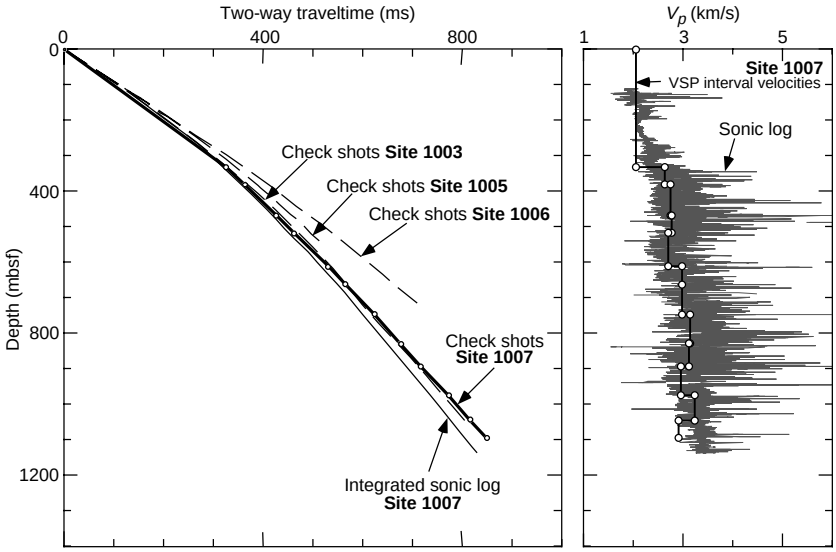

Figure 35. Left side: Time-depth curves for Leg 166 sites. VSP check shots of Site 1007 are displayed in thick line, and stations are marked by circles. The measured check-shot traveltimes have been compared with the integrated sonic log of Site 1007 and with check-shot results of the other Bahamas Transect sites. Right side: Plot of VSP-derived interval velocities between the 12 stations compared with sonic log data.

Table 18. Check-shot stations of VSP survey in Hole 1007C.

Check-shot station	Depth (mbsf)	TWT below seafloor (msbsf)	TWT below sea level (msbsl)
Seafloor	0	0.0	863.6
1	331	323.3	1187.0
2	379	360.0	1224.0
3	467	424.4	1288.0
4	516	459.8	1323.0
5	611	530.6	1394.0
6	661	564.2	1428.0
7	746	621.5	1485.0
8	826	672.6	1536.0
9	891	714.4	1578.0
10	973	770.1	1634.0
11	1044	814.1	1678.0
12	1093	847.9	1712.0

SSB C lies within the interval of 25–50 mbsf that is characterized by a succession of high-velocity layers (Fig. 25).

Pliocene Sequences

At the more proximal Sites 1003 and 1005, the uppermost Pliocene Sequence *d* is a thin unit, whereas at Site 1007 this sequence is 175 m thick. Lithologically, Sequence *d* consists of unlithified peloidal biowackestones that are slightly dolomitized in the lower part (Subunits IC and ID). This monotonous lithology is reflected in petrophysical data and in the logs by little variation throughout the sequence (see "Downhole Logging" and "Physical Properties" sections, this chapter). A biostratigraphic hiatus lasting from 2 to 2.4 Ma is observed near the top of the sequence (50 mbsf), just below a zone with two hardgrounds. The base of the sequence is placed at 220 msbsf (TWT) or 210 mbsf, which is only 4 m below the hiatus that straddles the early/late Pliocene boundary. This boundary can also clearly be recognized in the XRD data by a drastic decrease in aragonite content from values of 60%–80% in Sequence *d* to <5% in the early Pliocene. Taking the average depth between the first late Pliocene marker and the last early Pliocene marker places the hiatus at 200 mbsf. SSB D correlates with this hiatus, which lasted from 3.2 to 4.2 Ma. SSBs D and E cannot be separated seismically at Site 1007, probably as a result of erosion during the formation of SSB D (Fig. 34). The early Pliocene Sequence *f* extends to 300 msbsf (TWT) or 300 mbsf. This depth coincides with the top of the Miocene, which

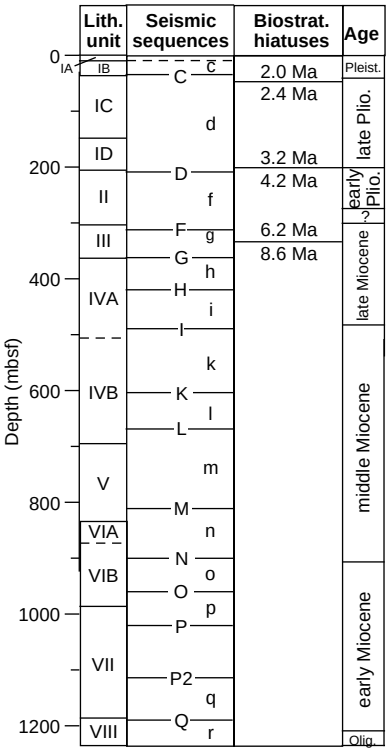

Figure 36. Correlation chart of lithologic units, sequence boundaries, and biostratigraphic ages.

is either a hiatus or alternatively a package deposited with very reduced sedimentation rate during the end of the Messinian (see "Biostratigraphy" section, this chapter). The abrupt lithologic change, the presence of a sharp spike in the gamma log, and the positive velocity anomaly with gradual downhole decreasing velocities underneath SSB F support the hiatus alternative. In this case, SSB F would correlate with the Messinian sea level fall. In any case, Sequence *f* is of early Pliocene age. This sequence was not datable in the more proximal sites as a result of the absence of age diagnostic fossils.

Miocene Sequences

The three upper Miocene sequences (*i*, *h*, and *g*) are well developed at Site 1007 (Figs. 34, 35). Sequence *g* is the thinnest. It extends from 310 to 365 mbsf and coincides with lithologic Unit III. Sequence *g* consists of variably indurated wackestones, chalks, and limestones. This variability is well recorded in the petrophysical and log data that display large variations in velocity, density, and gamma-ray values. SSB G is placed at 365 mbsf. The seismic reflection at SSB G is probably the sum of reflection events from three closely spaced horizons between 340 and 360 mbsf, all of which are marked in the logging data by spikes in gamma-ray values, resistivity, and velocity (discrete DSV velocities >5 km/s). The underlying Sequence *h* is 55 m thick and SSB H at its base is placed at 390 msbsf (TWT) or 420 mbsf. The sequence consists of bioturbated wackestones that are characterized by a uniform signal in the log data. The sequence boundary, dated at 9.4 Ma, is not marked by any discernible lithologic change. On the log data, however, a series of high-velocity horizons between 420 and 430 mbsf coincide with the depth calculated for SSB H. Sequence *i* also consists of bioturbated wackestones in the upper part, but several turbidites and a slump occur within the lower 20 m of the sequence. A clay layer in the middle of these gravity flow deposits indicates that mass wasting occurred during a time when siliciclastic input was higher, suggesting a sea-level lowstand. These redeposited units are recorded in the log data by an increase in velocity and bulk density, whereas the clay layers display an increase in the gamma-ray values. SSB I is dated as 10.9 Ma just above the late/middle Miocene boundary.

The middle Miocene Sequence *k* extends to a depth of 520 msbsf (TWT) or 600 mbsf and displays a facies distribution similar to Sequence *i*. It also consists of bioturbated wackestones in the upper part and intercalations of turbidites and a clay layer in a foraminifer wackestone in the lower portion. SSB K is dated as 12.2 Ma. In Sequence *l* the same facies succession is repeated, although the sequence is somewhat thinner. The log characteristics again show a more monotonous upper part and an increase in density in the lower part of the sequence. The sedimentation rate within Sequence *l* is high in the upper part and low in the basal part, which indicates a reduced platform input above the sequence boundary. SSB L, at 570 msbsf (TWT) or 670 mbsf, coincides with the base of the low sedimentation rate interval and is dated as 12.5 Ma. In underlying Sequence *m* the facies succession changes. Redeposited carbonates are also found in the middle of the sequence while only a few turbidites with bioclasts are present in the lower portion. The logs reflect these intercalations with increased values in both intervals. SSB M is placed at 660 msbsf (TWT) or 810 mbsf. A high gamma-ray peak at 800 mbsf indicates that the lithologic boundary might be approximately 10 m higher. SSB M is dated as 15.1 Ma. The fourth middle Miocene Sequence *n* extends to 720 msbsf (TWT) or 900 mbsf. In the upper portion of this sequence several firmgrounds occur while several slump packages are present in the lower half. The background sediments consist of a cyclic alternation between well cemented and less cemented, more compacted biowackestones (see "Lithostratigraphy" section, this chapter). SSB N, at the base of a slump, coincides with an interval with a reduced sedimentation rate at approximately the middle/early Miocene boundary. Its age is estimated between 16.2 and 16.4 Ma. This SSB is also marked by a distinct change in mineralogical composition (Fig. 20). Whereas the middle Miocene still contains significant amounts of aragonite (<20%) and very little insolubles (<5%), the lower Miocene does not have any aragonite, but has an increased amount of insolubles (5%–20%).

The first early Miocene Sequence *o* extends to 960 mbsf to the top of a firmground that is overlain by a clay layer, both of which are also recognized by strong gamma-ray signals in the logging data. This clay layer is a strong indication of the complete shutoff of platform-derived sedimentation during a sea-level lowstand. The underlying Sequence *p* consists of a cyclic alternation of cemented and more compacted clay-rich wackestones. The basal SSB P is placed at 1020 mbsf, which coincides with a couplet of clay-rich intervals overlain by some turbidites. These turbidites are responsible for a pattern of high-velocity signatures at the base of petrophysical Unit V, which is accompanied in the logging data by two prominent spikes in resistivity. This high-velocity zone above SSB P forms a velocity inversion because the top of the underlying sequence is characterized by low and monotonous velocity values. The remainder of the lower Miocene can be split into two sequences, *p2* and *q*. Biostratigraphic data indicate a possible hiatus or at least very reduced sedimentation rate between 1100 and 1118 mbsf (23.2–20.5 Ma). The concordant seismic reflection at 860 msbsf (TWT) or 1115 mbsf lies within the section below the first seafloor multiple, although it can still be precisely correlated with a horizon at Site 1003 at 1190 mbsf, which is characterized there by a hiatus ranging approximately from 22.5 to 19.4 Ma. We therefore postulate the existence of an additional sequence, *p2*, ranging at Site 1007 from 1020 to 1115 mbsf and at Site 1003 from 1165 to 1190 mbsf. Underlying Sequence *q* ranges in depth from SSB P2 down to SSB Q at 915 msbsf (TWT) or 1190 mbsf. Both Sequences *p2* and *q* approximately compose lithologic Unit VII, characterized by bioturbated wackestones that show cyclic alternations of well-cemented, light-colored layers and compacted, darker, and less cemented layers, with a slump unit just above SSB P2. These alternations result in the high-frequency succession of gamma-ray spikes seen in the logs, which are caused by the dark layers. The basal Neogene SSB Q is picked at a seismic reflection at 910 msbsf (TWT) (1190 mbsf) and lies 20 m above the biostratigraphic Oligocene/Miocene boundary.

Oligocene Sequences

The boundary to seismic Sequence *r* correlates with the base of petrophysical Unit VII and lithologic Unit VIII at 1190 mbsf, whereas the biostratigraphic Oligocene/Miocene boundary is 20 m deeper. The reflection of SSB Q is a result of the sudden increase in V_p and density in Sequence *r* in contrast with the relatively low values above (Fig. 23). Although lithologic Unit VIII is lithologically similar to the Miocene sequences above, there is a dramatic decrease in gamma-ray. The changes in physical properties indicate a significant change in the depositional or diagenetic signature across SSB Q. Assuming that the biostratigraphic markers and the time-depth correlation are accurate (note that lowest VSP station is at 1093 mbsf), these prominent physical changes as well as the seismic reflection event occur slightly above the Oligocene/Miocene boundary.

SUMMARY AND CONCLUSIONS

Site 1007 is located at the toe-of-slope of the western GBB. A 1235.4 mbsf deep hole penetrated the entire Neogene-Holocene section and 20 m of Oligocene sediments, providing the complete sedimentary record of the Neogene sea-level changes. Its position at the base of the slope makes it the link between the slope Sites 1003, 1004, and 1005 and the basinal Site 1006. Good overall recovery and the presence of many planktonic foraminifers and nannofossil marker species allow for a detailed biostratigraphy for the entire Neogene section. Site 1007, therefore, completed the data set needed to address all the questions in regard to sea-level changes as well as fluid flow within a stratigraphic framework. A precise foraminifer and nannofossil biostratigraphy provides the age control on the depositional changes related to sea-level fluctuations and the resulting sequence boundaries. This will add to the database that is needed to eventually establish the global synchrony of sea-level changes. Furthermore, the well-preserved foraminifers in this and Site 1006 pro-

vide the unique opportunity to compare the sedimentary record with the oxygen isotopic proxy for sea-level changes. This comparison will potentially assess the causal relationship between the stratal pattern and sea-level changes.

The geochemical profiles at Site 1007 indicate that, like the other sites, there is active fluid flow in the upper portion of the strata. With increasing depth, diffusive processes become the dominant transport mechanism.

The Facies of the Toe-of-Slope

The seismic data at the toe-of-slope of modern GBB display a geometry of basinward thinning distal portions of prograding clinoforms in the older Miocene section. In the upper Miocene, sediment drift deposits interfinger with the clinoforms. In the Pliocene, a thick basinal wedge onlaps the margin sediments. This wedge is overlain by Pleistocene prograding sequences. This complicated architecture is the result of an interplay among the change in platform-to-basin morphology, sea-level variation, and ocean currents and is reflected in the sedimentary succession. The Pleistocene prograding tongues are characterized by an alternation between carbonate-rich periplatform sediments and silt- and clay-rich intervals. These alternations are similar to the cycles observed in the Pleistocene section at Site 1006, where the clay-rich intervals are interpreted to reflect erosion of continent-derived siliciclastics during sea-level lowstands and incipient sea-level rise, whereas the carbonate-rich intervals indicate deposition during the following platform flooding.

The onlapping wedge is a succession of platform-derived, fine-grained sediment; mass gravity flow deposits, especially turbidites; and thin laminated beds that are interpreted as current deposits. The large amount of redeposited carbonates indicate that the toe-of-slope was the depocenter for the mass gravity flow deposits that bypassed the upper slope.

A larger amount of turbidites and slumps than in the more proximal sites was also recovered in the prograding Miocene sequences. The background sediment, however, is similar to the Miocene section recovered at Sites 1003, 1005, and 1006. This sediment consists of alternating intervals of well-cemented, decimeter- to meter-scale, light-colored, clay-free intervals that show no evidence of compaction and decimeter-scale, dark-colored, relatively clay-rich intervals that show evidence of compaction. These alternations are interpreted to reflect changes in the rate of neritic carbonate input as a result of platform flooding during sea-level highstands. In contrast, dark-colored, weakly cemented intervals reflect periods of decreased neritic input during sea-level lowstands. This alternation continues into the Oligocene section, although the color changes are less pronounced. Chert nodules give evidence of a changing sedimentary regime, probably dominated by cooler water temperatures.

The Sea-Level Record in the Seismic Sequences

The SSBs coincide with facies intervals that are indicative of sea-level lowstands. These facies are pelagic intervals or clay layers that punctuate the cyclic alternations. In addition, Miocene sequences in the lower portion contain redeposited carbonates, such as turbidites and slump packages, in a more pelagic background sediment (lowstands) whereas biowackestones, which have more platform-derived material, are in the upper portions of the sequences (highstands). With the transition into a steep-sided platform in the Pliocene, redeposited carbonates become more abundant in the upper parts of the sequences. This difference documents the relationship between platform morphology and highstand vs. lowstand shedding in carbonates. It is well documented that the modern steep-sided platform sheds most of its turbidites during sea-level highstands (e.g., Droxler and Schlager, 1985). In such a setting, the carbonate environment is 180° out of phase with the siliciclastic environment where most of the turbidites are shed during sea-level lowstands (Mullins, 1983; Schlager, 1992). The turbidites in the Miocene section of Site 1007 document that in a ramp-like platform/margin profile, differences between the two systems are diminished and carbonate turbidites also are shed during relative sea-level lowstands.

Facies and diagenesis act in concert to produce petrophysical differences within the sedimentary section. As a result, the logs closely image the sedimentary and stratigraphic record. Log-to-core correlation permits significant interpretations about variations in sedimentation patterns on the toe-of-slope of GBB from the earliest early Miocene to the Holocene. Small-scale and long-term excursions are superimposed over a general downhole trend. These variations reflect the lithologic and diagenetic variations in the core. Higher resistivity and velocity can be approximately correlated with firmgrounds, hardgrounds, or turbidites. In addition, logs display little variations through monotonous units. As a consequence the high values of the logs coincide with sequence stratigraphically important sedimentary units, and display lithologic sequence boundaries.

The exact positioning of the sequence boundaries in the cores and the good biostratigraphy enables the precise dating of the sequence boundaries. Seventeen seismic sequences were distinguished prior to drilling. The two youngest sequences could not be identified on the seismic section due to ghost reflections close to the sediment-water interface. Also prior to drilling, ages of the sequence boundaries were postulated from the biostratigraphic information of the adjacent sites. These predictions proved to be very accurate. In addition, the better preservation of the biostratigraphic markers at Site 1007 compared to the more proximal sites permits a refinement of some of the ages. For example, the lower Pliocene Sequence *f* was not datable in the more proximal Sites 1003 and 1005 due to the absence of age-diagnostic marker species. At this more distal site, a precise stratigraphy through this interval is possible, and the basal sequence boundary is now dated as the top of the Messinian. More important, the SSBs yield the same ages as in the adjacent sites when taking into account the seismic resolution in the depth assignment of the reflections. This age consistency of seismic reflections validates one of the basic assumptions of sequence stratigraphy, that there is a chronostratigraphic significance of seismic reflections.

At Site 1007, the biostratigraphic dating was of sufficient quality to provide, with sedimentation rates, an independent record of the platform-derived sedimentation during sea-level highstands and the reduced pelagic sedimentation during sea-level lowstands. In addition, current erosion during the Pliocene–Pleistocene can be documented by hiatuses. The average sedimentation rate for the Pleistocene interval is 5 cm/k.y. However, the top of Hole 1007B is older than 0.95 Ma. Obviously, current action at the toe-of-slope increased during the last 1 m.y. and caused erosion. A hiatus just below the Pliocene/Pleistocene boundary that lasted for approximately 0.4 m.y. might also be the result of current activity. The upper Pliocene interval is highly expanded with an average sedimentation rate of 21 cm/k.y. The increased sedimentation is the combined result of the accumulation of drift sediments and the deposition of platform-derived material that bypassed the upper slope and was deposited at the toe-of-slope at Site 1007. The lower Pliocene package is bounded by a hiatus. The duration of the hiatus spans the early/late Pliocene boundary and is approximately 1 m.y. (3.2–4.2 Ma). The sedimentation rate below this hiatus is 17.5 cm/k.y. Below 304 mbsf, an interval of poor preservation represents either an interval of very low sedimentation (<1 cm/k.y.) or contains a hiatus that straddles the Miocene/Pliocene boundary.

A late Miocene hiatus was detected that spanned a period of approximately 2 m.y. The low sedimentation rate of 1 cm/k.y. above the hiatus may provide evidence for some platform production during the Messinian, or it may represent a lowstand wedge. The late Miocene is characterized by a high sedimentation rate (13 cm/k.y.), indicating high sediment production on GBB during this time. The middle and

early Miocene sedimentation rates show four cycles with alternating low (<2 cm/k.y.) and high (>5 cm/k.y.) rates. Slow sedimentation intervals occurred from 9.5 to 11.5 Ma, 13 to 15 Ma, 16.5 to 17.5 Ma, and 20.5 to 23 Ma and correlate to hiatuses of similar duration at Site 1003. Periods of faster deposition occurred from 11.5 to 13 Ma, 15 to 16.5 Ma, 17.5 to 20.5 Ma, and older than 23 Ma, which corresponds to intervals at Site 1003 with similarly high sedimentation rates. These cycles represent the turning off and on of platform production in response to relative sea-level changes.

Fluid Chemistry and Diagenesis

The geochemical profiles at Site 1007 show three basic zones that relate to zones seen at the other sites. First, there is an upper flushed zone in which there are no changes in the conservative elements and only minimal changes in the nonconservative elements such as Sr^{2+}, Ca^{2+}, and alkalinity. This zone is similar to that found at the upper slope sites (Site 1003, 1004, and 1005), but differs in that minimal changes were observed in the concentration of Sr^{2+}. This difference makes Site 1007 similar to the more distal site, Site 1006. Below the flushed zone, the concentration of the conservative elements (Cl^- and Na^+) shows a diffusional relationship to the bottom of the hole. The concentration of K^+ shows a major decrease between 900 and 1000 mbsf, which is related to diagenesis of clay minerals. Beneath the flushed zone, concentrations of the nonconservative elements (Sr^{2+}, SO_4^{2-}, Ca^{2+}, NH_4^+, and alkalinity) show changes that are related to local reactions such as the degradation of organic material and the recrystallization of carbonate minerals. Immediately below the flushed zone, the SO_4^{2-} concentration decreases slightly as a result of the local oxidation of organic material. This is accompanied by an increase in the concentration of methane. The concentration of SO_4^{2-} rises again to seawater values at 400 mbsf and then decreases to zero below 600 mbsf. The removal of SO_4^{2-} marks the start of the third geochemical zone and corresponds to the appearance of isobutane concentrations of up to 10 ppm in the headspace samples that are probably of thermogenic origin. The concentration of Sr^{2+} in this interval is strongly controlled by the solubility of celestite. Once the SO_4^{2-} has been completely removed from the pore waters, the Sr^{2+} increases to over 5 mM at a depth of 950 mbsf. A maximum in the Ca^{2+} concentration between 350 and 400 mbsf indicates a probable zone of carbonate dissolution. When normalized to seawater Cl^- concentrations, this zone shows a net removal of Ca^{2+} from the pore waters.

The upper 900 m of sediment consists of over 90% carbonate. Below this depth concentration of carbonate decreases to between 60% and 80% with higher amounts of organic carbon (up to 1 wt%). The hole is dominated by LMC, although Unit I consists mainly of aragonite with small amounts of dolomite and HMC. Throughout the remainder of the hole, dolomite is a minor constituent with concentrations of up to 40% in small isolated intervals. Quartz is an ubiquitous component throughout the core, and there are documented occurrences of pyrite and clay minerals.

REFERENCES

Berner, R.A., 1970. Sedimentary pyrite formation. *Am. J. Sci.*, 268:1–23.

Canfield, D.E., 1989. Reactive iron in marine sediments. *Geochim. Cosmochim. Acta*, 53:619–632.

Chilingar, G.V., and Rieke, H.H., III, 1975. Chemistry of interstitial solutions in undercompacted (overpressured) versus well-compacted shales. *In* Baily, S.W. (Ed.), *Proc. Inter. Clay Conf.*, 673–678.

Droxler, A.W., and Schlager, W., 1985. Glacial versus interglacial sedimentation rates and turbidite frequency in the Bahamas. *Geology*, 13:799–802.

Eberli, G.P., and Ginsburg, R.N., 1989. Cenozoic progradation of NW Great Bahama Bank: a record of lateral platform growth and sea fluctuations. *In* Crevello, P.D., et al. (Eds.), *Controls on Carbonate Platform and Basin Evolution.* Spec. Publ.—Soc. Econ. Paleontol. Mineral., 44:339–355.

Emeis, K.-C., and Kvenvolden, K.A., 1986. Shipboard organic geochemistry on *JOIDES Resolution. ODP Tech. Note*, 7.

Fulthorpe, C.S., and Melillo, A.J., 1988. Middle Miocene carbonate gravity flows in the Straits of Florida at Site 626. *In* Austin, J.A., Jr., Schlager, W., et al., *Proc. ODP, Sci. Results*, 101: College Station, TX (Ocean Drilling Program), 179–191.

Maher, B.A., 1988. Magnetic properties of some synthetic sub-micron magnetites. *Geophys. J. R. Astron. Soc.*, 94:83–96.

Mullins, H.T., 1983. Comment on "Eustatic control of turbidites and winnowed turbidites." *Geology*, 11:57–58.

Schlager, W., 1992. Sedimentology and sequence stratigraphy of reefs and carbonate platforms. *AAPG Cont. Educ. Course Notes Ser.*, 34.

Schlager, W., and James, N.P., 1978. Low-magnesian calcite limestones forming at the deep-sea floor, Tongue of the Ocean, Bahamas. *Sedimentology*, 25:675–702.

Schlumberger, 1989. *Log Interpretation Principles/Applications:* Houston, TX (Schlumberger Educ. Services).

Scholle, P.A., Arthur, M.A., and Ekdale, A.A., 1983. Pelagic environments. *In* Scholle, P.A., Bebout, D.G., and Moore, C.H. (Eds.), *Carbonate Depositional Environments.* AAPG Mem., 33:620–691.

Serra, O., 1986. *Fundamentals of Well-Log Interpretation* (Vol. 2): *The Interpretation of Logging Data.* Dev. Pet. Sci., 15B.

Shipboard Scientific Party, 1991. Explanatory notes. *In* Davies, P.J., McKenzie, J.A., Palmer-Julson, A., et al., *Proc. ODP, Init. Repts.*, 133 (Pt. 1): College Station, TX (Ocean Drilling Program), 31–58.

Videtich, P.E., 1985. Electron microprobe study of Mg distribution in recent Mg calcites and recrystallized equivalents from the Pleistocene and Tertiary. *J. Sediment. Petrol.*, 55:421–429.

Ms 166IR-110

Note: Core description forms ("barrel sheets") and core photographs can be found in Section 3, beginning on page 377. Forms containing smear slides can be found in Section 4, beginning on page 831. Thin-section descriptions can be found in Section 5, beginning on page 849. See the Table of Contents for material contained on CD-ROM.

SHORE-BASED LOG PROCESSING

Hole 1007C

Bottom felt: 659 mbrf (used for depth shift to seafloor)
Total penetration: 1235.4 mbsf
Total core recovered: 503.3 m (53.9%)

Logging Runs

Logging string 1: DIT/SDT/HLDT/CNTG/NGT
Wireline heave compensator was used to counter ship heave.

Bottom-Hole Assembly

The following bottom-hole assembly depths are as they appear on the logs after differential depth shift (see "Depth shift" section) and depth shift to the seafloor. As such, there might be a discrepancy with the original depths given by the drillers on board. Possible reasons for depth discrepancies are ship heave, use of wireline heave compensator, and drill string and/or wireline stretch.

DIT/SDT/HLDT/CNTG/NGT: Bottom-hole assembly at ~110 mbsf.

Processing

Depth shift: No depth shift necessary as only one run was recorded.

Gamma-ray environmental corrections: Data have been processed to correct for borehole size and type of drilling fluid.

Acoustic data processing: The array sonic tool was operated in standard depth-derived, borehole compensated, long spacing (8–10 and 10–12 ft) mode. The logs have been processed to eliminate some of the noise and cycle skipping experienced during the recording.

Quality Control

Invalid density spikes were recorded at 142.5, 147, 154, and 188 mbsf.

Data recorded through bottom-hole assembly, such as the gamma ray data above 110 mbsf, should be used qualitatively only because of the attenuation on the incoming signal. Invalid gamma ray data were recorded at 96–100 mbsf.

Hole diameter was recorded by the hydraulic caliper on the HLDT tool (CALI).

Details of standard shore-based processing procedures are found in the "Explanatory Notes" chapter, this volume. For further information about the logs, please contact:

Cristina Broglia
Phone: 914-365-8343
Fax: 914-365-3182
E-mail: chris@ldeo.columbia.edu

Amal Chakraborty
Phone: 914-365-8358
Fax: 914-365-3182
E-mail: amalc@ldeo.columbia.edu

Hole 1007C: Natural Gamma Ray-Resistivity-Sonic Logging Data

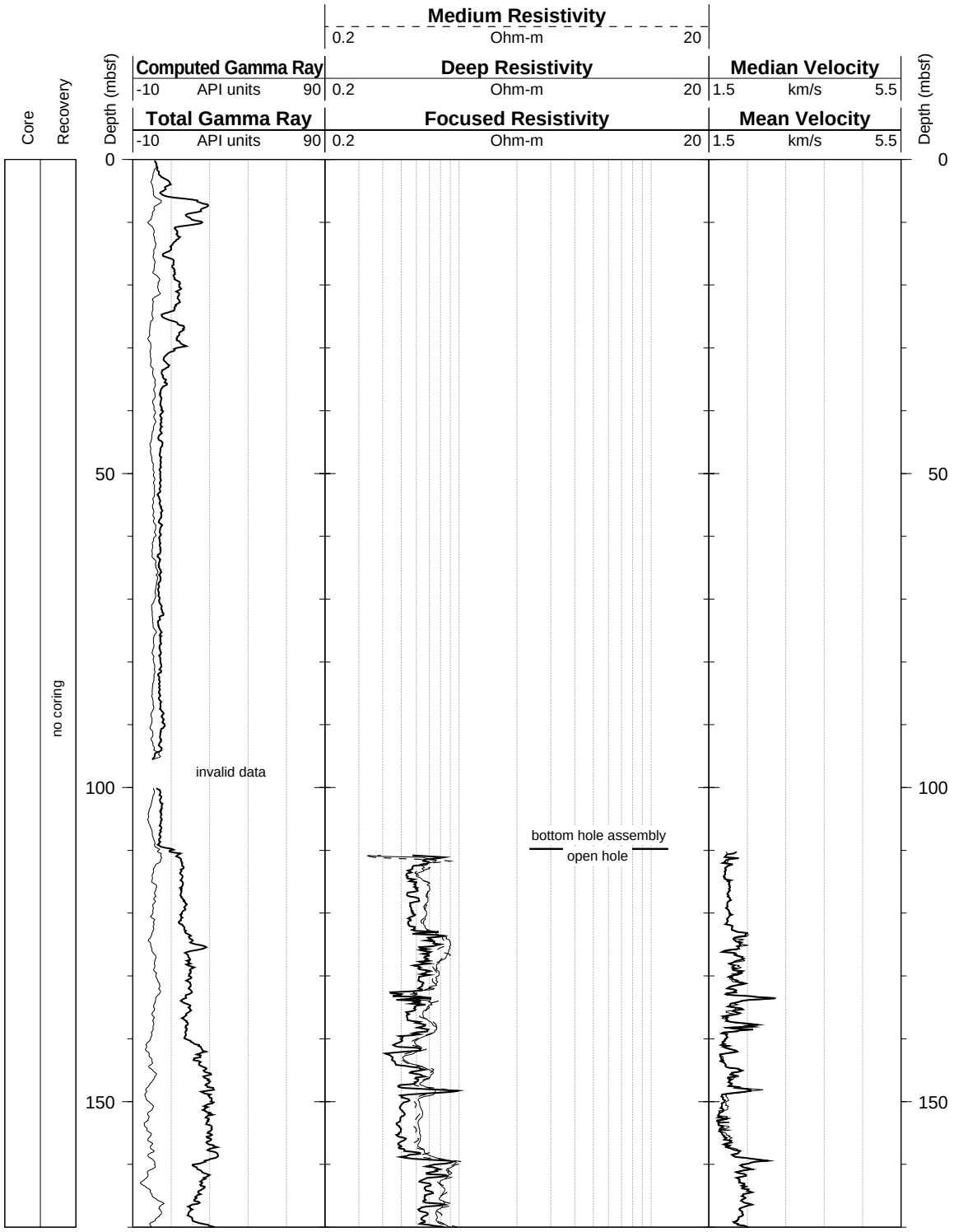

Hole 1007C: Natural Gamma Ray-Resistivity-Sonic Logging Data (cont.)

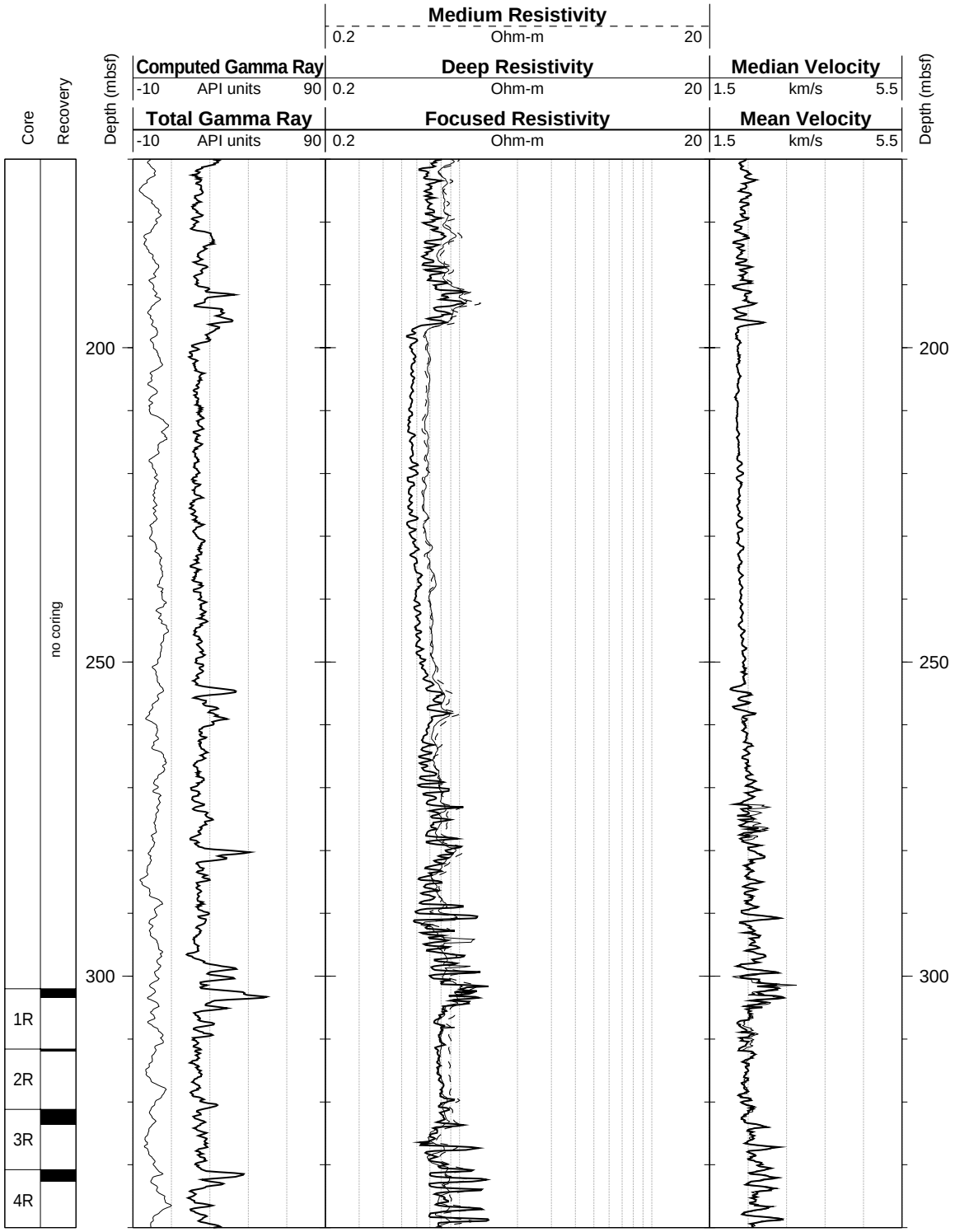

Hole 1007C: Natural Gamma Ray-Resistivity-Sonic Logging Data (cont.)

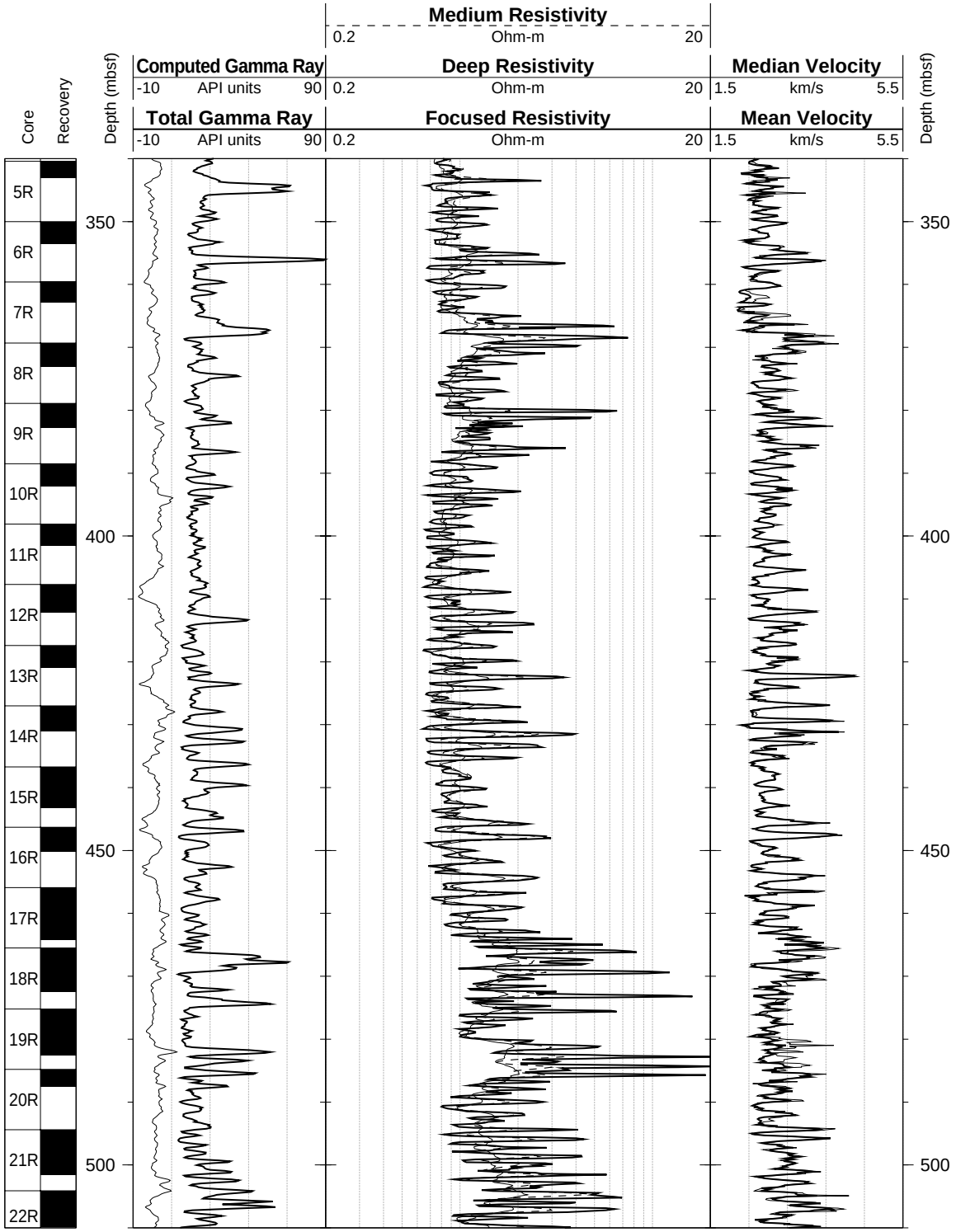

Hole 1007C: Natural Gamma Ray-Resistivity-Sonic Logging Data (cont.)

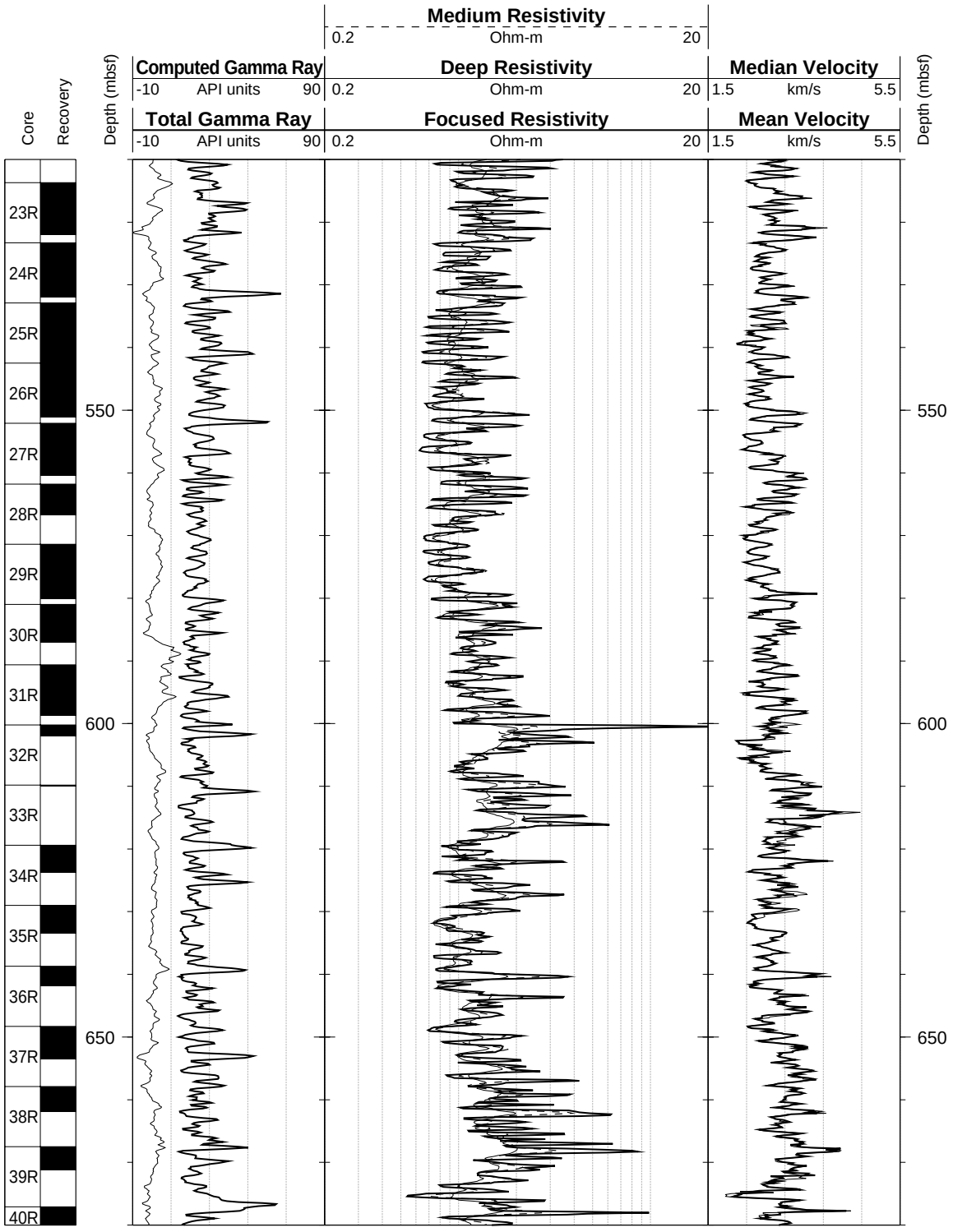

Hole 1007C: Natural Gamma Ray-Resistivity-Sonic Logging Data (cont.)

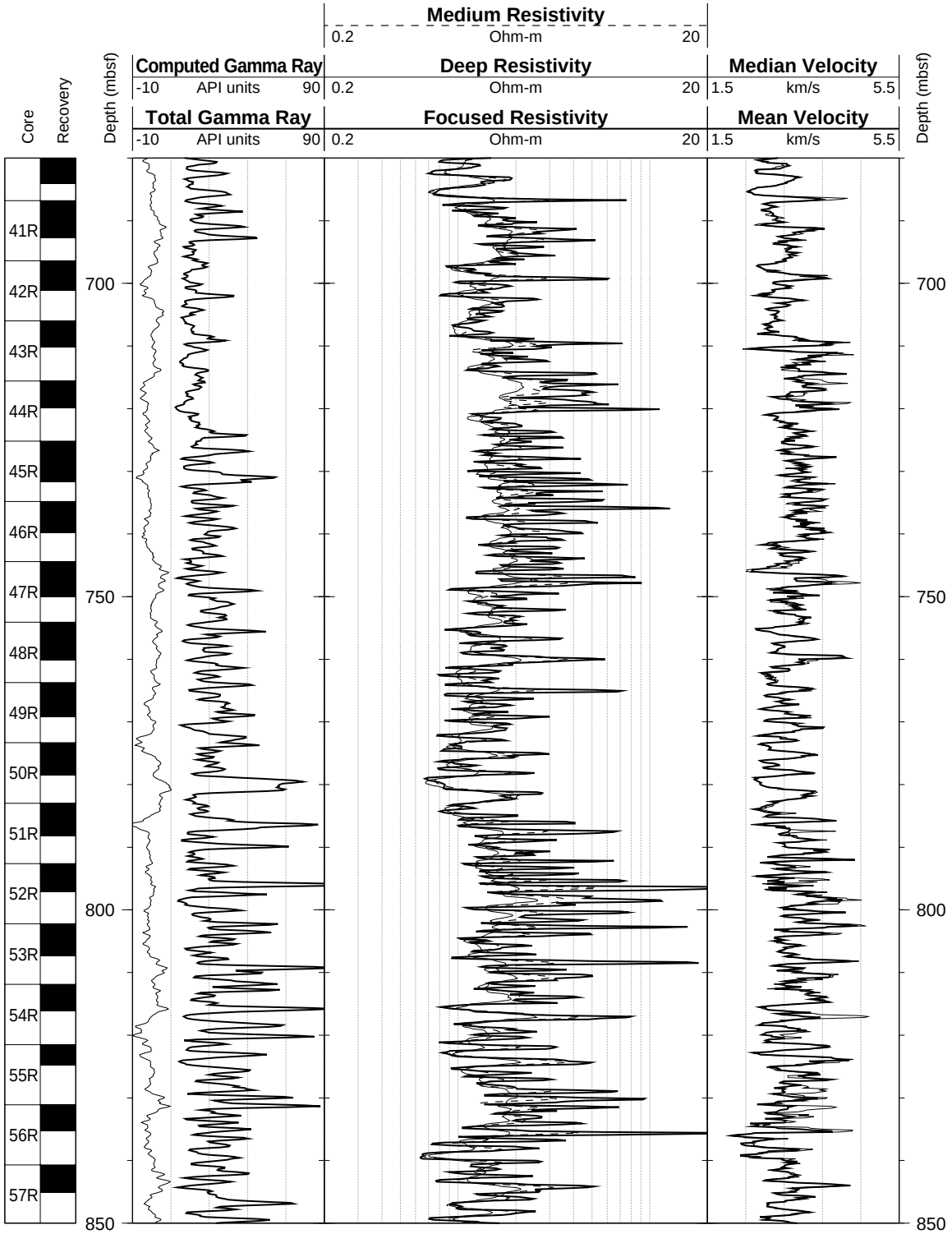

Hole 1007C: Natural Gamma Ray-Resistivity-Sonic Logging Data (cont.)

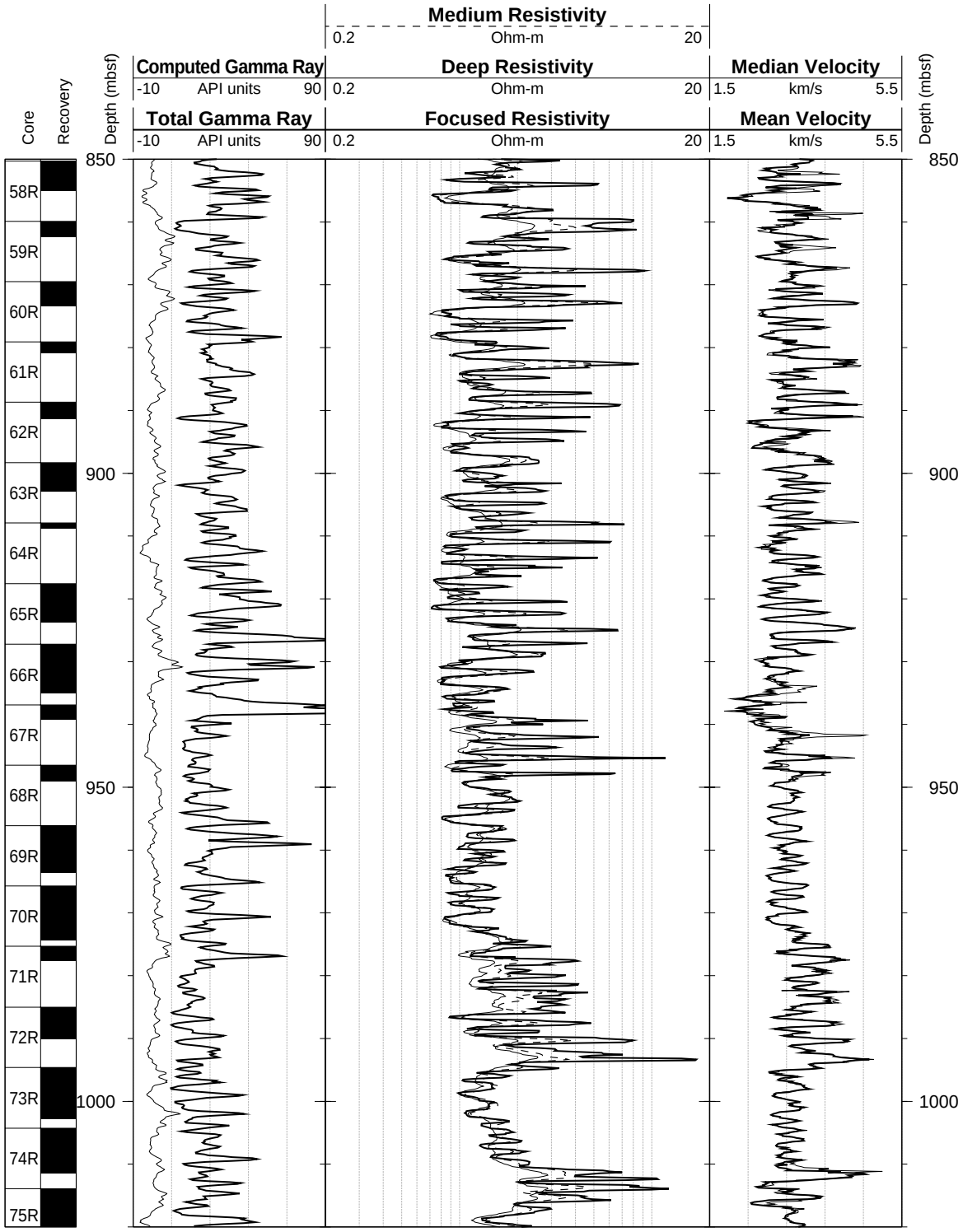

Hole 1007C: Natural Gamma Ray-Resistivity-Sonic Logging Data (cont.)

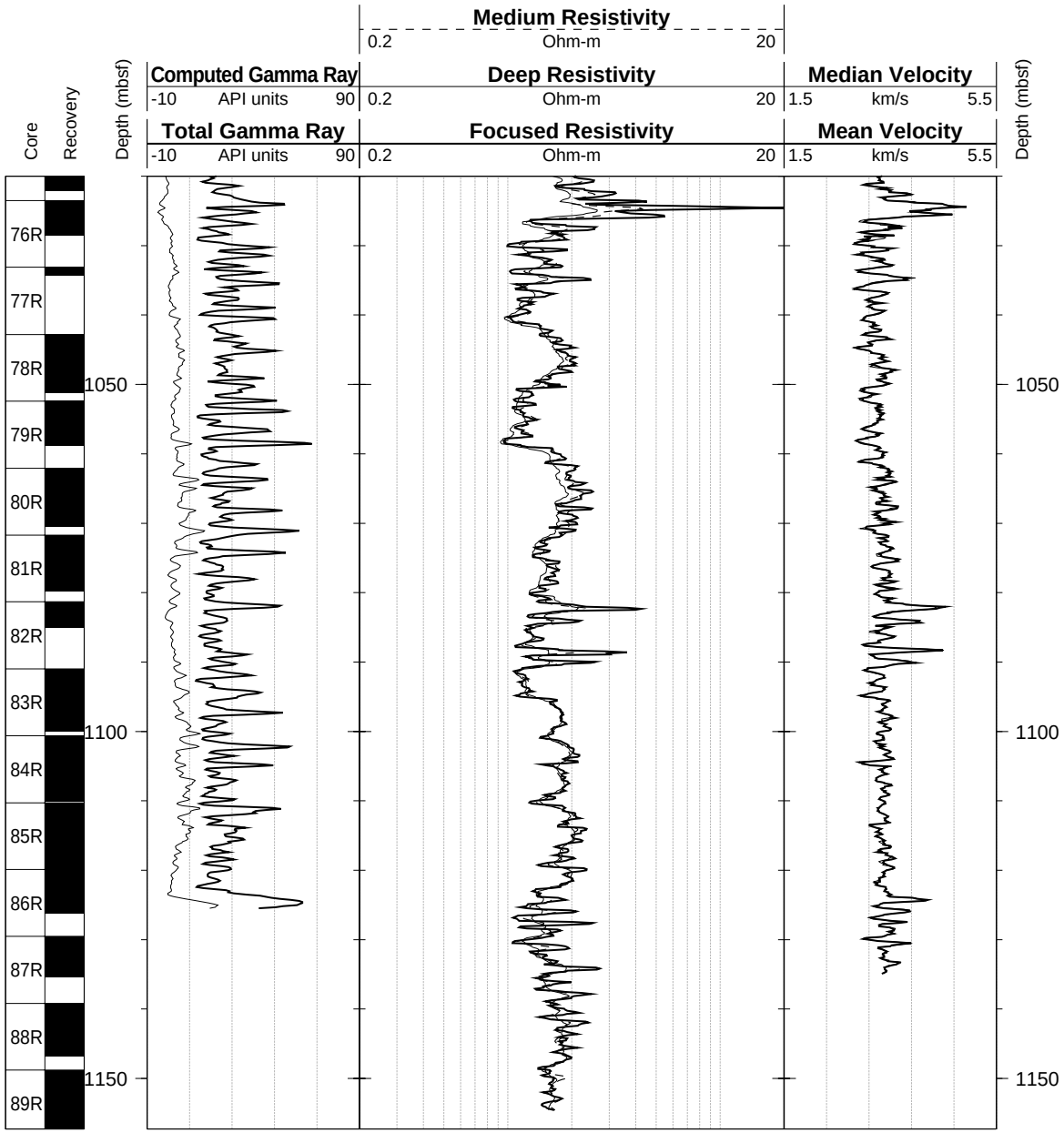

Hole 1007C: Natural Gamma Ray-Density-Porosity Logging Data

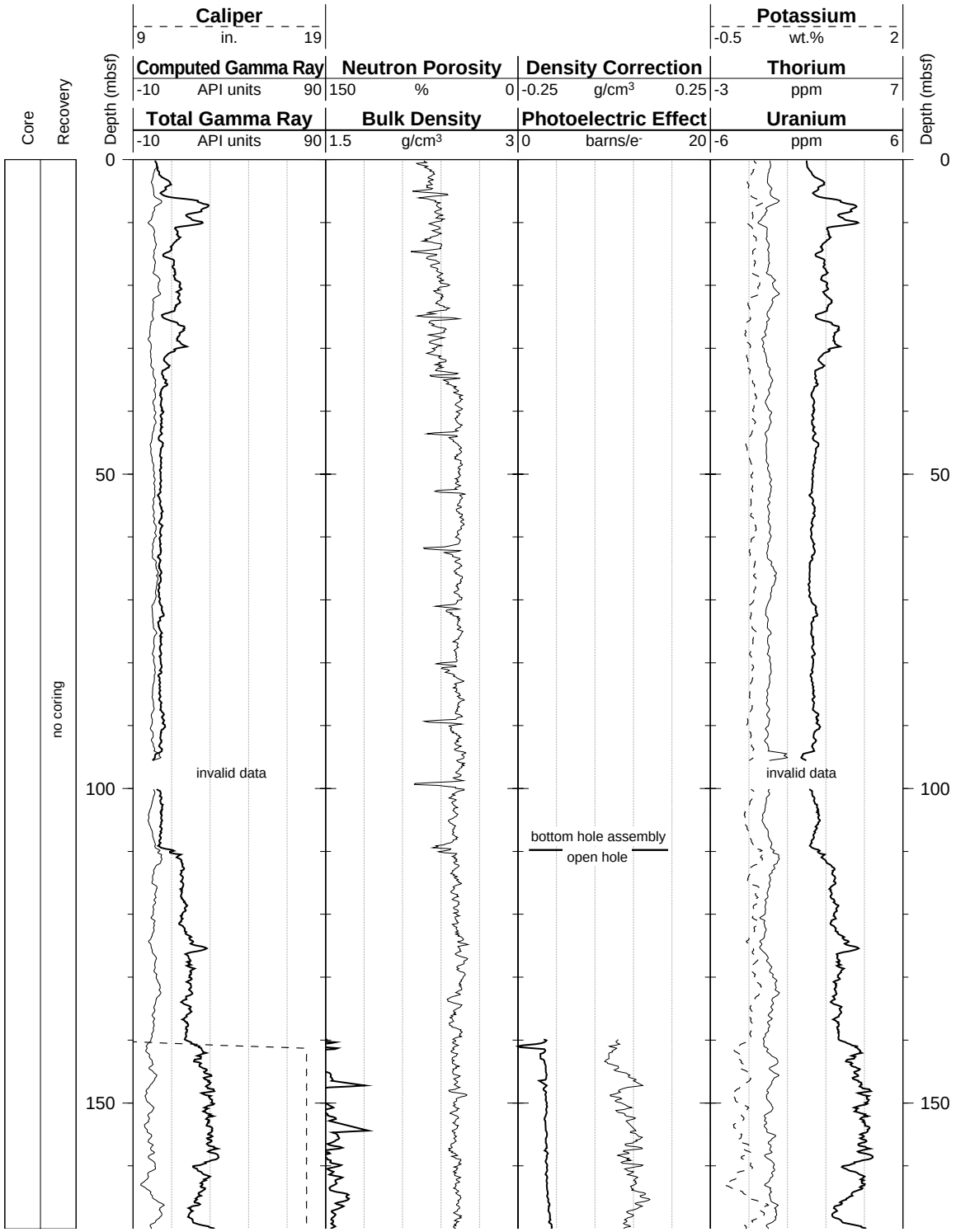

Hole 1007C: Natural Gamma Ray-Density-Porosity Logging Data (cont.)

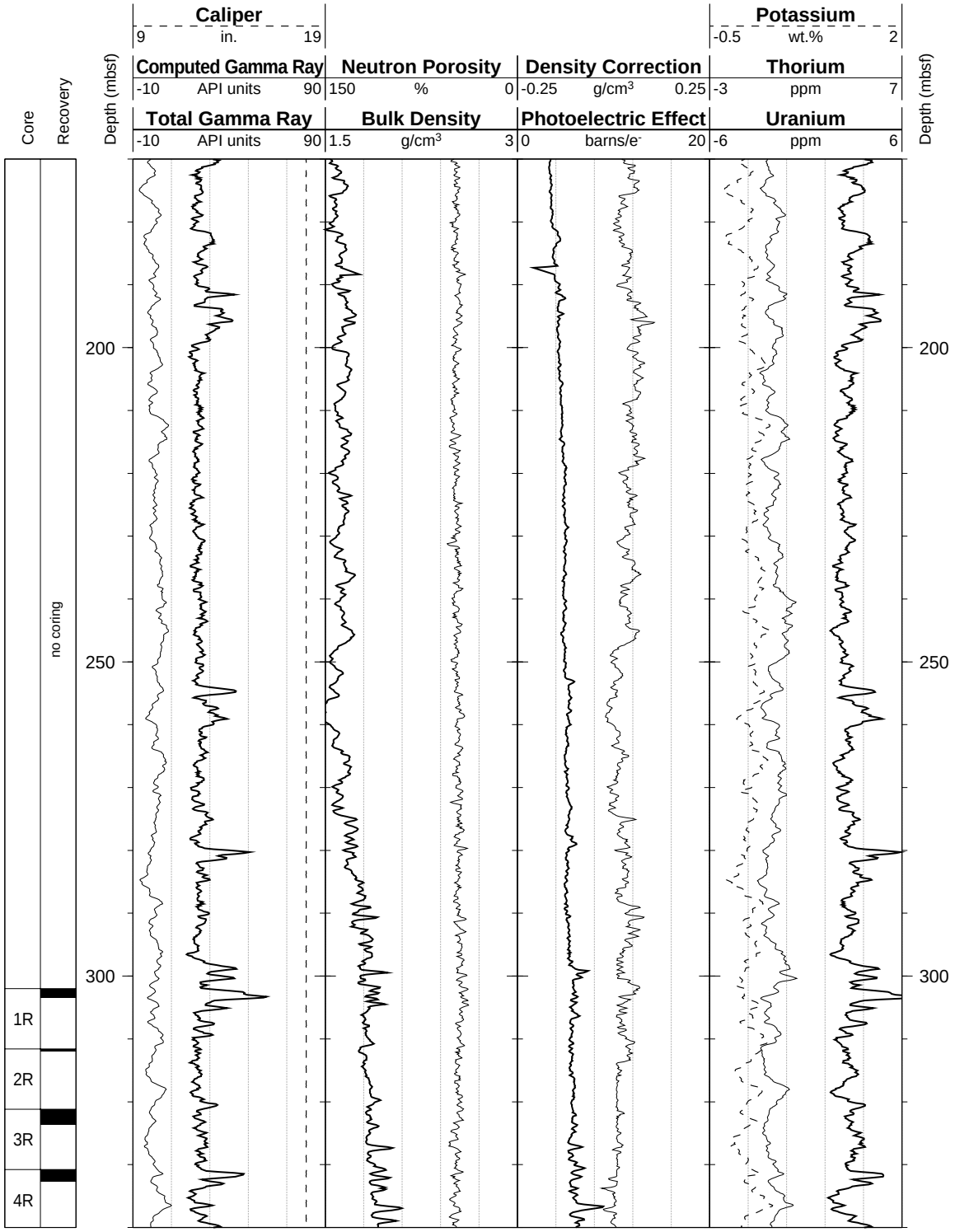

Hole 1007C: Natural Gamma Ray-Density-Porosity Logging Data (cont.)

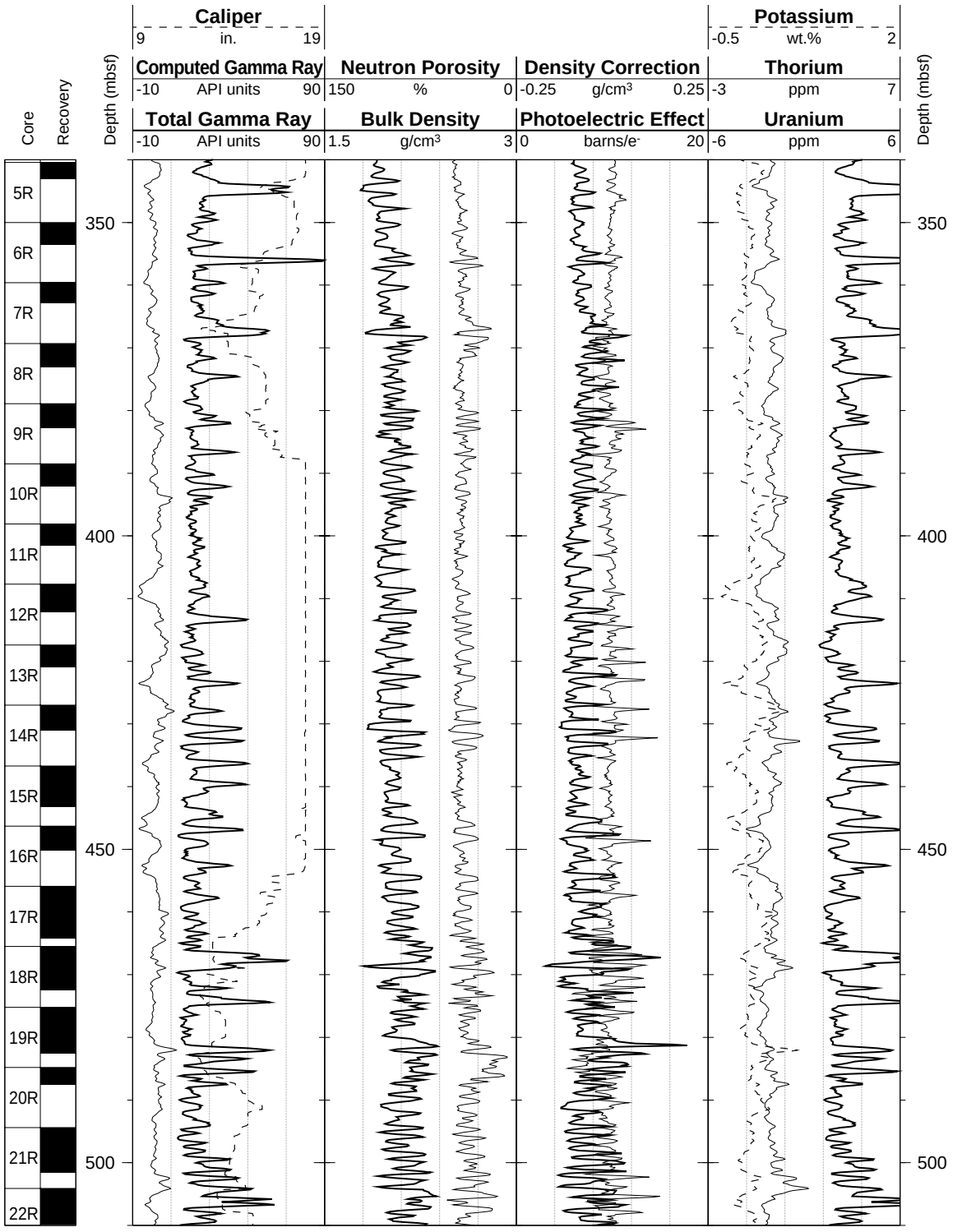

Hole 1007C: Natural Gamma Ray-Density-Porosity Logging Data (cont.)

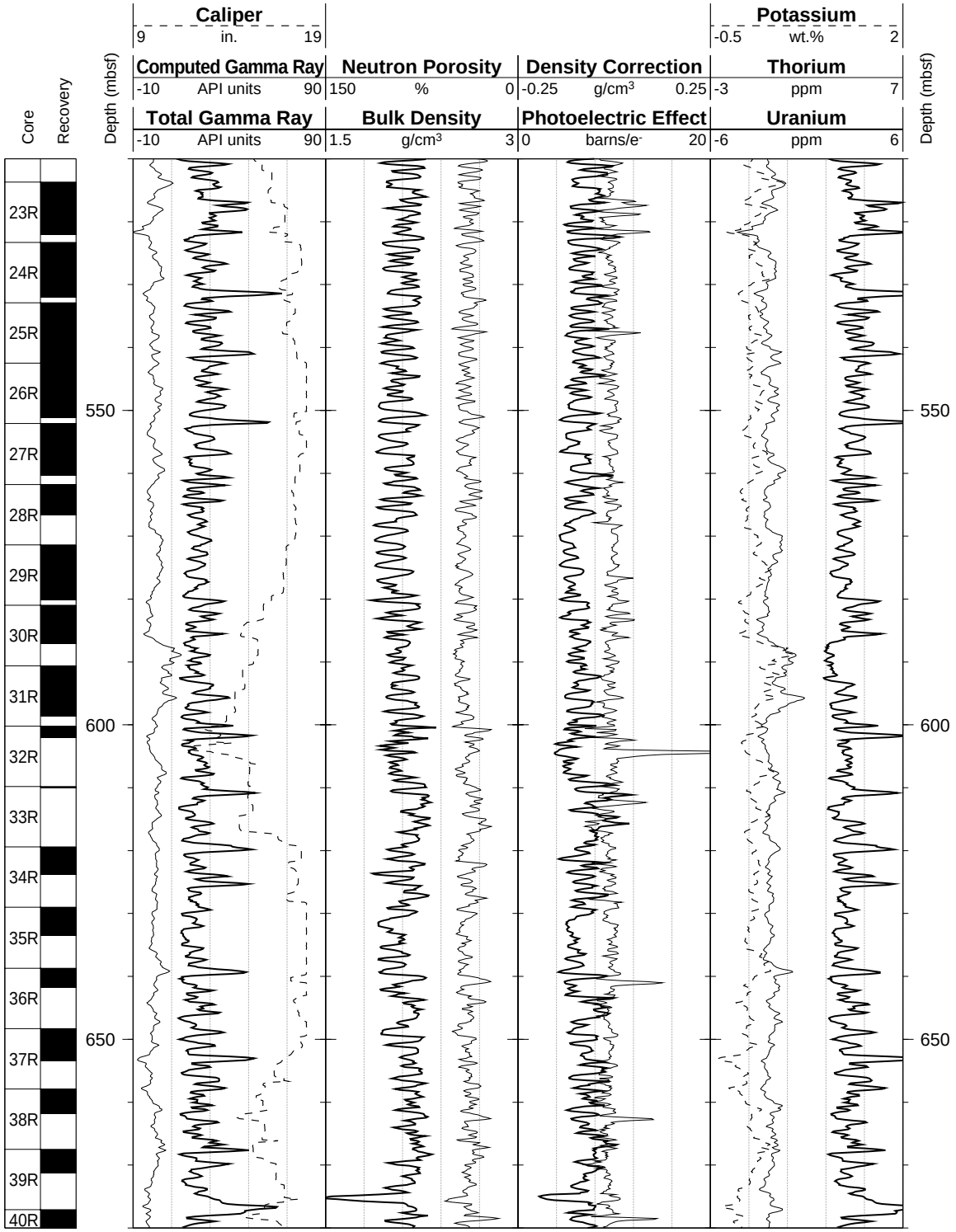

Hole 1007C: Natural Gamma Ray-Density-Porosity Logging Data (cont.)

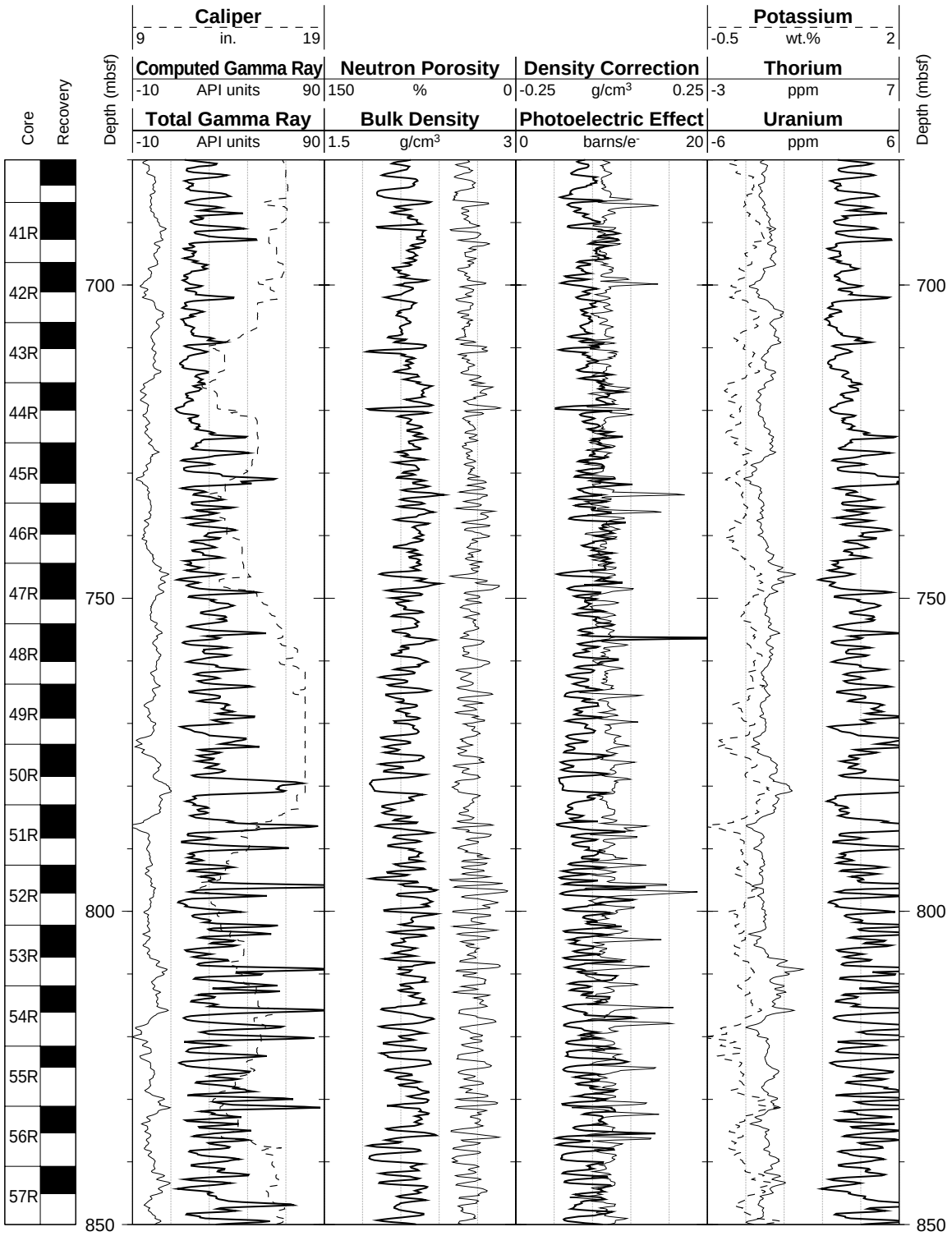

Hole 1007C: Natural Gamma Ray-Density-Porosity Logging Data (cont.)

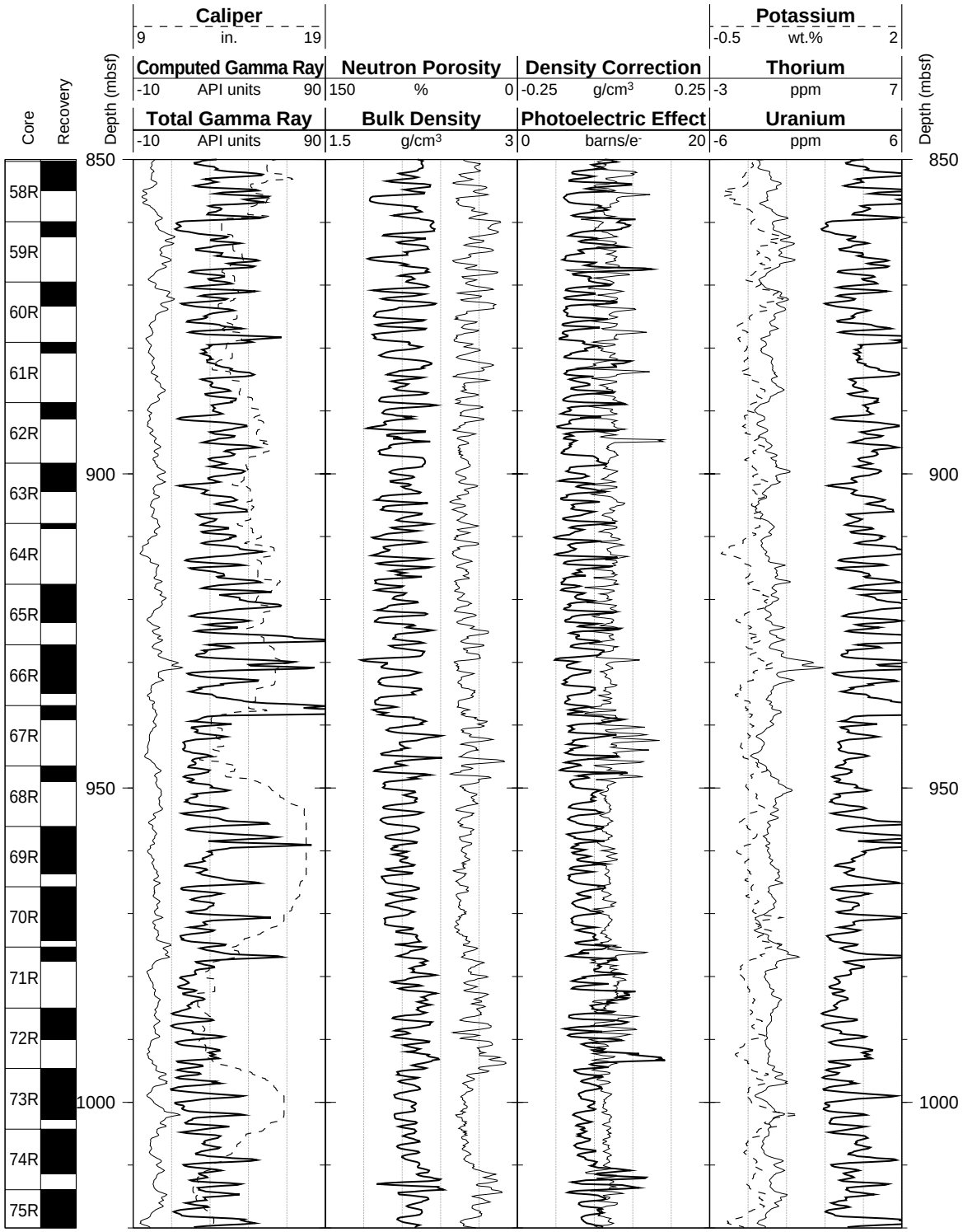

Hole 1007C: Natural Gamma Ray-Density-Porosity Logging Data (cont.)

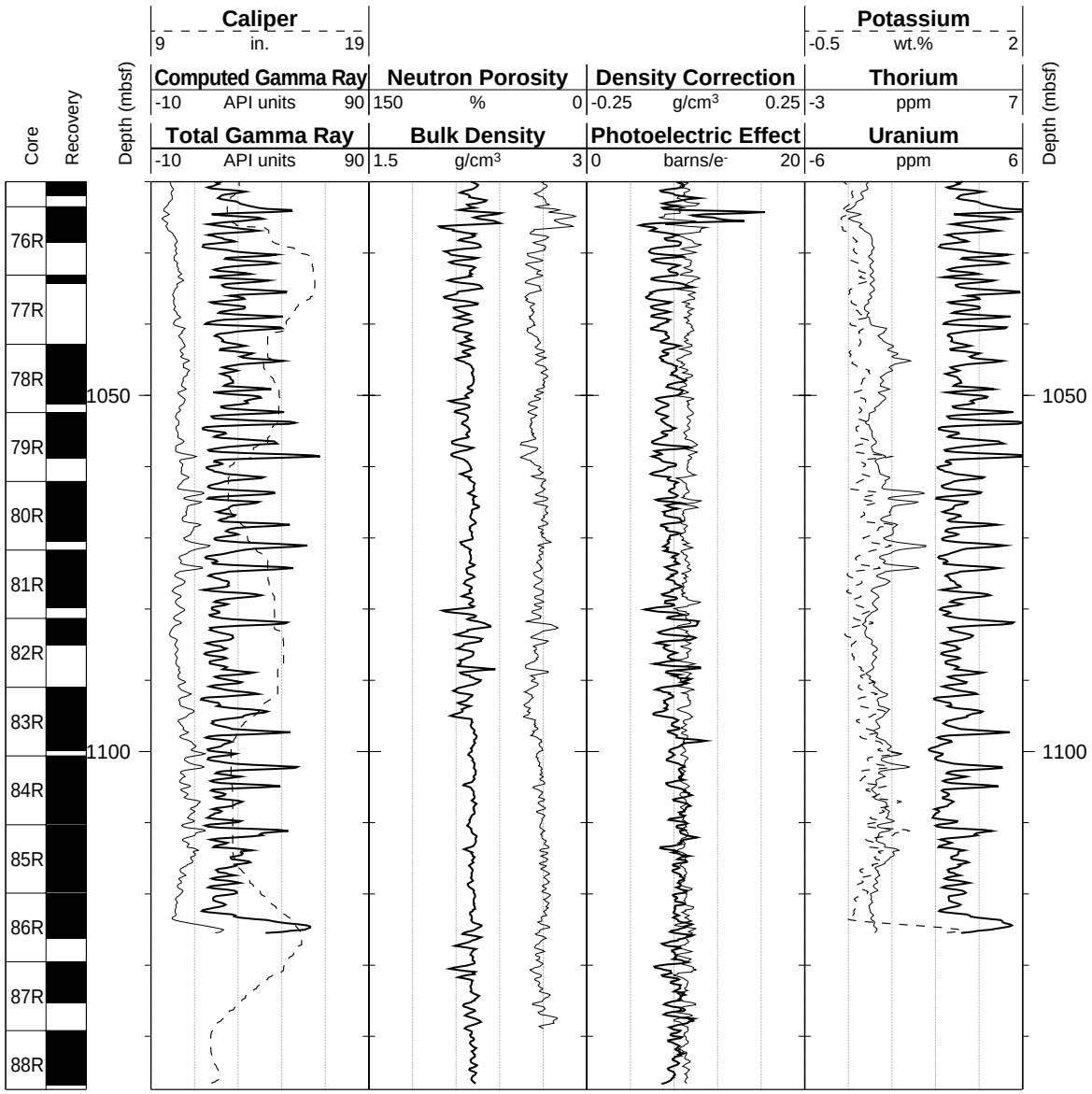

Previous Chapter Table of Contents Next Chapter